

STUDIES OF THE EFFECTS OF ELECTROLYTE ADDITIVES ON THE
PERFORMANCE OF LITHIUM-ION BATTERIES

by

Kathlyne Nelson

Submitted in partial fulfilment of the requirements
for the degree of Master of Science

at

Dalhousie University
Halifax, Nova Scotia
August 2014

© Copyright by Kathlyne Nelson, 2014

To my parents,

TABLE OF CONTENTS

LIST OF TABLES.....	vi
LIST OF FIGURES	vii
ABSTRACT.....	xii
LIST OF ABBREVIATIONS AND SYMBOLS USED.....	xiii
ACKNOWLEDGEMENTS.....	xv
CHAPTER 1. INTRODUCTION	1
1.1 MOTIVATION.....	1
1.2 LI-ION BATTERIES.....	2
CHAPTER 2. SOLID ELECTROLYTE INTERPHASES AND THE ROLE OF ELECTROLYTE ADDITIVES	10
2.1 SOLID ELECTROLYTE INTERPHASE	10
2.1.1 SEI AT THE NEGATIVE ELECTRODE.....	10
2.1.2 SEI AT THE POSITIVE ELECTRODE	17
2.2 ELECTROLYTE ADDITIVES	22
2.2.1 MOTIVATION.....	22
2.2.2 ADDITIVES IN THIS THESIS.....	39
CHAPTER 3. EXPERIMENTAL METHODS.....	41
3.1 POUCH CELLS, CELL CHEMISTRIES AND ELECTROLYTE SYSTEMS IN THIS THESIS	41
3.2 CYCLING EXPERIMENTS	42

3.3	STORAGE EXPERIMENTS.....	45
3.4	GAS EVOLUTION	49
3.5	ELECTROCHEMICAL IMPEDANCE SPECTROSCOPY	49
3.6	FREQUENCY RESPONSE ANALYZER (FRA)	56
CHAPTER 4. PES SYSTEM.....		57
4.1	CONCENTRATION STUDY	57
4.1.1	EXPERIMENTAL.....	57
4.1.2	RESULTS AND DISCUSSION.....	58
4.1.3	CONCLUSION.....	67
4.2	HIGH TEMPERATURE STORAGE STUDY.....	67
4.2.1	EXPERIMENTAL.....	67
4.2.2	RESULTS AND DISCUSSION.....	68
4.2.3	CONCLUSION.....	70
4.3	“211” COMBINATION STUDY	71
4.3.1	EXPERIMENTAL.....	71
4.3.2	RESULTS AND DISCUSSION.....	72
4.3.3	CONCLUSION.....	84
CHAPTER 5. TAP SYSTEM AND FRA MEASUREMENTS		85
5.1	CONCENTRATION STUDY	85
5.1.1	EXPERIMENTAL.....	85
5.1.2	RESULTS AND DISCUSSION.....	87

5.1.3	CONCLUSION.....	95
5.2	FRA STUDY	96
5.2.1	EXPERIMENTAL.....	96
5.2.2	RESULTS AND DISCUSSION.....	97
5.2.3	CONCLUSION.....	111
CHAPTER 6.	CONCLUSION.....	112
6.1	CONCLUSIONS.....	112
6.2	FUTURE WORK.....	113
REFERENCES	119

LIST OF TABLES

Table 2.1 Structure and function of additives for Li-ion cells.....	24
Table 3.1 Equivalent circuit models and their calculated impedance.....	52

LIST OF FIGURES

- Figure 1.1 Schematic of a Li-ion cell with a graphite negative electrode (right) and a lithium transition metal oxide positive electrode (left). The arrow indicates the direction of the flow of electrons and Li ions during a charge. 5
- Figure 1.2 The chemical structure of commonly used salts for electrolytes in Li-ion cells. 6
- Figure 1.3 The chemical structure of commonly used solvents for electrolytes in Li-ion cells. 8
- Figure 2.1 Schematic of the negative electrode SEI, adapted from Peled et al.¹⁸ 12
- Figure 2.2 The chemical structures of the electrolyte additives used in this thesis. 40
- Figure 3.1 Photograph of an NMC111/graphite wound pouch cell from Whenergy. 42
- Figure 3.2 A voltage-capacity curve for an NMC111/graphite pouch cell. The inset is a close up indicating the shift in capacity to higher values as the cycle number increases. 45
- Figure 3.3 Representative voltage-capacity curve for an NMC111 electrode (solid line) and for a graphitic electrode (dashed line). 46
- Figure 3.4 Schematic of the cell voltage as a function of time during a typical storage experiment. The time axis is not to scale. Adapted from Sinha et al.⁶⁰ 48
- Figure 3.5 A voltage-capacity curve of an NMC111/graphite cell filled with control electrolyte for the discharge capacities before and after a 500 hours storage period at 50°C. 48
- Figure 3.6 Schematic of the SEI formed on the electrode surface. The resulting layers of charge are analogous to a double layer capacitor. Li-ions and electrons can pass through the SEI. 53
- Figure 3.7 A Nyquist plot of a positive electrode in electrolyte (a) and a full Li-ion cell (b). A Bode plot of the real component of impedance (c) and the imaginary component of impedance (d) of a full Li-ion cell. The circuit values used are: $R_S = 10 \Omega$, $C_{DL} = 0.001 \text{ F}$, $R_{ct} = 20 \Omega$, $C_p = 0.005 \text{ F}$, and $R_p = 50 \Omega$. \mathcal{R} represents the combination of charge transfer resistances (both negative and positive electrodes) and resistance due to motion of ions through the SEI layers (both negative and positive electrodes). 54

- Figure 3.8 An example impedance spectra before the experimental setup contribution has been subtracted. 55
- Figure 4.1 Gas evolution during formation at 40°C measured using Archimedes principle. The dotted blue line highlights that of 2% VC. 59
- Figure 4.2 EIS spectra of the NMC111/graphite cells collected at 3.8 V and 10°C after formation. 60
- Figure 4.3 Gas evolution during storage at 40°C (a) and during cycling at 40°C (b) and the the combination of charge transfer resistances (both negative and positive electrodes) and resistance due motion of ions through the SEI layers (both negative and positive electrodes, \mathcal{R} measured using EIS at 3.8 V and 10°C after storage (c) and after cycling (d). 61
- Figure 4.4 (top) The drop in open circuit voltage from 4.2 V during 500 hours of storage at 40°C; (bottom) The difference between the discharge capacity before the storage period and the discharge capacity after a full charge following the storage period. 62
- Figure 4.5 The normalized discharge capacity of the cycled-only cells (a) and the stored-before-cycled cells (d); the normalized charge end point capacity of the cycled-only cells (b) and the stored-before cycled-cells (e); the coulombic efficiency of the cycled-only cells (c) and the stored-before-cycled cells (f), all plotted versus cycle number. The cells were cycled at C/20 between 2.8 and 4.2 V at 40.°C. 64
- Figure 4.6 a) The normalized charge end point capacity of the cycled-only cells and b) the stored –before-cycled cells, both versus cycle number. The cells were cycled at C/20 between 2.8 and 4.2 V at 40°C. 65
- Figure 4.7 The coulombic efficiency of the cycled-only cells (left) and the stored-before-cycled cells (right) as a function of time. The zero of time marks the point after EIS was measured after formation for all the cells. The cells were cycled at C/20 between 2.8 and 4.2 V at 40°C. The black dotted line represents an extrapolation of the CE for 2% VC-containing cells and the magenta dotted line represents an extrapolation of the CE for 2% PES containing cells. 66
- Figure 4.8 Gas evolution during formation at 40°C (a) and during storage at 60°C (c) and the EIS spectra collected at 3.8 V and 10°C after formation (b) and after storage (d). 69
- Figure 4.9 The drop in open circuit voltage from 4.2 V during 500 hours of storage at 60°C. 70

Figure 4.10 Gas evolution during formation at 40°C measured using Archimedes principle.	73
Figure 4.11 EIS spectra of the NMC111/graphite cells collected at 3.8 V and 10°C after formation.	74
Figure 4.12 Gas evolution during storage at 40°C (a) and during cycling at 40°C (b) and the impedance spectra measured using EIS at 3.8 V and 10°C after storage (c) and after cycling (d).	76
Figure 4.13 The drop in open circuit voltage from 4.2 V during 500 hours of storage at 40°C.	77
Figure 4.14 The normalized discharge capacity of the cells (a); the normalized charge end point capacity of the cells (b); and the coulombic efficiency of the cells (c), all plotted versus cycle number. The cells were cycled at C/22 between 2.8 and 4.2 V at 40°C	79
Figure 4.15 Gas evolution during storage at 60°C and 4.4 V measured using Archimedes principle. Cells were not degassed after charging to 4.4 V for the first time.	80
Figure 4.16 Volume of gas evolved during formation at 70°C in NMC442/graphite cells as a function of voltage. Data courtesy of Connor Aiken, Dalhousie University.	81
Figure 4.17 The drop in open circuit voltage from 4.4 V during 600 hours of storage at 60°C	83
Figure 4.18 The discharge capacity of NMC111/graphite cells as a function of cycle number. The cells were cycled at 55°C and C/2.5 between 2.8 and 4.2 V. Data courtesy of Jian Xia and Lin Ma, Dalhousie University.	83
Figure 5.1 Gas evolution during formation at 40°C measured using Archimedes principle.	88
Figure 5.2 EIS spectra of the NMC442/graphite cells collected at 3.8 V and 10°C after formation.	89
Figure 5.3 Gas evolution during cycling at 40°C (a) and the impedance spectra measured using EIS at 3.8 V and 10°C after cycling (b).	90
Figure 5.4 The normalized discharge capacity of the cells (a); the normalized charge end point capacity of the cells (b); and the coulombic efficiency of the cells (c), all plotted versus cycle number. The cells were cycled at C/22 between 2.8 and 4.4 V at 40°C.	92

- Figure 5.5 Schematic of voltage-capacity curves are a cell with no impedance growth (a) and with large impedance growth (b). 93
- Figure 5.6 The difference between the average charge and discharge voltages of the cells as a function of cycle number. 94
- Figure 5.7 A close up of the normalized discharge capacity of the cells (top); and the coulombic efficiency of the cells (bottom), all plotted versus cycle number. The cells were cycled at C/22 between 2.8 and 4.4 V at 40°C. 95
- Figure 5.8 Discharge capacity as a function of cycle number for the original eight cells undergoing cycling tests and FRA measurements at 40°C. 98
- Figure 5.9 The combination of charge transfer resistances (both negative and positive electrodes) and resistance due to motion of ions through the SEI layers (both negative and positive electrodes), \mathcal{R} as a function of voltage for the original eight cells measured every 11 cycles. 99
- Figure 5.10 Discharge capacity as a function of cycle number for the cell chosen for continued cycling tests and FRA measurements at 40°C. 102
- Figure 5.11 A Bode representation of the raw data, calibration data, and final data of an example cell containing 2% TAP. 103
- Figure 5.12 Impedance spectra of the 2% TAP-containing cell for every FRA cycle, measured at 4.4 V. 104
- Figure 5.13 Impedance spectra of the 2% TAP-containing cell at every voltage measured during cycle 149. 105
- Figure 5.14 The combination of charge transfer resistances (both negative and positive electrodes) and resistance due to motion of ions through the SEI layers (both negative and positive electrodes), \mathcal{R} as a function of voltage for the cells chosen for continued testing measured every 11 cycles. 106
- Figure 5.15 The combination of charge transfer resistances (both negative and positive electrodes) and resistance due to motion of ions through the SEI layers (both negative and positive electrodes), \mathcal{R} measured at 4.4 V as a function of cycle number for the cell containing 2% PES (a), PES211 (b), and 2% TAP (c). 110
- Figure 6.1 Chromatogram (total ion counts) of extracted electrolyte from NMC111/graphite cells initially containing 2% DTD or 2% DTD + 2% VC. 115

Figure 6.2 Discharge capacity for NMC442/graphite cells undergoing cycling tests with a 24 hour hold at 4.4 V and 40°C. 117

Figure 6.3 The combination of charge transfer resistances (both negative and positive electrodes) and resistance due to motion of ions through the SEI layers (both negative and positive electrodes), \mathcal{R} as a function of voltage for three cells for each measured FRA sequence. 117

ABSTRACT

Electrolyte additives are an effective way to improve the lifetime and performance of Li-ion cells. Electrolyte additives can modify the solid electrolyte interphase layers on the positive and/or negative electrodes, resulting in improved Li-ion cells. However, the function of additives and why they work are poorly understood. Through a series of high precision cycling and storage experiments, combined with measurements of gas evolution and cell impedance, the effectiveness of electrolyte additives and additive combinations have been investigated. This combination of experimental methods proved to be useful and was used to probe the performance of additives and understand their role in Li-ion cells in a timely fashion. Cells containing a combination of additives resulted in better performance than those containing a single additive, demonstrating the distinctive contributions of each additive to improvements to cell performance and lifetime.

Li[Ni_{1-x-y}Mn_xCo_y]O₂/graphite pouch cells containing the additive prop-1-ene-1,3-sultone (PES) had equivalent performance to cells containing the “famous” additive vinylene carbonate, except that prop-1-ene-1,3-sultone nearly eliminated all gas production during cycling and storage at elevated temperature. Cells containing PES combined with methylene methane disulfonate (MMDS) and tris(trimethylsilyl) phosphite (TTSPi) exhibited superior performance during cycling and storage experiments. In general, the impedance of Li[Ni_{1-x-y}Mn_xCo_y]O₂/graphite cells varied strongly with voltage above 4.3 V, and was basically reversible during a single cycle, but increased slowly and continuously during dozens of charge-discharge cycles to 4.4 V or 4.5 V. Additive blends of PES combined with MMDS and TTSPi were very effective at reducing this impedance growth. Further work will address why this is the case.

LIST OF ABBREVIATIONS AND SYMBOLS USED

AC	Alternating current
C	Capacitance (further described by subscript)
CE	Coulombic efficiency
D	Discharge capacity (further described by subscript)
DEC	Diethyl carbonate
DMC	Dimethyl carbonate
DOD	Depth of discharge
DTD	Ethylene sulfate
EC	Ethylene carbonate
EDX	Energy dispersive X-ray spectroscopy
EIS	Electrochemical impedance spectroscopy
EMC	Ethyl methyl carbonate
ES	Ethylene sulfite
f	Frequency
FEC	Fluoroethylene carbonate
FRA	Frequency response analyzer
FTIR	Fourier transform infrared spectroscopy
GC/MS	Gas chromatography-mass spectrometry
HQ-115	Lithium bis (trifluoromethylsulfonyl) imide (LiN[CF ₃ SO ₂] ₂ , Li-TFSI)
i	Imaginary unit, $\sqrt{-1}$
L	Inductance (further described by subscript)
LEDC	Lithium ethylene dicarbonate
LiBetI	(LiN(SO ₂ CF ₂ CF ₃) ₂)
LiBOB	Lithium bis(oxalato)borate
LiDFOB	Lithium difluoro(oxalato)borate
LiFSI	Lithium bis(fluorosulfonyl) imide
Li-TFSI	See HQ-115
LMC	Lithium methyl carbonate
m	Mass
MCMB	Mesocarbon microbeads
MMDS	Methylene methane disulfonate
NMC	Li[Ni _{1-x-y} Mn _x Co _y] ₂ O ₂
NMR	Nuclear magnetic resonance spectroscopy
OCV	Open circuit voltage
ρ	Density
PC	Propylene carbonate
PES	Prop-1-ene-1,3-sultone
PES211	Electrolyte containing 2% PES + 1% MMDS + 1% TTSPi

PES411	Electrolyte containing 4% PES + 1% MMDS + 1% TTSPi
Q	Cell capacity (further described by subscript)
R	Resistance (further described by subscript)
\mathcal{R}	Combination of resistance from charge transfer and motion of ions through the SEI layers
SEI	Solid electrolyte interphase
t	Time
TAP	Triallyl phosphate
TEM	Transmission electron microscopy
TMOBX	Trimethoxyboroxine
TTSP	Tris(-trimethyl-silyl)-phosphate
TTSPi	Tris(-trimethyl-silyl)-phosphite
UHPC	Ultra high precision charger
V	Cell voltage (further described by subscript)
v	Volume
VC	Vinylene carbonate
ω	Angular frequency
XPS	X-ray photoelectron spectroscopy
Z	Impedance (further described by subscript)

ACKNOWLEDGEMENTS

I would like to thank the NSERC CREATE DREAMS program along with 3M for their partial funding of this work.

I would like to thank my supervisor, Dr. Jeff Dahn, to whom I am very grateful for the opportunity to learn from his extensive experience in the world of batteries. His support, enthusiasm and motivation has been invaluable, and I look forward to another few years under his supervision. I would also like to thank my committee member, Dr. Mark Obrovac, for his help and advice. I would also like to thank Tanya Timmins and the rest of the staff in the physics office for their help.

I would like to thank all the members of the Dahn lab, both former and current, that I have interacted with for their support, encouragement, and teamwork. Particularly, I would like to thank the chickens for making time in the coop enjoyable, fun, and (mostly) productive. To Eric, Laura, Remi, and John for welcoming me and ensuring grad school was a balance of good work and good fun. I'd also like to thank Remi for his continual help and advice; his enthusiasm for research is infectious. Thanks also go to Lin whose positivity always brightens my day and to David Stevens for making every day amusing and every group lunch delicious.

I would like to thank Patrick Connolly for his love and support and his silliness, which was much needed during the writing of this thesis.

Lastly I would like to thank my parents for their everlasting love, encouragement, and support (financially and otherwise) and for being such admirable role models for me in all aspects of their lives. To my siblings who have also grown into significant role models for me, I am so grateful for your companionship, even when I'm far away.

CHAPTER 1. INTRODUCTION

1.1 MOTIVATION

Lithium-ion (Li-ion) batteries, first commercialized by Sony in 1990¹, are the most common rechargeable batteries on the market.² Li-ion batteries used in phones, laptop computers, medical devices and, most recently, electric vehicles, play a crucial role in transitioning away from the non-renewable sources of energy currently being used. Li-ion batteries offer both high specific energy and energy density as well as long cycle life.

Despite the good performance of current Li-ion batteries, the development of technology, such as electric vehicles and energy storage, require lifetimes of 10-30 years and thus require improved Li-ion batteries. Due to parasitic reactions that occur in Li-ion cells every cycle, electrolyte is consumed and lithium is trapped such that Li is no longer electrochemically active. Parasitic reactions lead to the eventual failure of the cell. Predicting cell failure and understanding the parasitic reactions that occur are necessary to design and manufacture improved Li-ion batteries.

Electrolytes are an ionic conductor and electronic insulator that facilitates ion transfer in a cell. Electrolyte additives are very important as they can reduce the rate of parasitic reactions, improve safety, decrease the degradation of active materials, and ultimately improve the cycle and calendar life of Li-ion batteries.^{1,3-6}

In May 2014, Nissan sold 3117 Leafs⁷ (fully electric vehicles), which was the most they have sold in a month to date. The number of electric vehicles sold was 2.5% of Nissan's

total vehicle sales for the month.⁷ In May 2014, GM sold 1684 Volts⁸ (plug-in hybrid vehicles) which made up 0.6% of GM's total vehicle sales for the month.⁸ The extremely low percentage of electric vehicles sold compared to gasoline powered vehicles made by the same company is evidence that longer lasting, safer batteries that are affordable need to be produced in order for the general population to begin and continue using electric vehicles.

1.2 LI-ION BATTERIES

A battery is a device that converts chemical energy contained in its active materials directly into electrical energy. This occurs via an electrochemical oxidation-reduction (redox) reaction. A secondary battery, such as a Li-ion battery, can be recharged through a reversal of the redox reaction.

Lithium-ion batteries work via intercalation, a process in which Li ions transfer between the positive and negative electrodes. Both electrode materials are Li intercalation compounds so that lithium ions can be inserted or removed from the interstitial space between atomic layers in the active materials in a reversible manner. The electrode materials should be chosen such that as Li ions are inserted and removed, there is no significant change in the structure of the host material. Therefore, typical electrode materials have a layered or framework structure. Electrode materials should also be selected to achieve a high operating cell voltage and high capacity, while obtaining high energy density at a low cost. Electrode materials should be chosen such that reactions with other cell components are minimized to minimize degradation.

The negative electrode is typically a graphitic carbon with a layered structure, on a copper current collector. Sony initially employed petroleum coke as a negative electrode material.² Lithium metal has been used for negative electrodes but has several safety issues due, in part, to the changing safety properties with the changing morphology of Li as cells were cycled.² Carbon electrodes have consistent safety properties during the lifetime of a cell due to stability in the morphology as lithium ions intercalate between the sheets of graphite.

The theoretical specific capacity of graphite is 372 mAh/g,⁹ which is significantly lower than the theoretical capacity of some alloys used as negative electrode materials, such as 3579 mAh/g for silicon in $\text{Li}_{15}\text{Si}_4$.¹⁰ However, silicon can expand up to 280% in volume during cycling leading to poor cycle life and cell design difficulties.¹¹

The positive electrode is typically a layered metal oxide on an aluminum foil current collector. When a layered metal oxide is used as the positive electrode material, lithium intercalates between the layers. Tunnel structures, such as the spinel or olivine structures, are also used and Li intercalates through the tunnels.

Lithium cobalt oxide (LiCoO_2), a layered structure, has good electrochemical performance and good safety properties as a positive electrode material.² However, cobalt is an expensive material and thus increases the cost of the cell.

Lithium nickel manganese cobalt oxide ($\text{Li}[\text{Ni}_{1-x-y}\text{Mn}_x\text{Co}_y]\text{O}_2$), or NMC, was first proposed by Lu et al. as a positive electrode material with improved performance, better thermal stability, increased safety, and lower cost.¹² The substitution of Ni and Mn in

place of cobalt in LiCoO_2 makes NMC a high performing, safe, inexpensive positive electrode material. Various forms of NMC including $\text{Li}[\text{Ni}_{1/3}\text{Mn}_{1/3}\text{Co}_{1/3}]\text{O}_2$ (NMC111) and $\text{Li}[\text{Ni}_{0.4}\text{Mn}_{0.4}\text{Co}_{0.2}]\text{O}_2$ (NMC442) have been used to maximize lifetime and performance while minimizing cost.¹³

Figure 1.1 shows a schematic of a Li-ion cell with a graphite negative electrode and a lithiated transition metal oxide positive electrode. The arrows indicate the flow of electrons and ions when a current is applied to the cell during charge. Lithium ions de-intercalate into the electrolyte from the positive electrode and intercalate into the negative electrode during charge. The reverse occurs during discharge. The positive electrode shown in Figure 1.1 could be LiCoO_2 if the transition metal is cobalt, or NMC if the transition metal is a combination of Ni, Mn and Co.

In order for charge to actually transfer between the positive and negative electrodes, there must be an electrolyte between the electrodes. Although electrolytes are sometimes solid, liquid electrolytes are used primarily. A liquid electrolyte typically consists of a salt dissolved in a mixture of solvents to achieve good ionic conductivity. Electrolyte salts must have high ionic conductivity and be able to fully dissolve in nonaqueous electrolytes. Commonly used salts in Li-ion cells include lithium hexafluorophosphate (LiPF_6), lithium tetrafluoroborate (LiBF_4), and lithium bis (trifluoromethylsulfonyl) imide ($\text{LiN}[\text{CF}_3\text{SO}_2]_2$, Li-TFSI, or HQ-115). The chemical structures of these salts are shown in Figure 1.2.

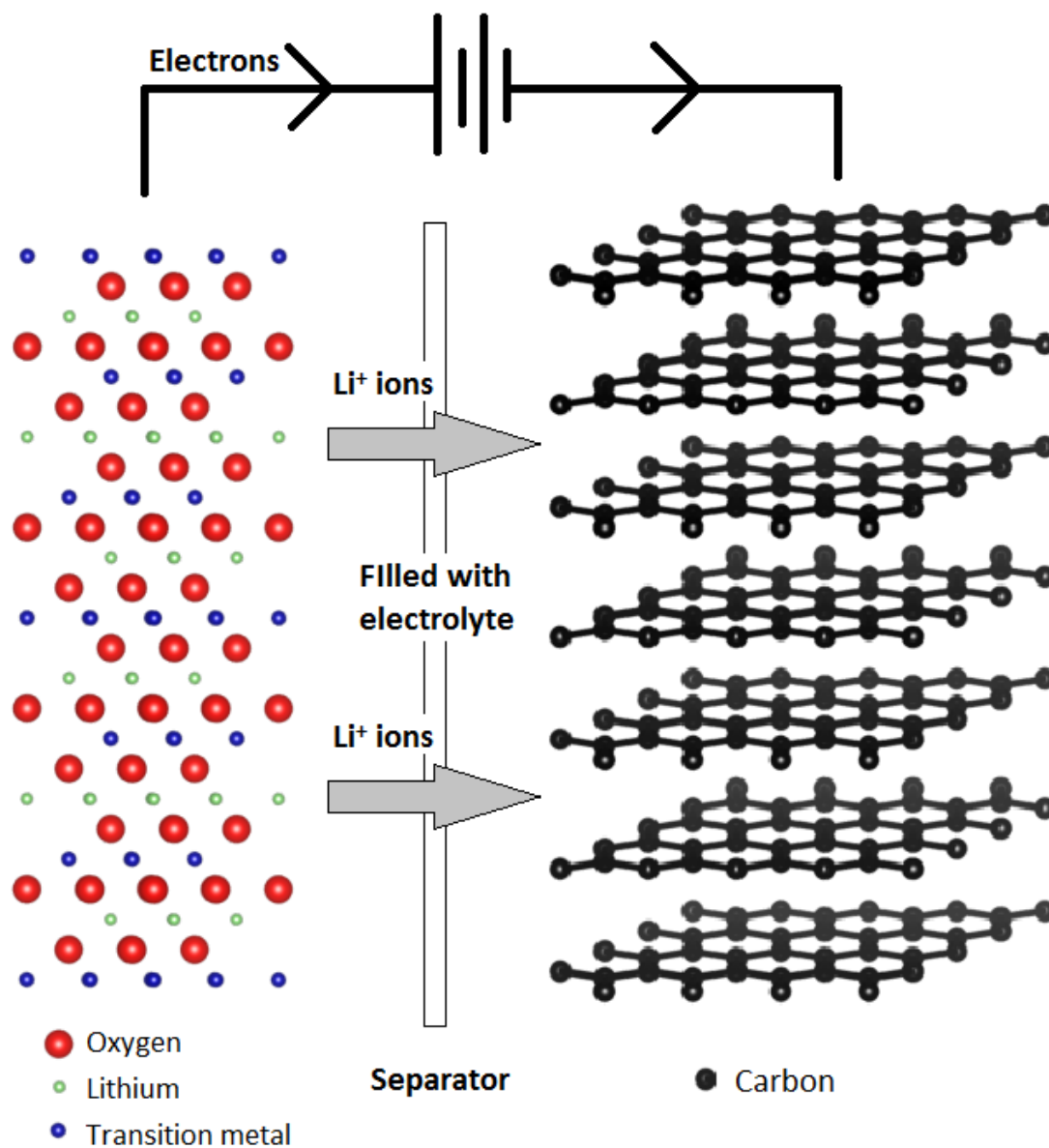


Figure 1.1 Schematic of a Li-ion cell with a graphite negative electrode (right) and a lithium transition metal oxide positive electrode (left). The arrow indicates the direction of the flow of electrons and Li ions during a charge.

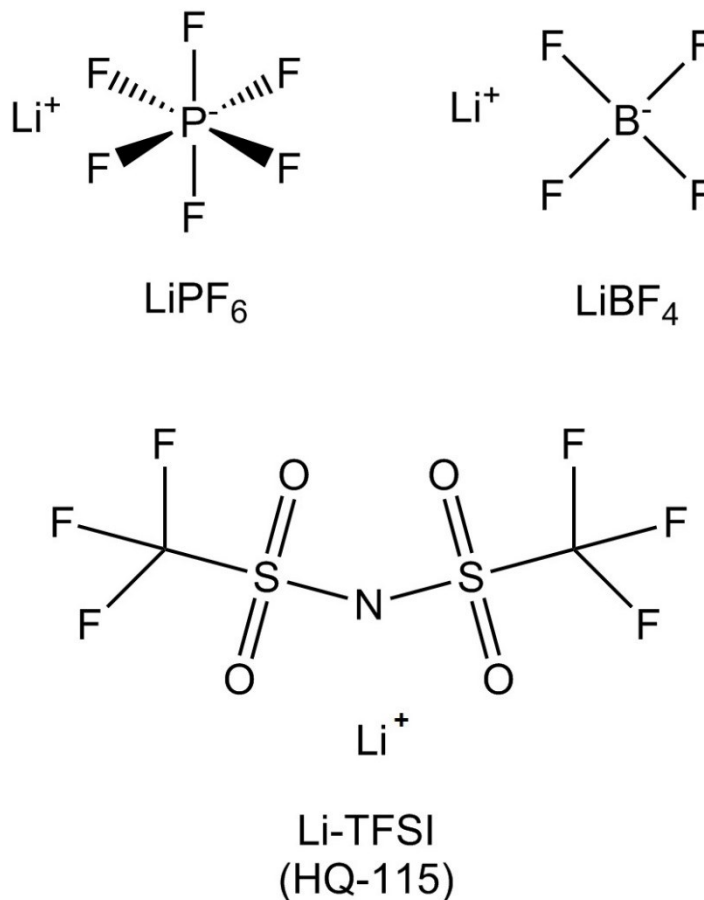


Figure 1.2 The chemical structure of commonly used salts for electrolytes in Li-ion cells.

LiBF₄ is advantageous due to its high safety and thermal stability, but has only moderate conductivity. Li-TFSI has good thermal stability and is highly conducting, but is expensive and corrodes the aluminum current collector at the positive electrode. LiPF₆ has a combination of properties that is better than any single other salt. LiPF₆ is highly conducting, particularly when dissolved in a mixture of carbonate solvents, although high purity manufacture is necessary to reduce the formation of hydrofluoric acid which is harmful to the cell in terms of safety and performance.

Solvents should be liquid over a wide temperature range in addition to being safe, non-toxic, and low in cost. Solvents should also be as stable as possible at positive and negative electrode potentials. Carbonate solvents are attractive as they are nonaqueous with a high dielectric constant and can dissolve high concentrations of Li salts. The most common carbonate solvents are ethylene carbonate (EC), ethyl methyl carbonate (EMC), diethyl carbonate (DEC), dimethyl carbonate (DMC) and propylene carbonate (PC). The chemical structures of these solvents are shown in Figure 1.3.

PC was originally used as a solvent due to its high dielectric constant and wide liquid range. However, PC can cause degradation in graphitic electrodes during a process called exfoliation, which leads to capacity fade, Li-plating and poor cycling.¹⁴ EC is a similar molecule to PC, but forms an effective passivating film on the negative electrode (called the solid electrolyte interphase or SEI), preventing further electrolyte decomposition, which PC is unable to do. The reversibility of Li-ion intercalation in graphitic negative electrodes in cells containing EC and PC was investigated by Fong et al.¹⁴ EC results in low capacity fade and low irreversible capacity but is solid at room temperature. By combining EC with other solvents, such as EMC or DEC, the freezing point of the electrolyte is reduced while still maintaining the beneficial properties of EC. For these reasons, EC:EMC is a very common and useful solvent mixture and will be used almost exclusively in the remainder of this thesis.

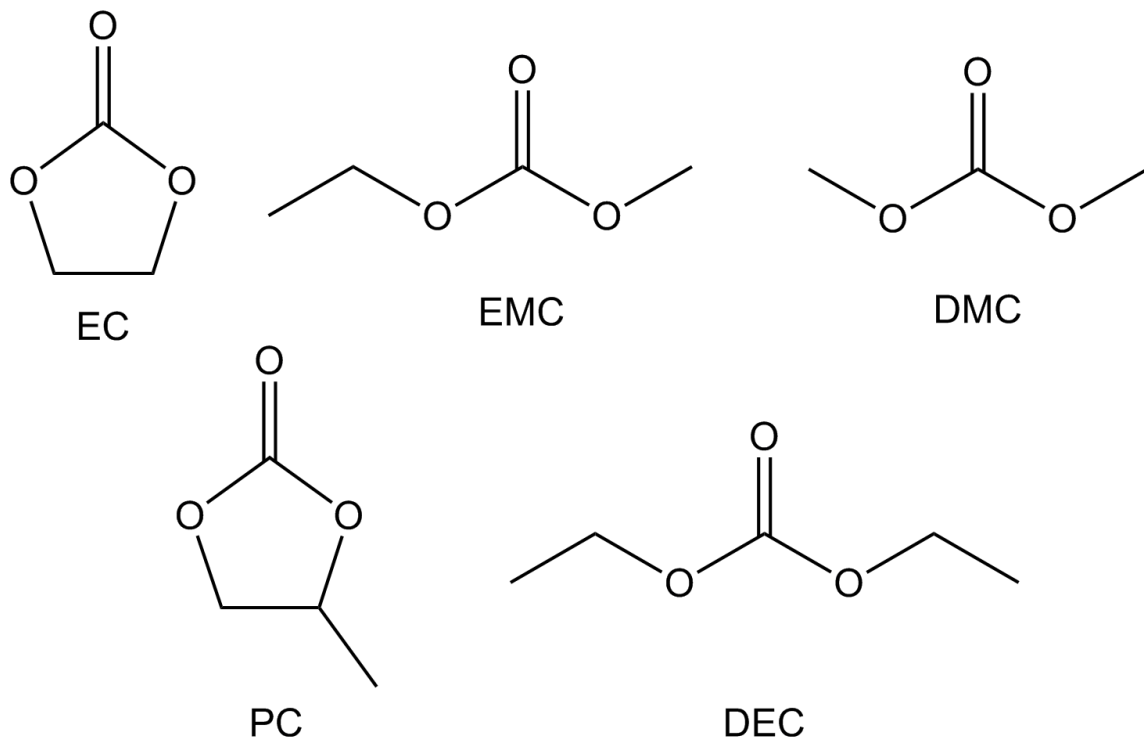


Figure 1.3 The chemical structure of commonly used solvents for electrolytes in Li-ion cells.

In a practical Li-ion cell, there is also a separator between the positive and negative electrode, typically made of polypropylene/polyethylene. The separator mechanically separates the two electrodes, avoiding an internal short, but is permeable to the electrolyte so that ionic conductivity is maintained.

Chapter 2 discusses the role of electrolyte additives and their influence on the solid electrolyte interphase. Chapter 3 outlines the various experimental techniques used to study electrolytes and electrolyte additives in a timely fashion as well as understand the complex function of these additives. Chapter 4 discusses experiments focused on understanding the additive prop-1-ene-1,3-sultone (PES). Chapter 5 discusses experiments focused on understanding the additive triallyl phosphate (TAP). Chapter 6

summarizes the work presented in this thesis and concludes by outlining future work to advance the knowledge and understanding of electrolyte additives for lithium-ion batteries.

CHAPTER 2. SOLID ELECTROLYTE INTERPHASES AND THE ROLE OF ELECTROLYTE ADDITIVES

2.1 SOLID ELECTROLYTE INTERPHASE

The lifetime of a lithium-ion battery is not infinite mainly because of parasitic reactions that occur every cycle. These reactions consume electrolyte and can render lithium electrochemically inactive. The electrodes are thermodynamically unstable in the charged state toward the solvents and salt in electrolytes. Despite the instability of the electrodes in contact with electrolyte, lithium-ion batteries are able to function due to a passivating layer called the solid electrolyte interphase (SEI) by Peled.¹⁵ SEI layers form on the positive and negative electrodes and both behave very differently.

2.1.1 SEI AT THE NEGATIVE ELECTRODE

During the first charge of a Li-ion cell, electrolyte is reduced on the graphitic negative electrode which causes the formation of a passive layer of insoluble products from the reaction of Li with the electrolyte.¹⁶ The SEI has properties of a solid electrolyte – it is an ionic conductor and an electronic insulator. The SEI consists of organic and inorganic compounds, from both solvent and salt decomposition products.¹⁶ It has been suggested that a layer of dense inorganic compounds are on the surface of the graphitic negative electrode and that a layer of porous organic compounds are close to the electrolyte interface in the SEI.¹⁷⁻¹⁹ By blocking electron transport but allowing ion transport, further electrolyte degradation and decomposition is almost entirely prevented by the SEI and the consumption of lithium is slowed.

Although much of the negative electrode SEI forms during the first charge of the cell, the SEI continues to grow during the lifetime of the cell.^{20,21} The SEI growth rate is proportional to $t^{-1/2}$, where t is the time since the beginning of cycling.^{20,21} As this layer continues to form, more Li is trapped resulting in further irreversible capacity loss. Changes in the SEI can be more pronounced at high temperature where the rate of parasitic reactions may increase. Ideally, the SEI is formed such that it prevents all further reactions and therefore prevents capacity loss and electrolyte decomposition.

Types of carbon, pretreatment of carbon and the composition of the electrolyte used are major factors that influence the formation and growth of the SEI.¹⁶ The components of the SEI and their ability to reduce the rate of parasitic reactions can be modified through cell design, choice of battery operating conditions, electrode materials and electrolyte components. For example, the reduction products when EC is used as an electrolyte solvent are insoluble and form a stable passivating film which is not evident when PC is used as a sole solvent.²² This is further evidence for the merit of using a mixture of carbonate solvents with EC in electrolytes for Li-ion cells.

For ideal safety and performance of Li-ion batteries, the SEI that forms should contain stable, insoluble passivating agents that are flexible and adhere well to the negative electrode. The SEI should have uniform morphology and composition so that the current distribution during charging and discharging is homogeneous.

Peled et al. introduced an “advanced model” of the SEI on the negative electrode in 1997.¹⁸ They described the SEI structure as a mixture of insoluble products on the

negative electrode that results from reactions between reduced species and the bulk electrolyte. A schematic of their proposed model is shown in Figure 2.1. Peled et al. thought that the order in which electrolyte components were reduced on the negative electrode dictated where certain species were located within the SEI.¹⁸

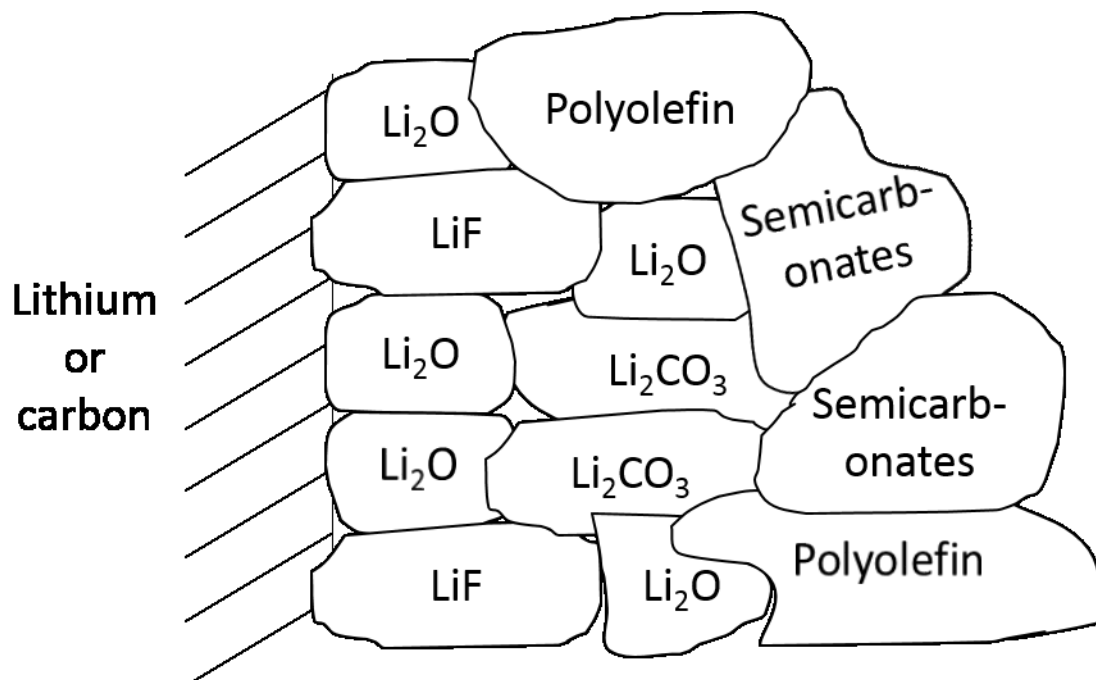


Figure 2.1 Schematic of the negative electrode SEI, adapted from Peled et al.¹⁸

Ganesh et al. performed ab initio molecular dynamics simulations of the negative electrode SEI to learn about electrolyte reduction.²³ They determined that cyclic carbonates are reduced on the graphitic electrode and that Li_2CO_3 should be expected near the electrode surface in the SEI. As LiPF_6 in the electrolyte decomposed, LiF formed on the graphitic electrode surface. Ganesh et al. determined that the surface of the electrode and the presence of LiPF_6 in the electrolyte have a strong impact on the type of species that are reduced on the electrode surface.²³ They determined that inorganic

species remain close to the graphitic electrode surface while organic species are closer to the electrolyte.²³ This is because the inorganic species are more ionic than the organic species.

Although there have been several models of the SEI proposed¹, it has been difficult to analyze and characterize the components of the SEI because the layer is thin and analysis is difficult due to the sensitivity of the SEI to water and oxygen. Several factors affect the formation, growth, and stability of the SEI and many techniques have been used in attempt to determine the SEI composition, and understand its function. Fourier transform infrared spectroscopy (FTIR) and X-ray photoelectron spectroscopy (XPS) can be used to analyze the SEI composition. Cycling and storage techniques described in Chapter 3 can be used to determine the effect of electrolytes and electrolyte additives on the SEI.

There has been controversy over the components of the negative electrode SEI. For example, several researchers believe that while semicarbonates exist in the negative electrode SEI, Li_2CO_3 is only found to be present as an artifact due to poor moisture management.^{19,24} According to a computational study by Shi et al., Li_2CO_3 is present in the negative electrode SEI.²⁵ However, Aurbach et al.²⁴ and Zhuang et al.²⁶ claimed that this compound is not present on the negative electrode side. Edström et al. detected Li_2CO_3 in the negative electrode SEI only when the sample was exposed to ambient atmosphere.¹⁹ They believed that the presence of Li_2CO_3 was an artifact, and could be formed from the reaction of Li_2O and CO_2 , which was confirmed by Harilal et al.²⁷

Zhao proposed that Li_2CO_3 was not present on freshly cycled electrodes, but was present on aged electrodes.²⁸ This was confirmed by Harilal et al. who detected lithium carbonate only in cells that underwent long-term cycling, as opposed to short-term cycling.²⁷ Dedryvère detected mainly Li_2CO_3 as an SEI component when a LiTFSI-based electrolyte was used, but detected both lithium carbonate and semicarbonates when a LiBeti ($\text{LiN}(\text{SO}_2\text{CF}_2\text{CF}_3)_2$) electrolyte was used.²⁹

Nie et al. recently studied the SEI composition using transmission electron microscopy (TEM) with energy dispersive X-ray spectroscopy (EDX) and nuclear magnetic resonance (NMR) spectroscopy.³⁰ Using binder-free graphite electrodes, Nie et al. determined that the SEI was mainly composed of lithium ethylene dicarbonate (LEDC) and lithium fluoride (LiF).³⁰ LEDC is the reduction product of EC. Nie et al. found that, in the presence of LiPF_6 in EC, the SEI was comprised of LEDC, LiF, and low concentrations of $\text{Li}_x\text{PF}_y\text{O}_z$.³⁰ These components were found throughout the SEI layer by Nie et al., suggesting that the SEI did not consist of a layer of dense inorganic compounds on the surface of the graphitic negative electrode and a layer of porous organic compounds close to the electrolyte interface in the SEI, as has been proposed by several researchers.^{1,17-19} Rather, Nie et al. detected inorganic compounds and semicarbonates throughout the SEI, suggesting there is not a clearly defined layer of either organic or inorganic compounds. Nie et al. found that, in the presence of LiPF_6 in EMC, the SEI was comprised of LEDC, LiF, and low concentrations of lithium methyl carbonate (LMC).³⁰ These components formed a non-uniform, thin SEI. Nie et al. found that, in the presence of LiPF_6 in EC:EMC, the SEI was comprised of LEDC, LiF and LMC.³⁰ These

components formed a thicker SEI than without EC. Nie et al. observed the SEI on the edge of graphite particles in all cases and did not detect Li_2CO_3 as an SEI component.

In another experiment, Nie and Lucht studied the effect of various salts in EC on the formation of the SEI.³¹ Among the salts studied, LiPF_6 , LiBF_4 , LiTFSI , and lithium bis(fluorosulfonyl) imide (LiFSI) formed an SEI of LEDC, with low concentrations of Li_2CO_3 .³¹ These findings are inconsistent with the previous work by Nie et al. in which Li_2CO_3 was not detected.³⁰ Nie and Lucht explained that the detection peaks of Li_2CO_3 overlap with the detection peaks of LEDC, and that perhaps a low concentration of Li_2CO_3 existed on the negative electrode surface. As suggested by Edström et al.¹⁹, the presence of Li_2CO_3 may be due to the brief exposure of the electrode to ambient atmosphere, or any source of CO_2 . When the salts lithium bis(oxalato)borate (LiBOB) and lithium difluoro(oxalato)borate (LiDFOB) were used, lithium oxalate and oxalate-containing species dominated the SEI in addition to LEDC, and the SEI was more complex. Nie and Lucht found that, due to the strong association of BF_4^- to the Li cation, LiBF_4 and LiDFOB resulted in the highest LiF concentration.³¹ LiPF_6 , LiTFSI and LiFSI all had similar concentrations on LiF in the formed SEI.

The presence of polymers in the negative electrode SEI has been another topic of controversy. Nie et al.³⁰ and Nie and Lucht³¹ did not report the detection of any polymeric products in the SEI. However, Nie et al. only used NMR, FTIR, and XPS to analyze the SEI composition between the first cycle and the fifth cycle. Nie has suggested that polymeric species form in subsequent cycles, while the inorganic and semicarbonate species are reduced preferentially on the graphitic electrode.³² This agrees with the

proposal by Peled et al. that the order in which species are reduced on the graphitic electrode determines the location of the species in the SEI. This may account for the differences observed by researchers on different cell chemistries and different cycling conditions. Certain salt and solvents may result in an SEI that is more divided into organic and inorganic compounds, whereas other electrolytes may result in an SEI that contains organic and inorganic compounds throughout. Dedryvère et al. have shown evidence for polymer species in the negative electrode SEI.^{29,33,34} Dedryvère et al. studied the SEI layers in $\text{LiMn}_{1.6}\text{Ni}_{0.4}\text{O}_4/\text{Li}_4\text{Ti}_5\text{O}_{12}$ cells using XPS. They found several organic and inorganic compounds on the surface of the negative electrode.³⁵ After one charge, LiF made up 25% of the negative electrode SEI surface, which decreased to 10% after 118 cycles. After one charge, Li_2CO_3 and lithium alkyl carbonates were detected, which increased in concentration during cycling. Solvent degradation during cycling led to a large amount of organic species at the negative electrode. After 118 cycles the negative electrode surface was made up of approximately 40% organic species. Dedryvère et al. proposed that organic species formed at the positive electrode due to solvent decomposition at high voltage may diffuse through the electrolyte to the surface of the negative electrode during long-term cycling.³⁵

There does not seem to be one model that is correct for the structure of the negative electrode SEI. The cell chemistry, electrolyte used, cycling conditions and cycling temperature all play a role in the formation and growth of the SEI, so there may not be any sole model that can describe the negative electrode SEI. Further experiments to determine the composition of the SEI under various conditions and understand the mechanism of the SEI are important to develop the next generation of Li-ion batteries.

2.1.2 SEI AT THE POSITIVE ELECTRODE

The SEI at the positive electrode has received significantly less attention from researchers than the negative electrode SEI. However, high voltage positive electrode materials can help enable higher energy densities and further investigation of the positive electrode SEI is required. Electrolytes capable of avoiding positive electrode degradation and electrolyte oxidation are required in the presence of high voltage positive electrode materials.

Moshkovich et al. studied the anodic stability and oxidation potential of several salts and solvents on Au, Pt, and Al metal electrodes.³⁶ The solvents studied were DMC, DEC and EC. The salts studied were LiClO₄, LiAsF₆, LiPF₆, HQ-115, and LiC(SO₂CF₃)₃. The onset oxidation potentials for all solutions tested were below 4 V vs Li/Li⁺.³⁶ Despite these low oxidation potentials, Li-ion cells with a variety of positive electrode materials have been shown to cycle to potentials above 4 V with good performance.³⁷⁻³⁹ Moshkovich et al. suggested that practical positive electrode materials in Li-ion cells inhibit the reactions that occurred on the metal electrodes (Au, Pt, Al). This inhibition is most likely a result from the passivating film that forms on the positive electrode in Li-ion cells. The positive electrode SEI that forms on a practical positive electrode material most likely suppresses the catalytic nature of the electrode surface. Therefore, the stability and passivating nature of the positive electrode SEI is important for Li-ion cells to be able to cycle up to potentials above 4 V.

Moshkovich et al. found that, even up to 6 V, there was no mass accumulation on the electrode surface, suggesting that the oxidation products were formed in solution and did

not precipitate on the electrode surface.³⁶ They believed that the oxidation products were formed in a layer in the solution very close to the electrode surface. Using FTIR, Moshkovich et al. found that the oxidation products were from decomposition of the solvents and that the salts did not affect the products formed during oxidation.³⁶ Solvent decomposition dominated the oxidation processes and consisted of organic compounds with carbonyl groups. They also observed the presence of CO and CO₂. CO₂ observed on the positive electrode SEI may diffuse toward the negative electrode, resulting in the detection of lithium carbonate in the negative electrode SEI.

In 1985, Goodenough et al. suggested that a passivating film formed on the positive electrode.⁴⁰ Shortly thereafter, Guyomard and Tarascon supported this suggestion after studying the decomposition of electrolyte due to oxidation at a Mn spinel positive electrode.⁴¹ Guyomard and Tarascon suggested that the decomposed electrolyte formed a passivating film on the positive electrode that prevented further electrolyte oxidation.⁴¹ Aurbach et al. found that the layer that formed on the positive electrode did not entirely prevent further electrolyte oxidation and that this layer continued to grow during cycling and storage.⁴² This claim was supported by a measured increase in impedance during cycling, suggesting that the positive electrode SEI was not stable and continued to grow.

Positive electrodes made of a lithiated transition metal oxide have a native surface film mainly composed of lithium carbonate.^{1,43} Acidic electrolytes, particularly Li salts containing fluorine that react to produce LiF and HF, can degrade the surface film.⁴⁴ Electrolyte oxidation and precipitation of LiF on the surface of the positive electrode can

then occur. Broussely et al. suggested that reduction products at the negative electrode diffuse to the positive electrode and oxidize, resulting in SEI growth.⁴⁴

Although electrolytes based on LiPF_6 and carbonate solvents oxidize around 4.5 V in practical Li-ion cells due to the formation of a passivating layer at the positive electrode, transition metal ions from the positive electrode can catalyze electrolyte decomposition at lower potentials.^{39,45} Transition metal dissolution can lead to structural changes in the positive electrode material and result in capacity fade. For example, cells with a LiMn_2O_4 positive electrode exhibited a large capacity fade due to Mn dissolution, which was accelerated at higher temperatures.⁴⁶

Yamamoto et al. investigated the effect of different positive electrode materials on cycling performance and stability of the positive electrode/electrolyte interface.⁴⁷ They discovered that a 50 nm thin-film electrode of LiCoO_2 gradually deteriorated during cycling and exhibited a 40% decrease in discharge capacity after 20 cycles, compared to a 70 nm thin-film electrode of LiFePO_4 that exhibited only a slight decrease in capacity after 20 cycles.⁴⁷ The severe capacity fade demonstrated by the LiCoO_2 cell is surprising as LiCoO_2 cells have been shown to have stable cycling performance for several months.⁴⁴ However, the cells in the work by Yamamoto et al. had electrodes that were deposited using pulsed laser deposition and the electrolyte used was 1M LiClO_4 in EC:DEC. Zhang et al. studied the effect of 1M LiClO_4 PC on high temperature thin-film LiCoO_2 electrodes deposited using pulsed laser deposition on capacity fade.⁴⁸ Zhang et al. found that the cells exhibited severe capacity fade during cycling due to mechanical

failure, Co ion dissolution, and inhomogeneous lithiation.⁴⁸ This may explain the surprisingly large capacity fade observed by Yamamoto et al.

For further study, Yamamoto et al. immersed the LiCoO₂ and LiFePO₄ electrodes in an organic electrolyte. The LiCoO₂ electrode had an unstable surface after immersion due to the reduction of Co ions at the electrode/electrolyte interface which led to irreversible changes during subsequent cycling. The LiFePO₄ electrode had a stable surface after immersion as the Fe ions were unaffected by contact with the electrolyte and the Fe ions were not reduced. The change in electronic structure of the LiFePO₄/electrolyte interface was found to be highly reversible during subsequent cycling. In conclusion, Yamamoto et al. were able to show a correlation between the cycling performance and the stability of the surface structure at the positive electrode/electrolyte interface of cells containing a particular positive electrode material.⁴⁷

Similarly to the work of Yamamoto et al.⁴⁷, Yogi et al. studied the surface of LiCoO₂ positive electrodes in the presence of the additive LiBOB.⁴⁹ Yogi et al. soaked the positive electrode in electrolyte and analyzed the SEI on the positive electrode. Without LiBOB, the SEI film comprised mostly of Li₂CO₃ formed instantly after being soaked in electrolyte. This film decomposed during cycling and caused poor cycling performance as the Li₂CO₃ surface was removed from the positive electrode and was replaced with organic carbonyl compounds from the decomposition of solvents, which is in agreement with the findings of Moshkovich et al.³⁶ With LiBOB, the SEI film, comprised mostly of Li₂CO₃, did not decompose upon subsequent cycling, which led to improved cycling performance. LiBOB can therefore form a protective SEI film on the positive electrode

that prevents further electrolyte oxidation normally induced by cycling.⁴⁹ Cells without LiBOB exhibited only a 60% capacity retention after 20 cycles, whereas cells with LiBOB had a capacity retention over 90% after 20 cycles.⁴⁹ The surprisingly large capacity fade of the LiCoO₂ cells containing 1M LiClO₄ EC:DEC may again be explained by the work by Zhang et al.⁴⁸ The effectiveness of LiBOB to form a protective SEI layer was reported by Dalavi et al. in 2011 during studies on high voltage LiNi_{0.5}Mn_{1.5}O₄ spinel positive electrodes.⁵⁰ Dalavi et al. also reported a reduction in cell impedance when 0.25-1% LiBOB was added by weight to the electrolyte.⁵⁰

Coatings on the positive electrode have been studied to enable cell cyclability at high voltage as well as increase the electrolyte oxidation stability at high voltage and decrease transition metal dissolution.¹ The coating can act as an artificial interphase similar to the SEI. With both LiCoO₂ and NMC positive electrodes, AlF₃ was found to be an effective coating.⁵¹ Chen et al. found that cells with LiCoO₂ as a positive electrode could be cycled up to 4.54 V with better capacity retention and rate capability when the positive electrode was coated with AlF₃.⁵¹ The coating provides a barrier between the active material and the electrolyte, while being highly Li-ion conducting. Sun et al. found that cells with NMC as a positive electrode had reduced reactivity of the positive electrode when in contact with electrolyte and had increased stability when the positive electrode was coated with AlF₃.⁵² They also found that transition metal dissolution due to acidic electrolytes decreased when the AlF₃ coating was used.⁵²

2.2 ELECTROLYTE ADDITIVES

2.2.1 MOTIVATION

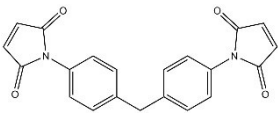
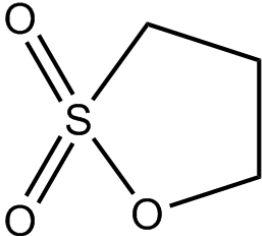
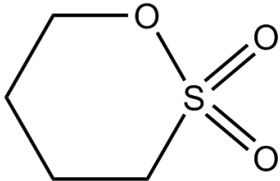
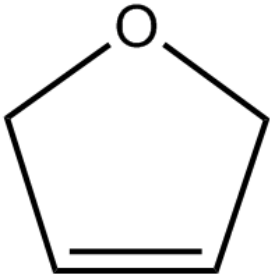
The components of the electrolyte play an important role in the formation and growth of both the positive and negative electrode SEI. Salts such as LiPF_6 and solvents such as EC and EMC demonstrate good performance in Li-ion cells, as described in Chapter 1, but they have drawbacks as well.^{1,3} The undesirable properties of electrolytes can be modified by using electrolyte additives. Electrolyte additives are components normally added at small concentrations to the electrolyte.

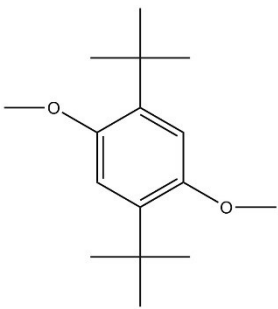
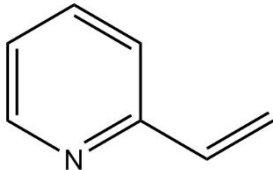
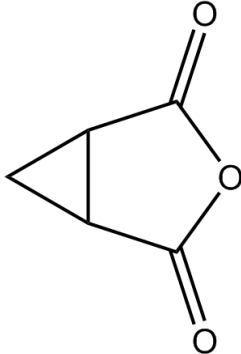
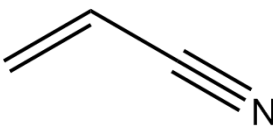
Electrolyte additives can be preferentially reduced or oxidized to greatly improve the formation and stability of the negative or positive electrode SEI, respectively. An improved SEI translates to improved lifetime of Li-ion cells. Aurbach et al. studied several additives and their effect on the positive and negative electrode SEI.^{53–55} Studies of the ability of additives to significantly improve the positive and negative electrode SEI have been an important topic of study in recent years.^{1,3,16,44} Electrolyte additives can extend the lifetime of cells⁵⁶, reduce capacity loss⁵⁷, and increase cell safety¹⁶. Additives can increase the cell operating temperature range by creating more stable reaction products and changing the viscosity of the electrolyte.² Additives can reduce the amount of gas produced during cycling and during storage as well as the impedance of the positive and negative electrode.^{5,57–59}

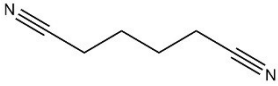
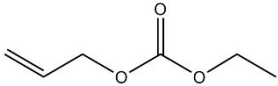
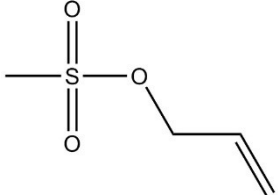
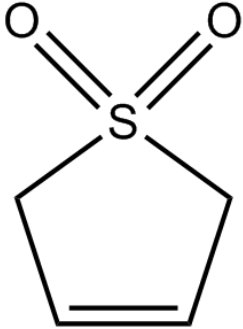
Vinylene carbonate (VC) is perhaps the most well-known additive for Li-ion batteries and has been shown to improve cycle and calendar life of Li-ion cells.⁴⁴ Sinha et al.⁶⁰

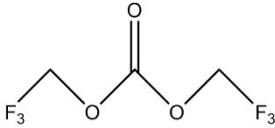
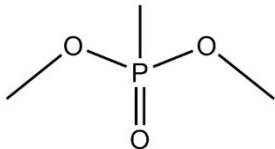
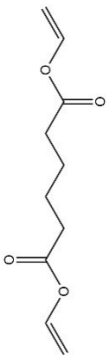
used storage studies to determine that VC is beneficial at the positive electrode by slowing the rate of electrolyte oxidation. Using high precision coulometry, Burns et al.⁶ determined that VC is beneficial at the positive electrode by reducing the rate of parasitic reactions. However, it has been shown that the performance of cells containing VC degrades at high temperatures due to electrolyte decomposition⁶¹ and at high voltages due to electrolyte oxidation.⁶² Sulfur-containing electrolyte additives have been studied in the hopes of overcoming the temperature sensitivity of VC.⁶³⁻⁶⁵ Prop-1-ene-1,3-sultone (PES) was found to have smaller irreversible capacity than VC-containing cells, and was suggested to be a stable SEI forming additive.⁶⁵ Table 2.1 lists a number of additives studied in the literature as well as comments about their function. Many of these additives have been studied in recent “monster comparisons” by Wang et al.^{38,66} The additives presented in this thesis have been highlighted in red in Table 2.1.

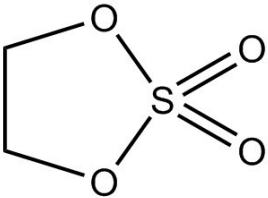
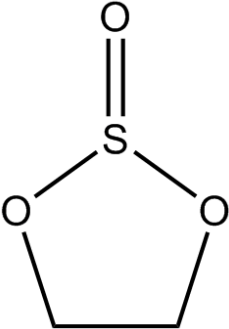
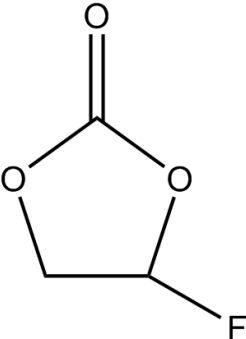
Table 2.1 Structure and function of additives for Li-ion cells.

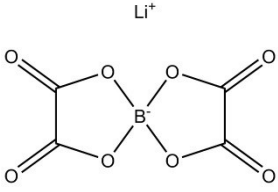
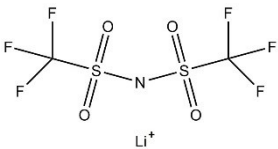
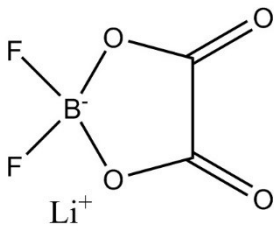
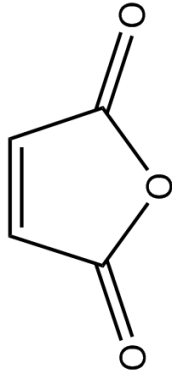
Additive Name	Structure	Notes About Function	Ref
1,1'-(methylenedi-4,1-phenylene)bismaleimide (BMI)		<ul style="list-style-type: none"> -functioned as a safety additive in 1M LiPF₆ EC:EMC:DMC 1:1:1 -rapidly solidified at 110°C and blocked off ion transport between the positive and negative electrode -did not diminish cycling performance compared to control 	67
1,3-propane sultone (PS)		<ul style="list-style-type: none"> -oxidatively stable to 4.8 V in 1M LiPF₆ EC:EMC 1:2 -reduced gas evolution -extended cycle life -formed fully stable SEI on the negative electrode during the first charge of the cell -preferentially reduced and slowed further reduction of solvents -improved discharge capacity after storage at -20°C and 80°C compared to without PS in PC:EC:EMC 1:1:3 	68,69
1,4-butane sultone (BS)		<ul style="list-style-type: none"> -formed a stable SEI on the negative electrode -significantly improved discharge capacity and cycling stability at room temperature compared to control 	70
2,5-dihydrofuran (DHF)		<ul style="list-style-type: none"> -decreased electrolyte oxidation at the positive electrode surface -formed a stable SEI on the positive electrode -improved the capacity retention of Li_{1.17}Mn_{0.58}Ni_{0.25}O₂ half cells cycled to 4.9 V -cells showed higher negative electrode stability 	39,45

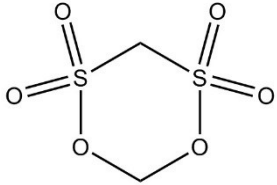
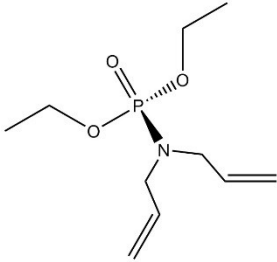
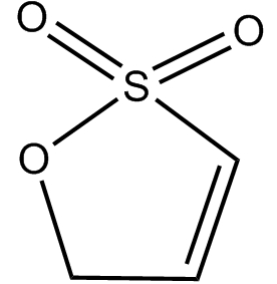
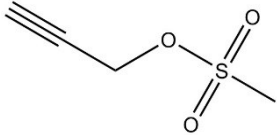
<p>2,5-ditertbutyl-1,4-dimethoxybenzene</p>		<p>-functions as an overcharge protection additive -demonstrated excellent redox shuttle behaviour at 3.85-3.92 V</p>	<p>71,72</p>
<p>2-vinyl pyridine (VP)</p>		<p>-suppressed degradation of negative electrode in LiMn₂O₄/graphite cells by forming a stable SEI -improved CE by preventing Mn dissolution -reduced cell impedance compared to control</p>	<p>3,73</p>
<p>3-oxabicyclo[3.1.0]hexane-2,4-dione (OHD)</p>		<p>-improved capacity retention while cycling at room temperature and 55°C with 0.1% and 0.2% OHD in EC:EMC 3:7 -formed a thin and stable SEI -reduced impedance after formation in MCMB/NMC111 cells</p>	<p>74</p>
<p>Acrylic acid nitrile (AAN)</p>		<p>-suppressed co-intercalation of PC in graphitic negative electrodes -oxidatively stable to 4 V in 1M LiClO₄ PC -formed a protective SEI on the positive electrode</p>	<p>3,75</p>

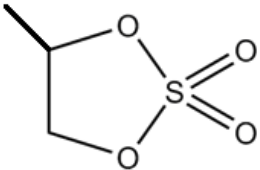
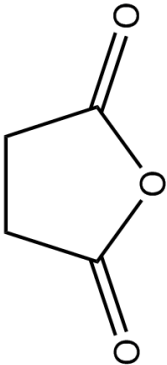
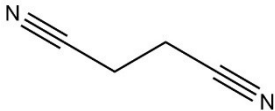
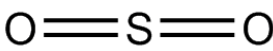
Adiponitrile		<ul style="list-style-type: none"> -improved over-discharge inhibition cycle characteristics -has a high oxidation potential and is stable at high voltage -can reduce the corrosion of metal parts of a battery 	76,77
Allyl ethyl carbonate (AEC)		<ul style="list-style-type: none"> -avoided exfoliation by suppressing co-intercalation of PC -formed a stable SEI on the graphitic negative electrode in 1M LiPF₆ PC:DEC 3:2 	3,78
Allyl methane sulfonate (AMS)		<ul style="list-style-type: none"> -has a higher reduction potential than VC -had a smaller impedance than both VC alone and 1M LiPF₆ EC:EMC 3:7 -mostly decomposed on negative electrode SEI, but had non-uniform morphology which led to poor discharge capacity and cell performance 	79,80
Butadiene sulfone (BSf)		<ul style="list-style-type: none"> -reduced impedance after cycling compared to control and 2% VC alone -improved CE and charge slippage compared to control, but was not superior to 2% VC alone 	66

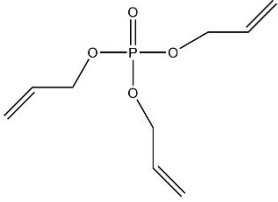
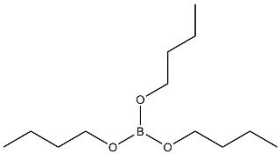
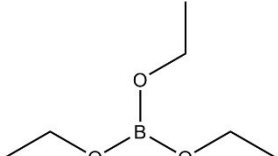
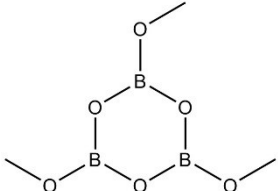
<p>Di-2,2,2-trifluoroethyl carbonate (TFEC)</p>		<ul style="list-style-type: none"> -enhanced oxidative stability of electrolyte -decreased flammability of electrolyte -formed protective and stable SEI 	<p>81-84</p>
<p>Dimethyl methyl phosphonate (DMMP)</p>		<ul style="list-style-type: none"> -functioned as a flame retardant additive -demonstrated high thermal stability -improved the capacity retention with 10% DMMP compared to 0% DMMP in 1M LiPF₆ EC:DEC 	<p>3,85</p>
<p>Dithiocarbonic anhydride (CS₂)</p>	<p>S=C=S</p>	<ul style="list-style-type: none"> -functioned as a film-forming additive for the SEI on the negative electrode -performed better than SO₂ in DEC based electrolytes 	<p>86</p>
<p>Divinyl adipate (ADV)</p>		<ul style="list-style-type: none"> -showed similar performance to vinyl acetate -initially demonstrated good cycling performance but the value of capacity was unstable, suggesting Li ions could not properly intercalate through the SEI 	<p>3,87</p>

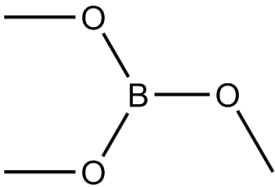
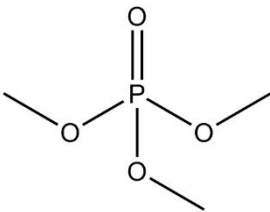
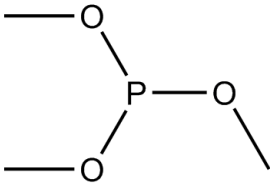
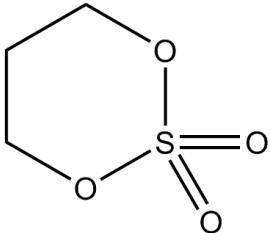
<p>Ethylene sulfate (DTD)</p>		<p>-functioned as a film forming additive for the SEI on the negative electrode -preferentially reduced and slowed further solvent reduction -had a capacity retention of 105.3% (1% DTD) and 96% (3% DTD) after 50 cycles, compared to 85.3% (0% DTD) in 1M LiPF₆ EC:EMC:DMC 1:1:1 -reduced the voltage drop during 40°C storage but produced a large volume of gas during formation -had a high CE and low charge slippage during cycling, but was not superior to 2% VC alone -gas evolution is reduced and the CE is improved when combined with VC</p>	<p>88,89</p>
<p>Ethylene Sulfite (ES)</p>		<p>-avoided exfoliation caused by PC solvent -formed protective SEI on the negative electrode in cells with a LiMn₂O₄ cathode</p>	<p>90,91</p>
<p>Fluoroethylene carbonate (FEC)</p>		<p>-increased capacity retention by 20% in 1M LiPF₆ EC:DEC:PC at 60°C in LiMn₂O₄/graphite cells -formed a thin, stable SEI layer on graphitic negative electrodes -can form a VC molecule with loss of an HF molecule -particularly beneficial in cells with Si negative electrodes</p>	<p>3,92</p>

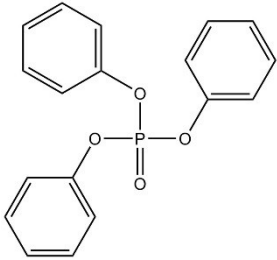
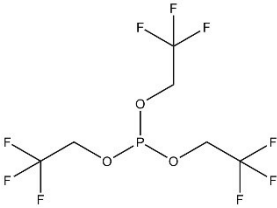
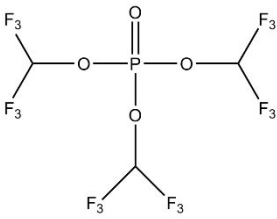
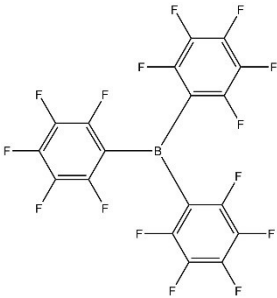
<p>Lithium bis(oxalate) borate (LiBOB)</p>		<p>-has a high reduction potential and formed a stable SEI on the negative electrode with LiBF₄ PC:EC:EMC 1:1:3 electrolyte -decreased the impedance and increased capacity retention and CE in cells cycled to 4.9 V -formed a thin SEI on the positive electrode and stabilized lithiated graphite over a wide temperature range with 1.1 M LiPF₆ EC:DEC 1:2 electrolyte -inhibited electrolyte oxidation</p>	<p>50,93 ,94</p>
<p>Lithium bis-trifluoromethane sulfonimide (HQ-115)</p>		<p>-reduced gas generation, particularly in combination with VC -reduced impedance at both positive and negative electrodes</p>	<p>6,59</p>
<p>Lithium difluoro(oxalate) borate (LiDFOB)</p>		<p>-formed stable SEI on the positive electrode -films formed by LiDFOB are more stable and have lower impedance than those with LiBOB -provided stable cycling performance with high-voltage LiCoPO₄ positive electrode</p>	<p>95,96</p>
<p>Maleic anhydride (MA)</p>		<p>-improved capacity retention compared to control electrolyte -avoided PC degradation with graphitic anodes and improved Li intercalation in graphite -had higher CE and longer cycle life with GBL based electrolytes -has a high reduction potential and formed a protective SEI on the negative electrode</p>	<p>74,97</p>

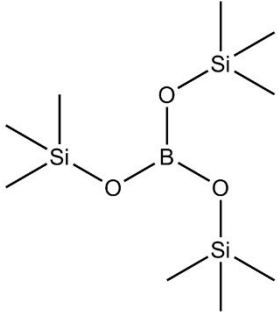
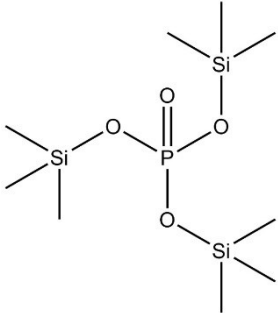
<p>Methylene methane disulfonate (MMDS)</p>		<p>- preferentially oxidized and reduced electrolyte oxidation at the positive electrode -reduced gas formation -decreased impedance and reduced the rate of parasitic reactions compared to cells without MMDS in LCO/graphite cells</p>	<p>63,98</p>
<p>N, N-diallyl - diethoxy phosphoramidate (DEDAPA)</p>		<p>-improved thermal stability of the electrolyte -used to control the properties of the SEI -functions as a fire retardant additive</p>	<p>99 100</p>
<p>Prop-1-ene-1,3-sultone (PES)</p>		<p>-smaller irreversible capacity than VC-containing cells -functions as a stable SEI forming additive -improved CE -reduced charge endpoint capacity slippage, self-discharge rates and gas evolution during storage -increased negative electrode impedance and decreased positive electrode impedance -virtually eliminated all gas production during storage at 4.2 V and 60°C (VC does not)</p>	<p>65 101</p>
<p>Propargyl methane sulfonate (PMS)</p>		<p>-demonstrated higher discharge capacity than VC alone which increased further by adding VC -produced less gas during formation than VC alone -preferentially reduced on negative electrode -improved cyclability even in PC based electrolyte</p>	<p>79,80 ,102</p>

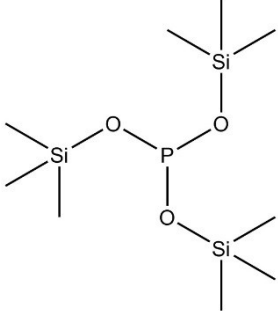
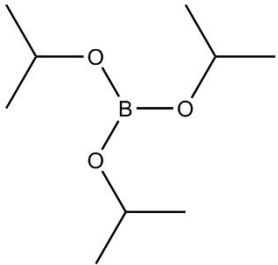
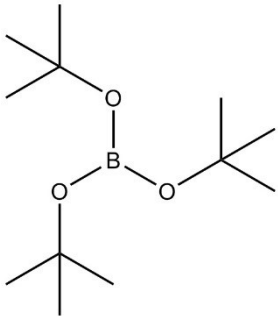
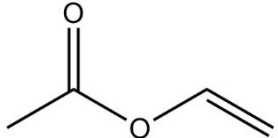
<p>Propylene sulfate (PLS)</p>		<p>-although studied due to its similar structure to TMS and DTD, PLS was found to be less useful than TMS and DTD -both PLS alone and PLS with VC demonstrated worse cycling performance compared to VC alone</p>	<p>89</p>
<p>Succinic anhydride (SA)</p>		<p>-reduced gas evolution -extended cycle life and improved discharge capacity after storage at -20°C and 80°C compared to without SA -formed a stable SEI at the negative electrode during the first charge of the cell -oxidatively stable to 4.8 V and prevented LiPF₆ decomposition</p>	<p>68</p>
<p>Succinonitrile (SN)</p>		<p>-can protect Cu current collector against corrosion -reduced gas produced at high temperature and improved thermal stability of LCO/graphite cells with EC based electrolytes -reduced parasitic reactions at the positive electrode</p>	<p>76,77 ,103</p>
<p>Sulfur dioxide (SO₂)</p>		<p>-formed fully stable passive SEI on the graphite electrode -preferentially reduced to inhibit electrolyte degradation in 1M LiPF₆ and 1M LiAsF₆</p>	<p>104</p>

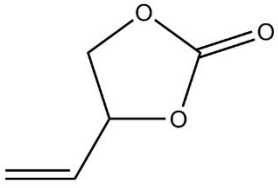
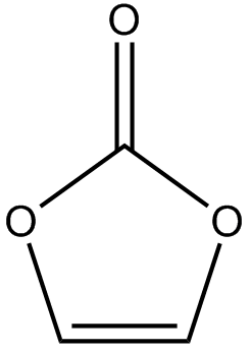
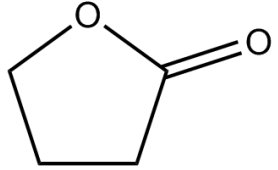
<p>Triallyl phosphate (TAP)</p>		<p>-found in “high voltage electrolyte” made by Capchem -suspected to reduce electrolyte oxidation and form a stable SEI at the positive electrode surface</p>	<p>105</p>
<p>Tributyl borate (TBB)</p>		<p>-demonstrated lower CE and higher charge slippage than control cells -even when combined with VC, the CE was lower than that of control cells -TBB is a poor performing additive</p>	<p>38 106</p>
<p>Triethyl borate (TEB)</p>		<p>-demonstrated lower CE and higher charge slippage than control cells -even when combined with VC, the CE was lower than that of control cells -TEB is a poor performing additive</p>	<p>38 106</p>
<p>Trimethoxy boroxine (TMOBX)</p>		<p>-reduced impedance and improved CE when less than 1% is added to 1M LiPF₆ EC:EMC 3:7 -had negative effects on impedance and cycling performance when more than 1.5% was added -used to control the formation of the SEI at the positive electrode -improved charge slippage and CE when used with VC</p>	<p>5,6, 59, 107</p>

<p>Trimethyl borate (TMB)</p>		<p>-demonstrated lower CE and higher charge slippage than control cells -even when combined with VC, the CE was lower than that of control cells -TMB is a poor performing additive</p>	<p>38, 106</p>
<p>Trimethyl phosphate (TMP)</p>		<p>-functions as a flame retardant additive -increased the thermal stability, but slightly degraded the electrochemical performance of electrolyte in LiNi_{0.8}Co_{0.2}O₂/Li cells</p>	<p>108, 109</p>
<p>Trimethyl phosphite (TMPi)</p>		<p>-functions as a flame retardant additive -increased the thermal stability and enhanced the electrochemical performance of electrolyte in LiNi_{0.8}Co_{0.2}O₂/Li cells -more stable than TMP</p>	<p>108, 109</p>
<p>Trimethylene sulfate (TMS)</p>		<p>-decreased cell impedance compared to control -improved CE and reduced the voltage drop during storage, but produced a large amount of gas in 1M LiPF₆ EC:EMC 3:7 -when combined with VC, no gas was produced, CE was improved, and impedance was reduced</p>	<p>89</p>

<p>Triphenyl phosphate (TPP)</p>		<p>-formed a stable SEI on the negative electrode but may impede ion transport -functions as a flame retardant additive that does not diminish capacity retention in NCA and NMC cells -had large impedances at both electrodes</p>	<p>108, 110, 111</p>
<p>Tris(2,2,2-trifluoroethyl) phosphite (TTFP)</p>		<p>-formed a stable SEI on negative electrode and thermally stabilized electrolyte -electrolyte became nonflammable with 15% TTFP -in PC:EC:EMC electrolyte, PC degradation was avoided and CE was improved</p>	<p>112, 113</p>
<p>Tris(hexafluoro-isopropyl) phosphate (HFIP)</p>		<p>-formed a stable, uniform, protective SEI on high voltage (5 V) positive electrode and on graphitic negative electrode -had significantly better capacity retention than control over 200 cycles up to 5 V in 1M LiPF₆ EC:EMC 3:7 -demonstrated small charge transfer resistance and improved cycle and rate performance in NMC/graphite cells</p>	<p>99, 114, 115</p>
<p>Tris(pentafluorophenyl) borane (TPFPB)</p>		<p>-improved CE and capacity retention in cells with LiPF₆ and LiBF₄ due to dissolution of LiF from the SEI -thermally stabilized LiPF₆ electrolyte</p>	<p>¹</p>

<p>Tris(trimethylsilyl) borate (TMSB)</p>		<p>-demonstrated lower CE and higher charge slippage than control cells and even when combined with VC, the CE was lower than that of control cells -TMSB is a poor performing additive in LCO cells -in LiFePO₄ cells, TMSB had higher capacity retention and improved cycling performance than cells without, and reduced impedance due to the thermal stability of TMSB</p>	<p>38, 106, 116</p>
<p>Tris(-trimethylsilyl)-phosphate (TTSP)</p>		<p>-reduced impedance compared to control and reduce impedance with VC compared to VC alone -demonstrated superior performance when combined with PES or VC and a sulfur containing additive -decreased the rate of parasitic reactions, reduced the charge end point capacity slippage and the impedance of NMC/graphite cells when in the presence of VC -discharge capacity increased by 10% when cycled to 4.5 V compared to control -had 91% capacity retention -effectively forms a stable SEI at the positive electrode</p>	<p>108, 117</p>

<p>Tris(-trimethylsilyl)-phosphite (TTSPi)</p>		<p>-reduced impedance and improved CE compared to control -improved CE and charge slippage with VC compared to VC alone -demonstrated superior performance when combined with PES or VC and a sulfur containing additive -demonstrated superior performance alone and with VC compared to TTSP alone</p>	<p>108</p>
<p>Trisopropyl borate (TiPB)</p>		<p>-demonstrated lower CE and higher charge slippage than control cells -even when combined with VC, the CE was lower than that of control cells -TiPB is a poor performing additive</p>	<p>38, 106</p>
<p>Tri-tert-butyl borate (TtBB)</p>		<p>-demonstrated lower CE and higher charge slippage than control cells -even when combined with VC, the CE was lower than that of control cells -TtBB is a poor performing additive</p>	<p>38, 106</p>
<p>Vinyl acetate (VA)</p>		<p>-significantly improved cell cycling performance and reduced impedance in cells with PC based electrolytes -formed a thin SEI in PC based electrolyte with a morphology similar to that formed in EC-based electrolytes</p>	<p>3,87</p>

<p>Vinyl ethylene carbonate (VEC)</p>		<ul style="list-style-type: none"> -improved capacity retention from 69% (0% VEC) to 85% (2% VEC) at 50°C, but showed only marginal improvements at room temperature -demonstrated better CE when combined with LiBOB compared to VEC alone and LiBOB alone -demonstrated better CE when combined with LiBOB and VC compared to VC alone 	<p>38, 118</p>
<p>Vinylene carbonate (VC)</p>		<ul style="list-style-type: none"> -improved cycle and calendar life of NMC and LCO/graphite cells. -beneficial at the positive electrode by slowing the rate of electrolyte oxidation -beneficial at the positive electrode by reducing the rate of parasitic reactions 	<p>6,44, 60</p>
<p>γ-butyrolactone</p>		<ul style="list-style-type: none"> -decreased electrolyte oxidation at the positive electrode surface -formed a stable SEI on the positive electrode -improved the capacity retention of $\text{Li}_{1.17}\text{Mn}_{0.58}\text{Ni}_{0.25}\text{O}_2$ half cells cycled to 4.9 V -cells showed higher negative electrode stability 	<p>45</p>

Recently, Xia et al.¹⁰¹ studied the effects of VC and/or PES as electrolyte additives in $\text{Li}[\text{Ni}_{1/3}\text{Mn}_{1/3}\text{Co}_{1/3}]\text{O}_2$ (NMC111)/graphite pouch cells up to concentrations as large as 3% by weight. They found that both PES and VC improved coulombic efficiency, reduced charge endpoint capacity slippage, decreased self-discharge rates, decreased gas evolution during storage, increased negative electrode charge transfer impedance and

decreased positive electrode charge transfer resistance. At a concentration of 2%, VC and PES impart very similar attributes to NMC111/graphite pouch cells **except** that PES virtually eliminates all gas production during storage at 4.2 V and 60°C while VC does not. This is the main advantage of PES over VC in the range of potentials below 4.2 V.

Burns et al. found that the cycle life of 18650-sized cells was extended by 20 times in cells containing additives compared to those without any additives.⁵⁶ Burns et al. also found that cells containing a combination of up to five additives had superior performance and extended the lifetime by a factor of five when compared to electrolytes containing just a single additive.⁵⁶

Ma et al. studied the effect of additive combinations in Li-ion pouch cells.³⁷ Ma et al. studied cells containing a combination of VC, a sulfur-containing additive, and tris(-trimethyl-silyl)-phosphate (TTSP) and/or tris(-trimethyl-silyl)-phosphite (TTSPi).³⁷ Ma et al. found that the ternary and quaternary additive mixtures improved the cycling performance and safety of the NMC111/graphite cells while reducing the impedance and parasitic reactions at the positive electrode when compared to VC alone in the electrolyte.³⁷

It is unlikely that any single additive will be able to overcome all undesirable properties of electrolytes. Studies of the combination of multiple additives and their effect on Li-ion batteries are essential.^{38,66} By understanding how electrolyte additives work, singly and in combination, the intelligent selection of additives for specific applications and operating conditions as well as the engineering of new additives may be possible. The effect of an

additive or combination of additives on the performance of a cell must be determined in a timely fashion. This can be done through careful experiments, which are discussed in Chapter 3.

2.2.2 ADDITIVES IN THIS THESIS

The effects of two additives on the performance of Li-ion cells are discussed in detail in this thesis. Chapter 4 discusses experiments involving prop-1-ene-1,3-sultone (PES). As an extension of the work of Xia et al.¹⁰¹, studies of a complete range of PES contents from 0.5% to 6.0% in NMC111/graphite pouch cells are discussed in Section 4.1. The superiority of PES over VC was investigated. In addition, the combination of PES with the additive lithium bis(trifluoromethylsulfonyl)imide ($\text{LiN}[\text{CF}_3\text{SO}_2]_2$ or Li-TFSI), called HQ-115, known to reduce gassing in combination with VC, is explored in Section 4.2.

Similarly to the work of Ma et al.³⁷ on ternary and quaternary electrolyte additive mixtures, the study of PES, a sulfur containing additive, and TTSP or TTSPi is described in Section 4.3. The sulfur containing additives studied were methylene methane disulfonate (MMDS) and ethylene sulfite (ES). MMDS and ES have been shown to improve the performance of Li-ion cells at high voltage due to the formation of a stable SEI.³⁹ MMDS has also been shown to reduce electrolyte oxidation at the positive electrode, reduce gas formation, decrease impedance and thus reduce the rate of parasitic reactions compared to cells without MMDS.⁶³

Studies of the additive triallyl phosphate (TAP) are discussed in Chapter 5. This additive has been found by Remi Petibon using gas chromatography-mass spectrometry (GC/MS)

in two “high voltage electrolytes” produced by Capchem (Shenzhen, China), a reputable electrolyte manufacturing company. The presence of fluoroethylene carbonate (FEC) was found by Remi Petibon using a GC/MS in one of the Capchem electrolytes. Investigation of the performance of the Capchem electrolytes and a complete range of TAP contents from 0.5% to 6.0% in Li[Ni_{0.4}Mn_{0.4}Co_{0.2}]O₂ (NMC442)/graphite pouch cells is discussed in Chapter 5. High voltage studies of Li-ion cells containing these additives in electrolyte are compared to cells with PES and VC-containing electrolytes, and are presented in Chapter 5 as well. The chemical structures of the additives presented in this thesis are shown in Figure 2.1, and these additives have been highlighted in red in Table 2.1 as well. The chemical structure of HQ-115, which can be used as a salt or an additive, was shown in Figure 1.2.

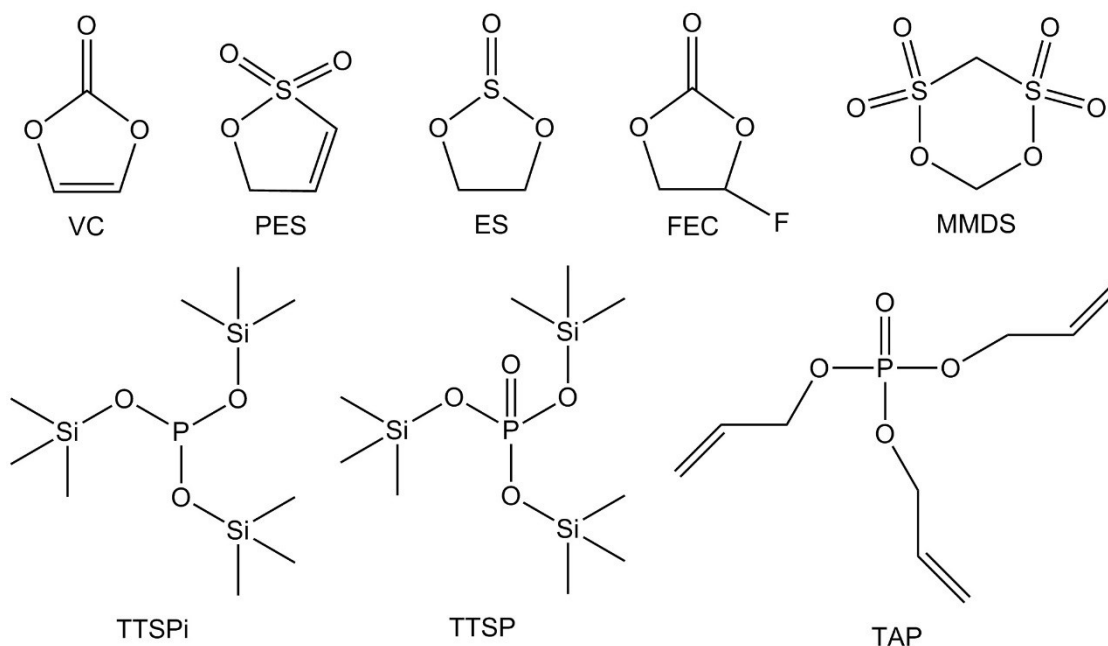


Figure 2.2 The chemical structures of the electrolyte additives used in this thesis.

CHAPTER 3. EXPERIMENTAL METHODS

3.1 POUCH CELLS, CELL CHEMISTRIES AND ELECTROLYTE SYSTEMS IN THIS THESIS

Lithium-ion cells can come in cylindrical, prismatic, or pouch cell casings. Cylindrical 18650-sized cells are used in Tesla vehicles and pouch cells are typically used in cell phones, such as the Samsung Galaxy S series phones. The experiments described in this thesis used wound pouch cells. Dry machine-made wound pouch cells were obtained from reputable Li-ion battery manufacturer, Whenergy (Shandong, China). Pouch cells were manufactured and vacuum sealed in a dry room before shipping to Dalhousie University. Pouch cells were sent dry (no electrolyte added). The cells could then be filled with any electrolyte and electrolyte additives. Being machine-made, the pouch cells were highly repeatable, as shown through several experiments. Any differences between cells during experiments were attributed solely to the electrolyte in the cell.

Figure 3.1 shows a photograph of a dry NMC111/graphite pouch cell as received from Whenergy (Shandong, China). The labelled jelly roll contains the wound electrodes and separators. The vacuum seals are indicated as well as the positive and negative electrode tabs. Please note there is also a vacuum seal at the tab edge.

The work presented in this thesis involved experiments using machine made 220 mAh $\text{Li}[\text{Ni}_{1/3}\text{Mn}_{1/3}\text{Co}_{1/3}]\text{O}_2$ (NMC111)/graphite wound pouch cells balanced for 4.4 V operation and machine made 240 mAh $\text{Li}[\text{Ni}_{0.4}\text{Mn}_{0.4}\text{Co}_{0.2}]\text{O}_2$ (NMC442)/graphite wound pouch cells balanced for 4.7 V operation. The control electrolyte used for all experiments

was 1M LiPF₆ in EC:EMC 3:7 by weight. As explained in Chapter 1, LiPF₆, EC, and EMC have properties which lead to good cycling performance. Both types of pouch cells required 0.9 grams of electrolyte.

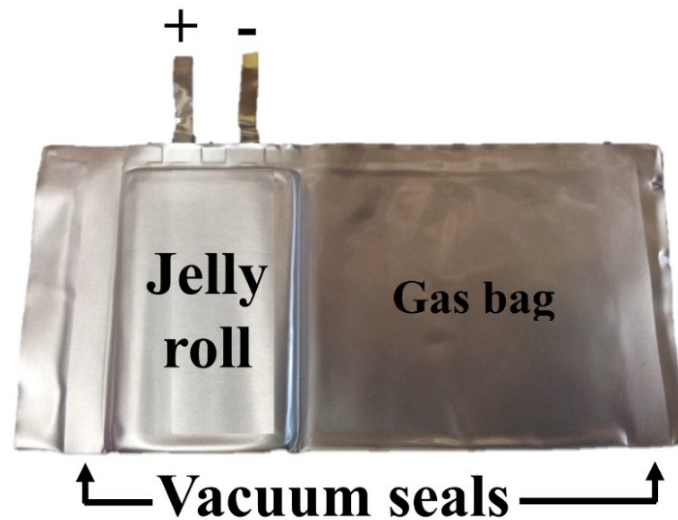


Figure 3.1 Photograph of an NMC111/graphite wound pouch cell from Whenergy.

As the cobalt content in NMC decreases, the thermal stability increases and the cost decreases. However, the rate capability of NMC also decreases with decreasing Co content.¹³ Therefore, NMC111 has higher energy density and better rate capability while NMC442 has higher thermal stability and lower raw material costs.

3.2 CYCLING EXPERIMENTS

Cycling experiments, including short-term high precision tests and long-term tests, are essential to probe electrolyte additives and determine if an additive is beneficial in a certain cell chemistry. Broussely et al. have done several impressive tests of the effect of

cycling and rest on the aging mechanisms of Li-ion cells, some of which spanned more than four years.⁴⁴ Fathi et al. performed tests on cells, all with the same cell chemistry, that had aged up to 12 years to learn about aging mechanisms.¹¹⁹ While these long-term experiments are incredibly valuable, rapid and accurate measurements of the effects of electrolyte additives on cell performance are also necessary. In order to remain relevant in the field and have a positive impact on society, beneficial additives need to be distinguished from non-beneficial additives in a timely fashion. Through careful measurements of the charge capacity and discharge capacity of a cell, it is possible to determine the effect of an additive on cell cycling performance in experiments that can last less than a month.

Due to parasitic reactions, the amount of charge apparently stored in the cell during charge is greater than that actually delivered during discharge. The ratio of the discharge capacity of the cell, Q_d , to the previous charge capacity, Q_c , is the coulombic efficiency (CE). If this ratio is exactly 1.000... the Li-ion cell should last forever. Accurately measured values of the CE can be used to compare the effect of different electrolyte additives on the performance of machine-made Li-ion cells. Using the CE, the lifetime of cells can be ranked and cells with higher performance can be determined.

For a meaningful comparison, the CE must be measured to at least $\pm 0.01\%$. Dalhousie University has two built-in-house ultra high precision chargers (UHPC).¹⁰⁷ These chargers have an accuracy of 0.003% and a precision of 0.001%, which is more accurate than commercially available chargers and thus is an important asset for academic researchers.¹⁰⁷

The validity of CE measurements made using the high precision charger to predict the lifetime of cells was shown by Burns et al.⁵⁶ Burns et al. measured the CE of cells containing up to five additives in combination during 16 low-rate cycles and compared the values to the discharge capacity of the same cells during long-term cycling at high rate.⁵⁶ Burns et al. found that the CE measurements clearly distinguished the cells containing different additives and were generally able to correctly rank the cells with longer lifetime.⁵⁶

In addition to measuring the coulombic efficiency, measurements of the discharge capacity and the charge end point capacity as a function of cycle number using the UHPC can be used to compare electrolyte additives. The discharge capacity of a cell typically decreases as a function of cycle number due to parasitic reactions that can consume electrolyte and can render lithium electrochemically inactive. Discharge capacity fade is an indicator of a decrease in the active supply of lithium and is useful for learning about the parasitic processes and the effectiveness of the SEI at the negative electrode.

Figure 3.2 shows a typical voltage-capacity curve for an NMC111/graphite pouch cell for 14 cycles. The inset of Figure 3.2 highlights the capacity shift at the top of charge as the cycle number increases. This shift in capacity is called the charge endpoint capacity slippage and can be measured using the UHPC. The charge endpoint capacity can be plotted versus cycle number, and the slope is the charge endpoint capacity slippage. Charge endpoint capacity slippage is an indicator of electrolyte oxidation and is a useful measurement for learning about the parasitic process and the effectiveness of the SEI at the positive electrode.¹²⁰

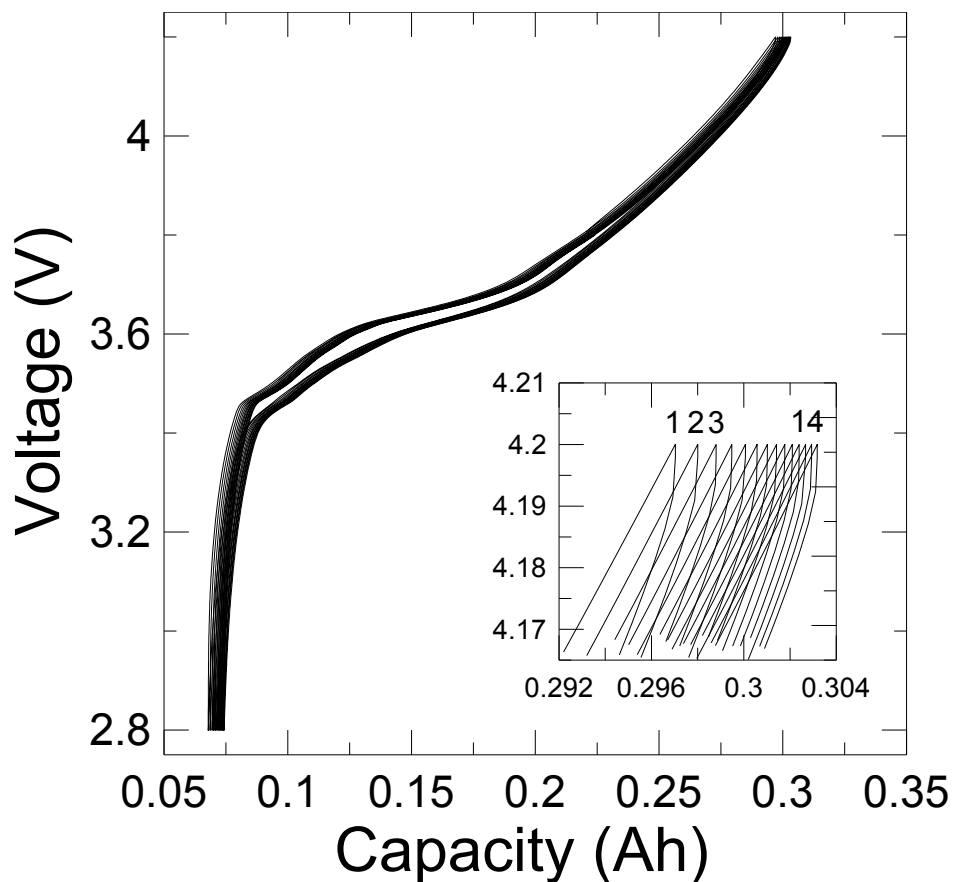


Figure 3.2 A voltage-capacity curve for an NMC111/graphite pouch cell. The inset is a close up indicating the shift in capacity to higher values as the cycle number increases.

3.3 STORAGE EXPERIMENTS

Storage experiments are useful to learn about aging mechanisms and parasitic reactions that occur in Li-ion cells during rest. Storage experiments on full cells are also very useful for learning about the reactions that happen at the positive electrode, including electrolyte oxidation, and can be helpful in understanding the positive electrode SEI.

Figure 3.3 shows a representative voltage-capacity curve for an NMC111 ($\text{Li}_x[\text{Ni}_{1/3}\text{Mn}_{1/3}\text{Co}_{1/3}]\text{O}_2$) positive electrode (the solid line) and a graphite (Li_xC_6) negative

electrode (the dashed line). The voltage of both electrodes is presented as a function of the percentage of available lithium. The difference between the two curves is the full Li-ion cell voltage. During storage at a full state of charge, parasitic reactions and electrolyte oxidation occur which can result in a decrease in the monitored open-circuit voltage. Due to the sloped voltage-capacity curve of the positive electrode and the flat voltage-capacity curve of the negative electrode when the cell is at a full state of charge, the voltage drop during the storage period is indicative of the parasitic processes occurring at the positive electrode. Processes that remove Li from the graphitic negative electrode will not contribute significantly to the drop in open-circuit voltage during storage because the voltage-capacity curve for the graphitic negative electrode is nearly flat during a full lithiation.

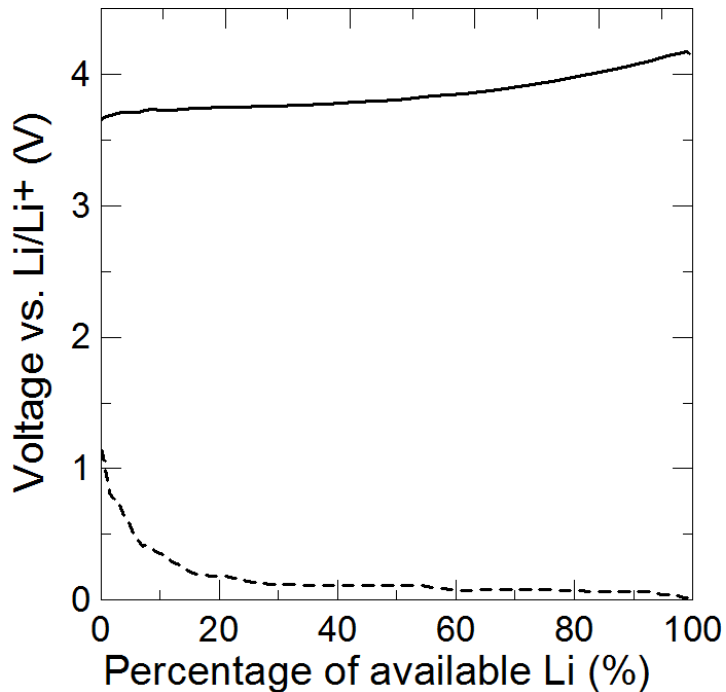


Figure 3.3 Representative voltage-capacity curve for an NMC111 electrode (solid line) and for a graphitic electrode (dashed line).

Figure 3.4 shows a schematic of a typical storage experiment. After the SEI formation cycle, the pouch cells undergo a “precycle” of 1.5 cycles at low rate (C/20). The rate of charge of a cell (C-rate) indicates the current applied to a cell during cycling. A C-rate of 1C means that a full charge takes approximately 1 hour. For a 220 mAh cell, a C-rate of C/20 means that a full charge will take 20 hours, and that 11 mA will be applied to the cell. Once the cells are cycled so they are at a full state of charge, they are then left at open-circuit at a constant temperature for a storage period. The storage period is typically 500 hours at either 40°C or 60°C. Following the storage period, in which the open-circuit voltage is monitored every 6 hours, the cells undergo a “postcycle” in which the cells are cycled 1.5 times at low rate. The discharge capacity before storage and after storage can be analyzed to measure the total capacity loss of the full cell during storage. D_0 represents the discharge capacity immediately before storage. D_1 represents the discharge capacity immediately after storage. D_2 represents the discharge capacity following a full charge after storage.

Figure 3.5 shows a voltage versus normalized capacity curve for an NMC111/graphite cell filled with control electrolyte. Typically, the discharge capacities should rank as $D_0 > D_2 > D_1$, as shown in Figure 3.5. The total capacity loss in the cell during storage is given by the difference between D_0 and D_1 . The difference between D_0 and D_2 is the irreversible capacity loss and the difference between D_2 and D_1 is the reversible capacity loss. By comparing both the change in open-circuit voltage during storage and the irreversible capacity loss of cells containing different additives, the most beneficial additives can be determined.

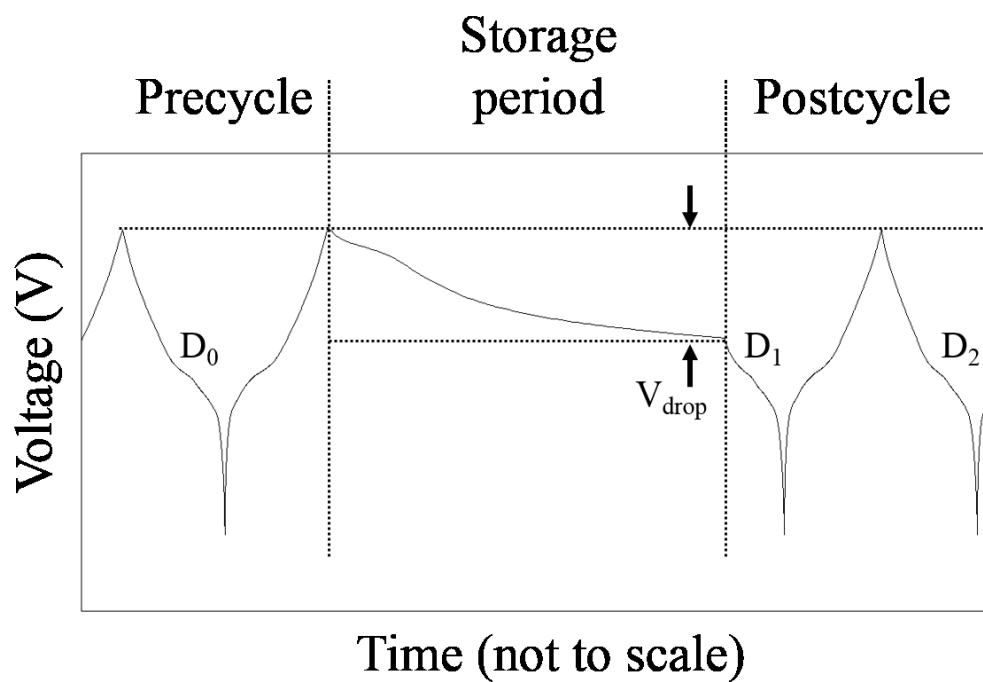


Figure 3.4 Schematic of the cell voltage as a function of time during a typical storage experiment. The time axis is not to scale. Adapted from Sinha et al.⁶⁰

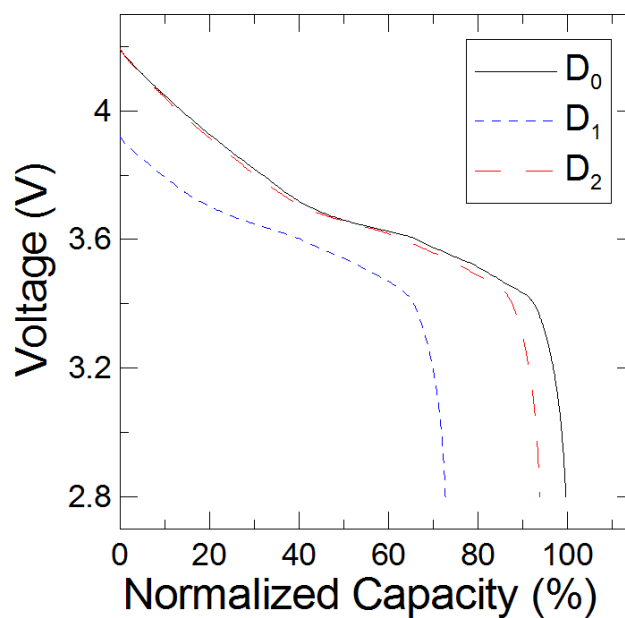


Figure 3.5 A voltage-capacity curve of an NMC111/graphite cell filled with control electrolyte for the discharge capacities before and after a 500 hours storage period at 50°C.

Sinha et al. described the design and operation of an automatic storage system, which they used to study the effect of the electrolyte additives HQ-115, VC, and TMOBX on the storage performance of LiCoO₂/graphite wound prismatic cells at 40°C and 60°C.⁶⁰ A similar automatic storage system was used for the experiments described in this thesis.

3.4 GAS EVOLUTION

During formation of the positive and negative electrode SEIs and during cycling and storage experiments, gas can be produced inside of Li-ion cells. Gas production can lead to battery safety issues, manufacturing difficulties, loss of electrical contact and change in cell volume. Preventing or reducing gas evolution is therefore important. Accurate measurements of the gas produced inside a cell are necessary to determine the effect of electrolyte additives on gas evolution. In-situ and ex-situ measurements of gas evolution employing Archimedes principle are possible for pouch cells. By suspending pouch cells from a balance and weighing the pouch cells in nanopure water with $\rho = 0.998 \text{ g/mL}$ (20°C), the change in mass, Δm , is a direct measure of the volume, Δv , of gas produced during formation, storage, or cycling as described by $\Delta v = \Delta m/\rho$. This procedure is discussed in depth by Aiken et al.¹²¹

3.5 ELECTROCHEMICAL IMPEDANCE SPECTROSCOPY

Electrochemical impedance spectroscopy (EIS) can be used to measure the real and imaginary components of cell impedance in response to a small AC signal over a range of frequencies. EIS measurements are attractive because they are quick and non-destructive

to the cell components and can provide insights about the effect of electrolyte additives on the positive and negative electrode SEI layers and on the electrolyte resistance.

EIS measurements can be used to investigate charge transfer processes, interfacial processes, and mass transfer effects. EIS measurements are important because the SEIs that form on both the positive and negative electrodes must be passivating films that allow Li-ions to pass through the layer. The resistances of the SEI layers can help determine the effectiveness of the SEI, and EIS measurements are therefore important.

An AC potential is applied to the cell with an amplitude on the order of mV to invoke a current response that is linear with the amplitude of the AC potential. The impedance, in ohms, is calculated at each frequency as the ratio of the applied voltage, in volts, to the measured current, in amps. The impedance, Z_{eq} , of circuit elements in series and in parallel are shown by Equation 3.1 and 3.2, respectively.

$$\text{Series: } Z_{eq} = Z_1 + Z_2 + \dots + Z_n \quad (3.1)$$


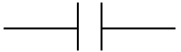

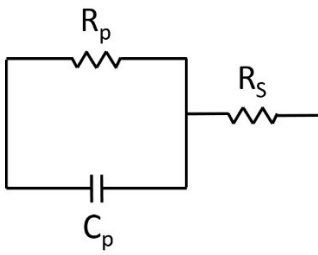
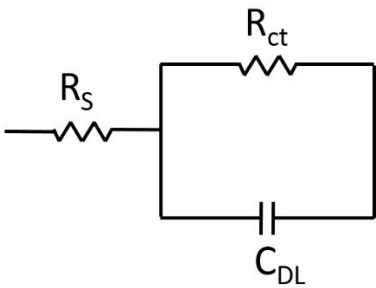
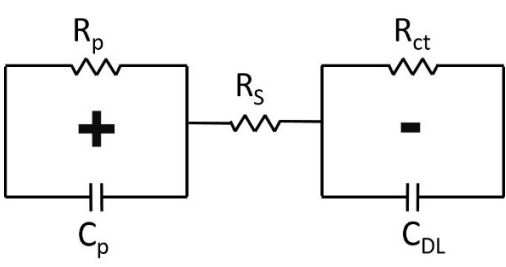
$$\text{Parallel: } Z_{eq} = \left[\frac{1}{Z_1} + \frac{1}{Z_2} + \dots + \frac{1}{Z_n} \right]^{-1} \quad (3.2)$$

Table 3.1 shows the schematic of simple circuit elements and their corresponding impedance in addition to simplified circuit models of electrodes and a full Li-ion cell. The capacitance of a capacitor, in farads, is represented by C , the resistance of a resistor, in ohms, is represented by R and the inductance of an inductor, in henrys, is represented by L . The angular frequency, ω , is equal to $2\pi f$, where f is the frequency in hertz.

In a full cell, the charge transfer resistance and resistance due to motion of ions through the SEI can be represented by an effective resistance, \mathcal{R} . The negative electrode can be described by a circuit containing a resistor and a capacitor in parallel. The SEI on the negative electrode will have some resistance, R_{ct} , as Li moves from the active material into the electrolyte while passing through the SEI. The electrode, with the SEI layer, has some surface charge, and oppositely charged ions in the electrolyte are near the surface, such that there are two parallel layers of charge. These layers of charge are an electric double layer, and thus have a corresponding double layer capacitance, C_{DL} . The motion of Li^+ through the SEI and the electrical double layer is shown in Figure 3.6. The positive electrode can be described similarly, with effective resistance, R_p , and capacitance, C_p . The resistance of the electrolyte is represented by R_s . The schematic of a simplified circuit of a full cell and its impedance are shown in Table 3.1.

EIS spectra can be shown in either a Bode plot or a Nyquist plot. A Bode representation is a plot of either the real component of impedance or the imaginary component of impedance as a function of frequency on a logarithmic scale. This is useful as the impedance at each measured frequency is shown. A Nyquist representation is a plot of the imaginary impedance versus the real impedance. A Nyquist plot of a Li-ion cell typically has a semi-circular shape, and the real component of impedance normally decreases as frequency increases.

Table 3.1 Equivalent circuit models and their calculated impedance.

Component	Circuit Symbol	Impedance, $Z(\omega)$
Resistor		R
Capacitor		$1/(i\omega C)$
Inductor		$i\omega L$
Positive Electrode in Electrolyte		$R_s + \frac{R_p}{1 + \omega^2 C_p^2 R_p^2} - \frac{i\omega C_p R_p^2}{1 + \omega^2 C_p^2 R_p^2}$
Negative Electrode in Electrolyte		$R_s + \frac{R_{ct}}{1 + \omega^2 C_{DL}^2 R_{ct}^2} - \frac{i\omega C_{DL} R_{ct}^2}{1 + \omega^2 C_{DL}^2 R_{ct}^2}$
Simplified model of full Li-ion Cell		$R_s + \frac{R_p}{1 + \omega^2 C_p^2 R_p^2} - \frac{i\omega C_p R_p^2}{1 + \omega^2 C_p^2 R_p^2} + \frac{R_{ct}}{1 + \omega^2 C_{DL}^2 R_{ct}^2} - \frac{i\omega C_{DL} R_{ct}^2}{1 + \omega^2 C_{DL}^2 R_{ct}^2}$

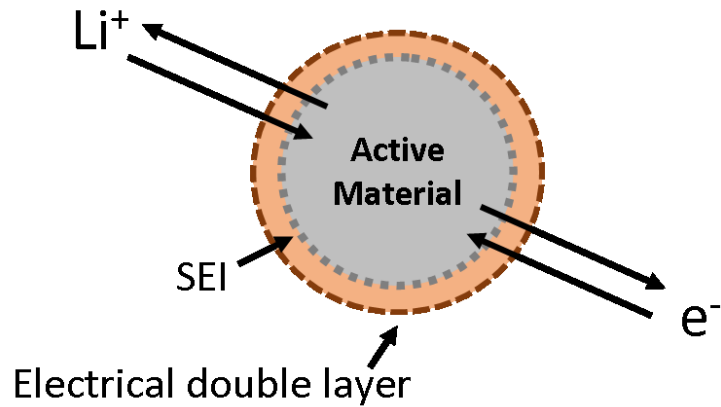


Figure 3.6 Schematic of the SEI formed on the electrode surface. The resulting layers of charge are analogous to a double layer capacitor. Li-ions and electrons can pass through the SEI.

Figure 3.7 shows example Nyquist and Bode plots from circuit model calculations. Figure 3.7a shows a Nyquist plot for a positive electrode in electrolyte. The shift of the start of the semi-circle from zero is the solution resistance, R_s . Figure 3.7b shows a Nyquist plot for an example full Li-ion cell. If both the positive and negative electrodes behave similarly at the same frequency, the Nyquist plot will retain a smooth semi-circular shape. Figure 3.7c shows a Bode plot of the real component of impedance of an example full Li-ion cell and Figure 3.7d shows the imaginary component of impedance of a full Li-ion cell.

In this thesis, the Nyquist representation will be used to analyze EIS spectra. Data will be presented in a Nyquist plot in which the solution resistance, R_s , and the resistance of the experimental set-up have been subtracted. Figure 3.8 shows a Nyquist plot of the impedance spectra of a full cell prior to any subtraction of the contribution of the experimental setup to the cell impedance. The sum of the charge transfer resistances and resistance due to motion of ions through the SEI layers can be extracted from a Nyquist

plot as the “diameter” of the “semicircle”, as indicated in Figure 3.7b, and it is this measurement, \mathcal{R} that will be used to compare electrolyte additives.

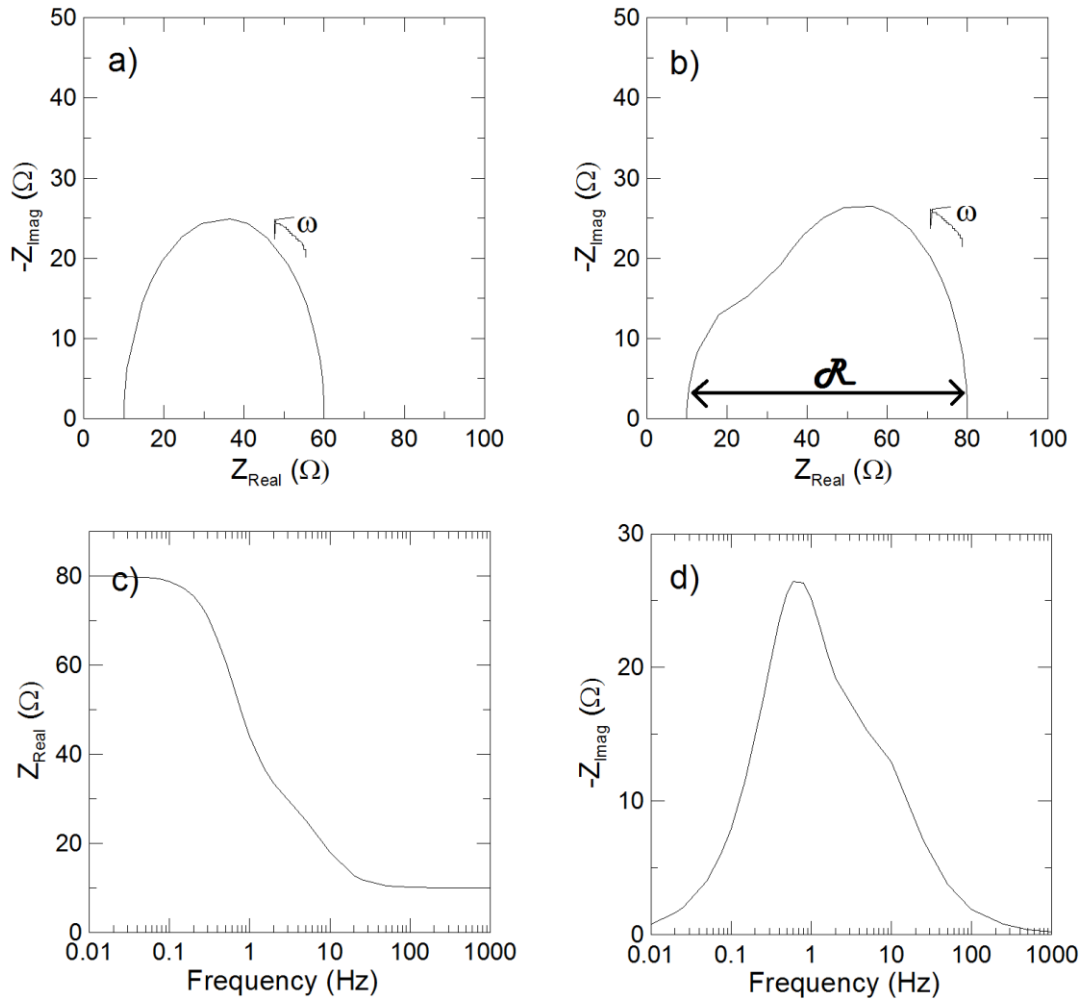


Figure 3.7 A Nyquist plot of a positive electrode in electrolyte (a) and a full Li-ion cell (b). A Bode plot of the real component of impedance (c) and the imaginary component of impedance (d) of a full Li-ion cell. The circuit values used are: $R_S = 10 \Omega$, $C_{DL} = 0.001 \text{ F}$, $R_{ct} = 20 \Omega$, $C_p = 0.005 \text{ F}$, and $R_p = 50 \Omega$. \mathcal{R} represents the combination of charge transfer resistances (both negative and positive electrodes) and resistance due to motion of ions through the SEI layers (both negative and positive electrodes).

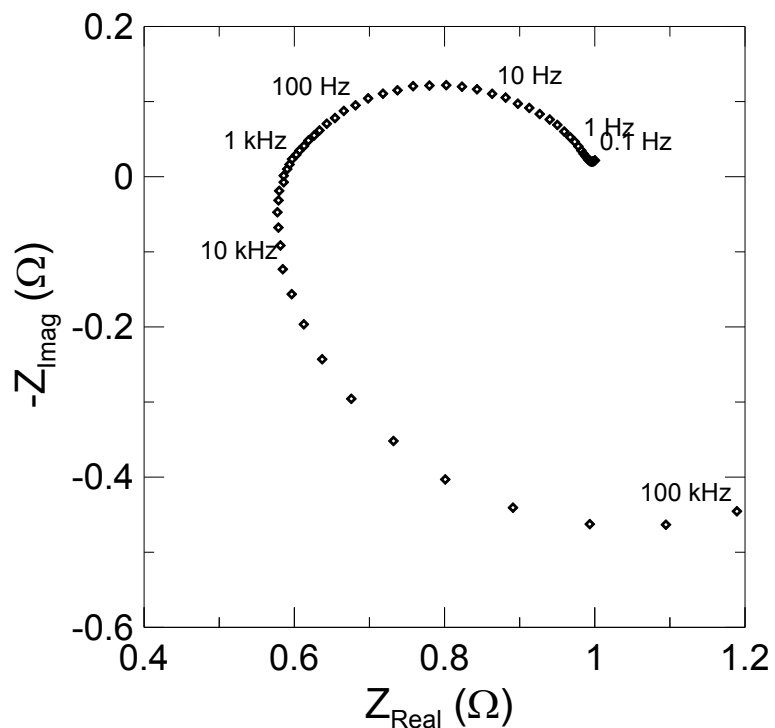


Figure 3.8 An example impedance spectra before the experimental setup contribution has been subtracted.

Since electrolyte additives modify the composition, formation, and growth of the SEI, the charge transfer resistance should vary with different additives. The goal is to determine additives that reduce the impedance of the full cell during formation, cycling, and storage experiments. EIS measurements in this thesis were taken at $10. \pm 0.1^\circ\text{C}$ when the cells were at 3.8 V. The temperature boxes used for these measurements are stable to $\pm 0.1^\circ\text{C}$, and are within one degree centigrade of the set temperature of 10°C . These measurements were taken at $10. \pm 0.1^\circ\text{C}$ so that differences in the impedance spectra due to different electrolyte additives were more pronounced. The measurements were taken from 100 mHz to 100 kHz. EIS measurements were taken using a BioLogic VMP3 battery tested equipped with an EIS board.

3.6 FREQUENCY RESPONSE ANALYZER (FRA)

A frequency response analyzer (FRA) setup can be used to perform in-situ electrochemical impedance spectroscopy measurements. By connecting a Maccor model FRA 0356 to a Maccor series 4000, impedance spectra can be collected at any desired voltage during cycling. While the FRA is measuring the impedance spectra of a cell, the cell remains at open circuit voltage.

A typical FRA experiment involves measuring the impedance spectra every 0.1 V as a cell is charged and discharged, followed by a fixed number of cycles. The FRA measurements and subsequent cycling are then repeated as desired. This allows for the investigation of the positive and negative electrode stability as a function of voltage and as a function of cycle number. By comparing the charge transfer resistance of a cell at various cycles, one can learn about cell aging and the growth of the SEI as a function of time. By comparing the charge transfer resistance of a cell containing one additive combination to a cell containing another additive combination, one can learn about the effects of electrolyte additives on the stability of the SEI layers as well as the cell cyclability at high voltage.

CHAPTER 4. PES SYSTEM

4.1 CONCENTRATION STUDY

The work of Xia et al.¹⁰¹ is extended to include studies of a complete range of PES contents from 0.5% to 6.0% in Li[Ni_{1/3}Mn_{1/3}Co_{1/3}]O₂ (NMC111)/graphite pouch cells. The Ultra High Precision Charger (UHPC) at Dalhousie University^{107,122} was used to monitor the coulombic efficiency, charge end point capacity slippage and discharge capacity versus time and cycle number of the cells. In addition, gas evolution measurements employing Archimedes principle¹²¹ and electrochemical impedance spectroscopy (EIS) measurements were performed. Improved UHPC methods, where storage was performed before UHPC, to help distinguish between additives with similar properties, are introduced here.

4.1.1 EXPERIMENTAL

Machine-made 220 mAh NMC111/graphite wound pouch cells balanced for 4.4 V operation were obtained dry (no electrolyte added) from Whenergy (Shandong, China). Pouch cells were manufactured and vacuum sealed in a dry room before shipping to Dalhousie University. After heating to 80°C for 14 hours under vacuum to remove any residual water, the pouch cells were filled with 0.90 g of 1M LiPF₆ in ethylene carbonate (EC): ethyl methyl carbonate (EMC) (Novolyte Technologies, now BASF) in a ratio of 3:7 (by weight) as the control electrolyte with purity greater than 99.9%. Additional cells were filled with control electrolyte containing 0.5, 1, 2, 4, and 6% of prop-1-ene-1,3-sultone (PES, Lianchuang Medicinal Chemistry Co., 98.20%) by weight and compared to cells containing 2% vinylene carbonate (VC, BASF, 99.97%). Cells were vacuum sealed

using a compact vacuum sealer (MTI Corp.) after electrolyte filling. All cells did a formation cycle at 40°C, consisting of a 24 hour hold at 1.5 V to ensure adequate electrolyte wetting followed by a C/20 charge to 4.2 V and a subsequent C/20 discharge to 3.8 V. After this step, cells were transferred into an argon-filled glovebox, cut open just below the heat seal to release generated gas and then vacuum sealed again. After degassing, electrochemical impedance spectroscopy (EIS) was used to measure the impedance of the cells at 3.8 V and 10. ± 0.1°C. AC impedance spectra were collected from 100 kHz to 100 mHz with a signal amplitude of 10 mV.

All these cells were part of one of two experiments. One set of cells were cycled using the Ultra High Precision Charger (UHPC) at Dalhousie University between 2.8 and 4.2 V at 40. ± 0.1°C and C/20 for 20 cycles. The second cells underwent a 500 hour storage period at 40. ± 0.1°C where their open circuit voltage was monitored and recorded every 6 hours before being cycled using the UHPC similarly to the first set of cells. This was done to observe the effect and potential benefit of a storage period prior to cycling experiments.

In addition, gas evolution measurements employing Archimedes principle were done on all cells before and after formation, storage, and cycling as described in the experimental section.

4.1.2 RESULTS AND DISCUSSION

Figure 4.1 shows the gas evolution during formation at 40°C. Error bars are the standard deviation of data from four nominally identical cells. Cells containing low

concentrations of PES and the control electrolyte produce large amounts of gas, leading to bulging of the pouch and possible loss of contact between separators and electrodes. Cells containing 2, 4, or 6% PES were comparable to 2% VC. Figure 4.2 shows the EIS spectra of the cells collected after formation in units of $\Omega \cdot \text{cm}^2$ in order to account for the electrode areas for various cell chemistries. The EIS data were collected at 3.8 V and 10°C. Figure 4.2 shows that increasing the PES content in the control electrolyte causes an increase in charge transfer resistance after formation. All cells show good repeatability for the four cells of each additive type.

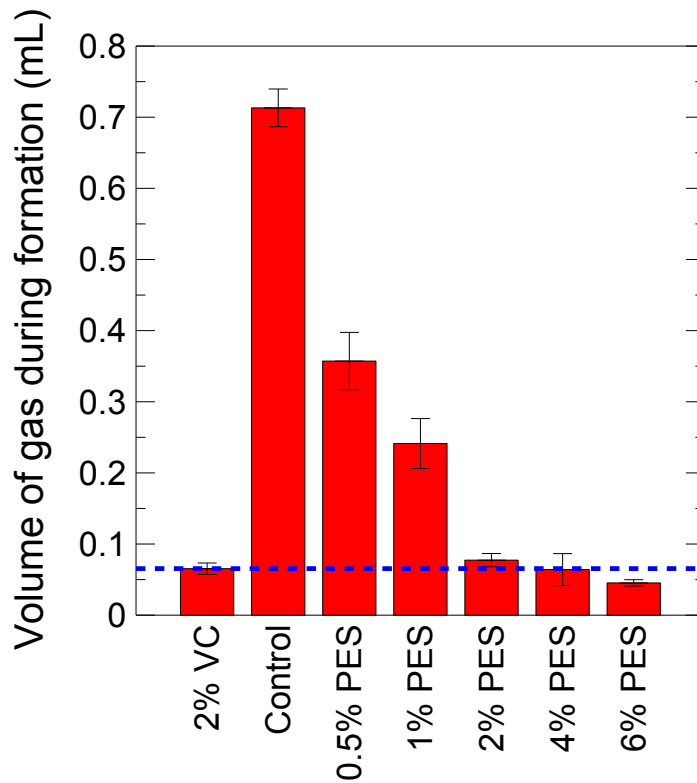


Figure 4.1 Gas evolution during formation at 40°C measured using Archimedes principle. The dotted blue line highlights that of 2% VC.

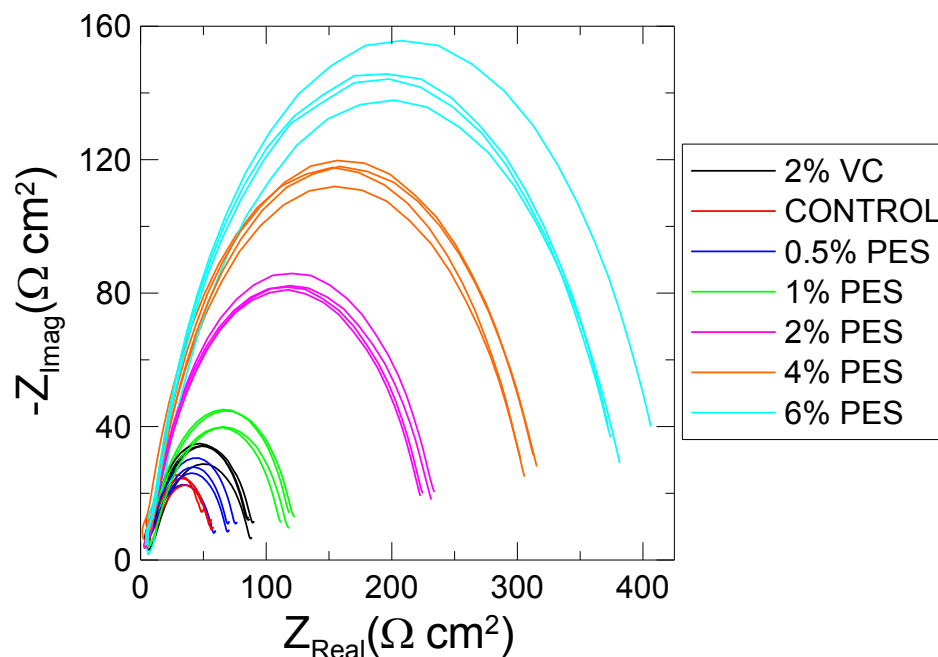


Figure 4.2 EIS spectra of the NMC111/graphite cells collected at 3.8 V and 10°C after formation.

Figure 4.3 summarizes the gas evolution and impedance measurements taken after 500 hours of storage at 40°C and UHPC cycling at 40°C. The error bars are the standard deviation of data from pair cells. Figures 4.3a and 4.3b show that all combinations studied show low gas evolution after storage and cycling. Negative volumes of gas indicate that no further gas was produced in the cells, and that at least some (if any) gas remaining in the cells after being degassed has been consumed. Figures 4.3c and 4.3d again show that increasing the content of PES caused an increase in impedance after both storage and cycling at 40°C. The impedance of all cells containing VC or PES additives was reduced after storage and cycling compared to the impedance measured after formation.

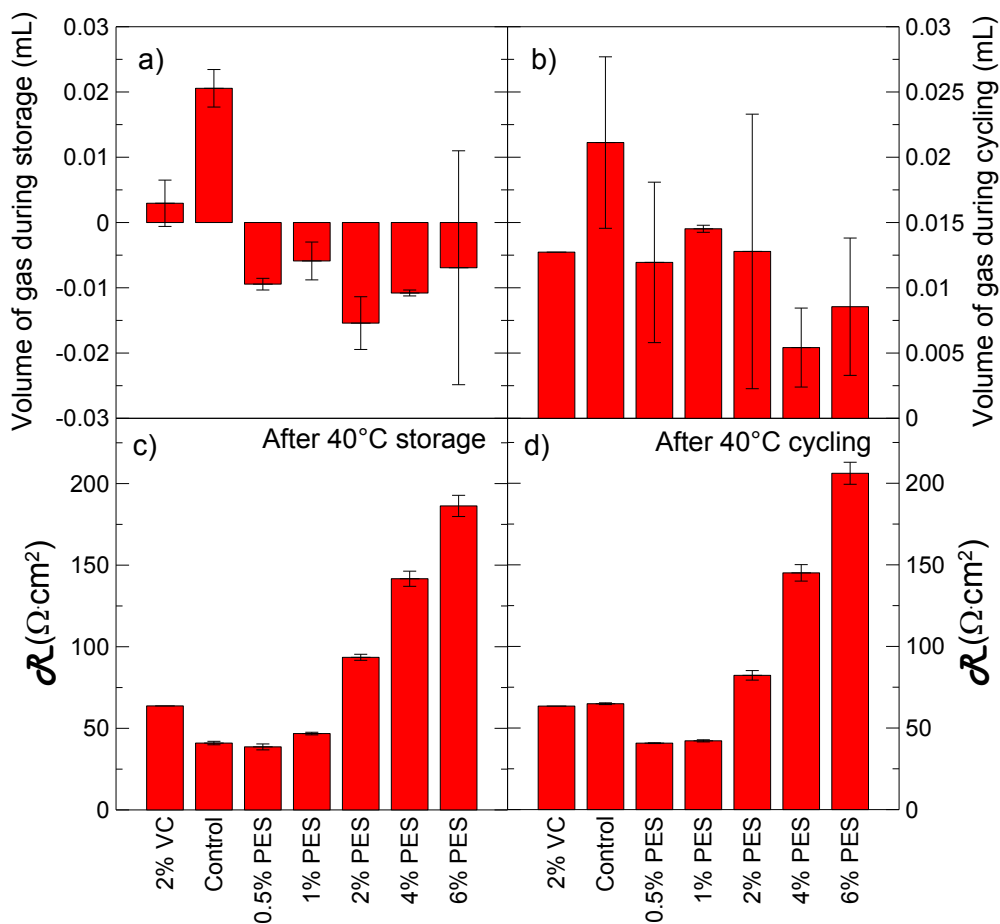


Figure 4.3 Gas evolution during storage at 40°C (a) and during cycling at 40°C (b) and the the combination of charge transfer resistances (both negative and positive electrodes) and resistance due motion of ions through the SEI layers (both negative and positive electrodes, R measured using EIS at 3.8 V and 10°C after storage (c) and after cycling (d).

Figure 4.4 shows a summary of the 40°C, 4.2 V storage experiment. The error bars are the standard deviation of data from pair cells. The top panel shows the total drop in open circuit voltage (OCV) from 4.2 V during the 500 hour storage period. The voltage at the end of the storage period was lower than the voltage at the beginning of the storage period. Cells containing low concentrations of PES and the control electrolyte lead to a large voltage drop and cells containing 2, 4, or 6% PES were comparable to 2% VC. The

bottom panel of Figure 4.4 shows the difference between the discharge capacity immediately before the storage period and the discharge capacity following a full charge after the storage period. This difference is the irreversible capacity loss of the cells resulting from parasitic reactions at the negative electrode which deplete the Li inventory. Although all cells exhibited low irreversible capacity loss, the PES-containing cells resulted in the smallest loss.

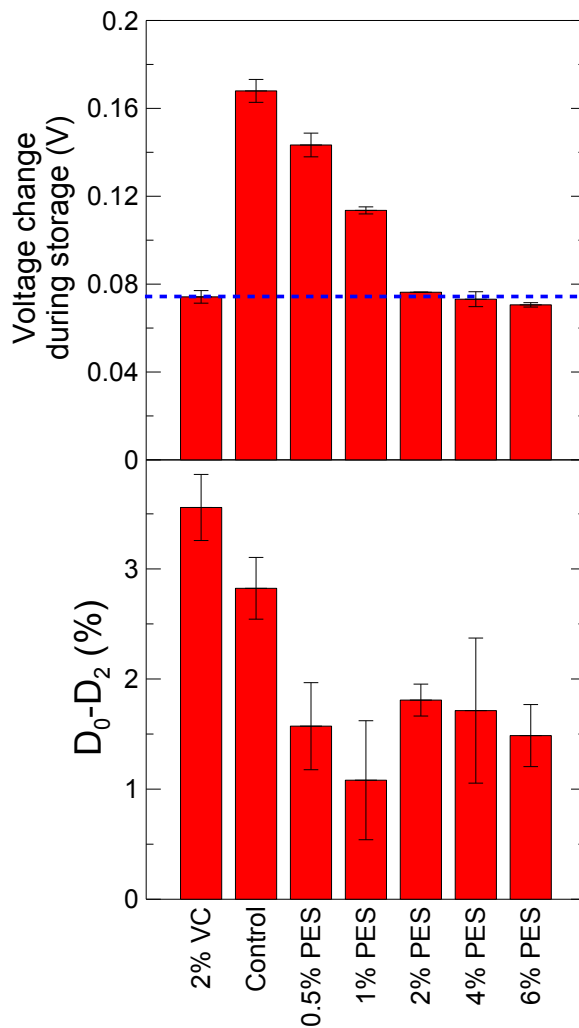


Figure 4.4 (top) The drop in open circuit voltage from 4.2 V during 500 hours of storage at 40°C; (bottom) The difference between the discharge capacity before the storage period and the discharge capacity after a full charge following the storage period.

Figure 4.5 shows the results of UHPC cycling for cells that underwent cycling only (Figures 4.5a to 4.5c) or cycling after a 500 hour storage period (Figures 4.5d to 4.5f). Figures 4.5a and 4.5d show the normalized discharge capacity, Figures 4.5b and 4.5e show the normalized charge end point capacity, and Figures 4.5c and 4.5f show the coulombic efficiency (CE), all plotted versus cycle number. The true discharge capacity of the cycling-only cells ranged from 208-225 mAh, and that of the storage before cycling cells ranged from 208-218 mAh. During storage at a full state of charge, lithium in the graphite slowly migrated to the overhang region of the anode. After the storage period, some of this lithium in the overhang, that above the average state of charge of the anode during 100% DOD cycling, was slowly made available during cycling, which caused the increase in capacity and decrease in CE shown in Figures 4.5d and 4.5f, respectively. This is an interesting effect which needs further exploration. Cells containing 2, 4, or 6% PES or 2% VC display high CE, low discharge capacity fade and small slippage of the charge end point capacity.

Figure 4.6 shows the charge end point capacity for the best performing cells. The increasing trend, or slippage, of the charge end point capacity was due to electrolyte oxidation at the positive electrode. Cells containing 4 and 6% PES were superior to 2% VC as shown by the small slippage and small slope. Figure 4.6 shows that UHPC cycling after storage gave a similar ranking of the additives as direct UHPC cycling, except in the case of 2% PES and 2% VC. Cells with 2% PES performed better than 2% VC when cells were cycled directly (Figure 4.6a) but performed worse when cells were cycled after the storage period (Figure 4.6b). The electrolyte oxidation rate, and correspondingly the charge endpoint capacity slippage, in cells with 2% VC decreased dramatically from one

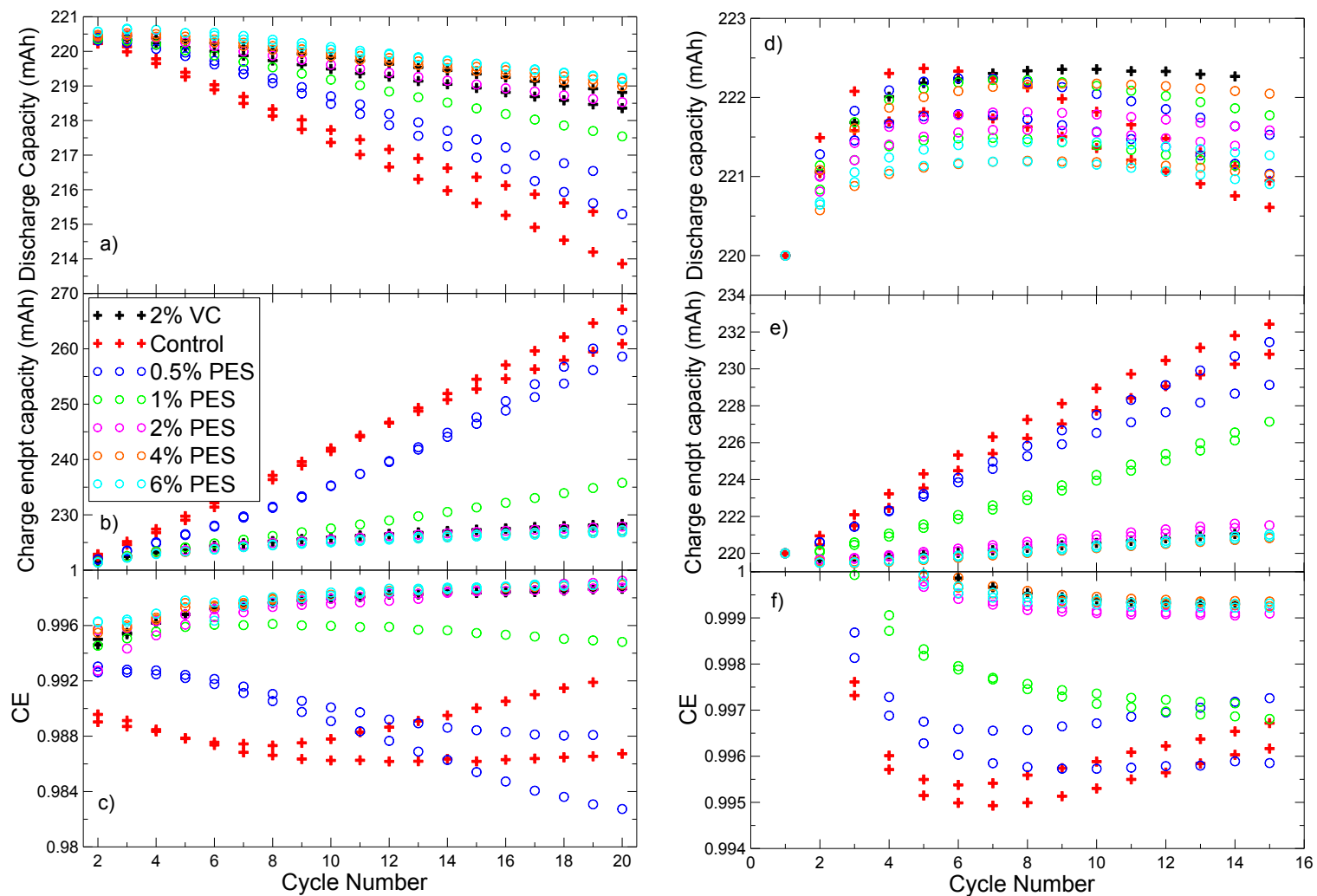


Figure 4.5 The normalized discharge capacity of the cycled-only cells (a) and the stored-before-cycled cells (d); the normalized charge end point capacity of the cycled-only cells (b) and the stored-before-cycled-cells (e); the coulombic efficiency of the cycled-only cells (c) and the stored-before-cycled cells (f), all plotted versus cycle number. The cells were cycled at C/20 between 2.8 and 4.2 V at 40.°C.

500 h storage period to the next as has been shown by Burns et al.^{56,58} Therefore, it is not surprising that the 2% VC cells appear better than the 2% PES cells when cycled after storage. By contrast, 4% and 6% PES outperformed 2% VC in both UHPC methods.

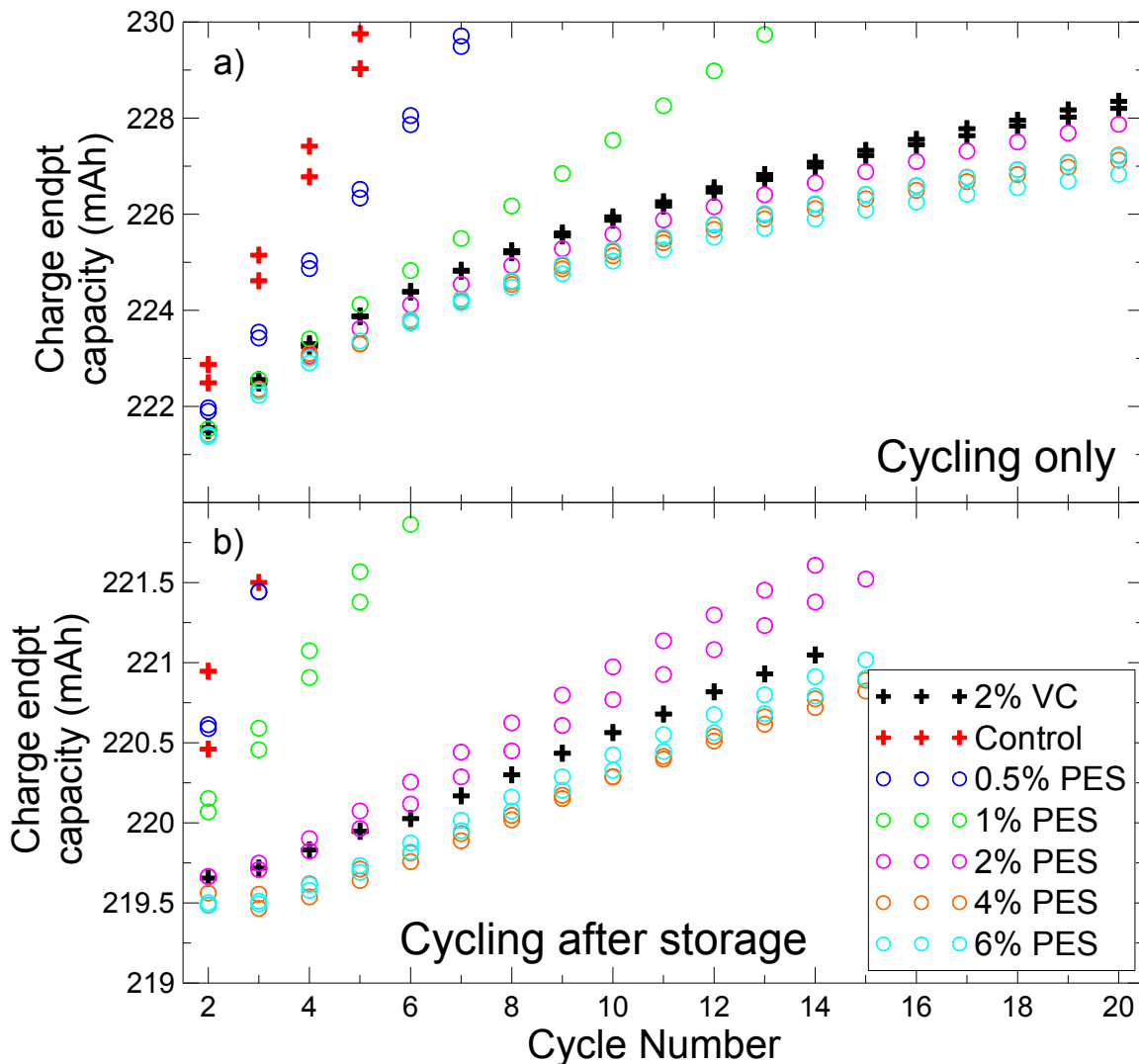


Figure 4.6 a) The normalized charge end point capacity of the cycled-only cells and b) the stored –before-cycled cells, both versus cycle number. The cells were cycled at C/20 between 2.8 and 4.2 V at 40°C.

Figure 4.7 shows the CE versus time after formation for the best performing cells. The cells that were cycled only are shown on the left and those that had a storage period prior

to cycling are on the right. Figure 4.7 shows the benefit of a storage period prior to UHPC cycling. A more stable value of CE can be observed in fewer cycles when a storage period precedes the cycling experiments, possibly due to the maturation of the negative electrode SEI during the storage period. There are several features in Figure 4.7 that are very interesting. First, the CE versus time data for the PES-containing cells appear to extrapolate well from the cycling only experiment to the store-before-cycling experiment as one might expect. However, the data for 2% VC –containing cells that were stored before cycling is clearly shifted upwards relative to the extrapolation of the cycling-only cells. This is consistent with the results from Figure 4.6. From the cycling and storage data at 40°C (Figures 4.4 and 4.6), the performance of 4 and 6% PES proves to be comparable to or better than 2% VC.

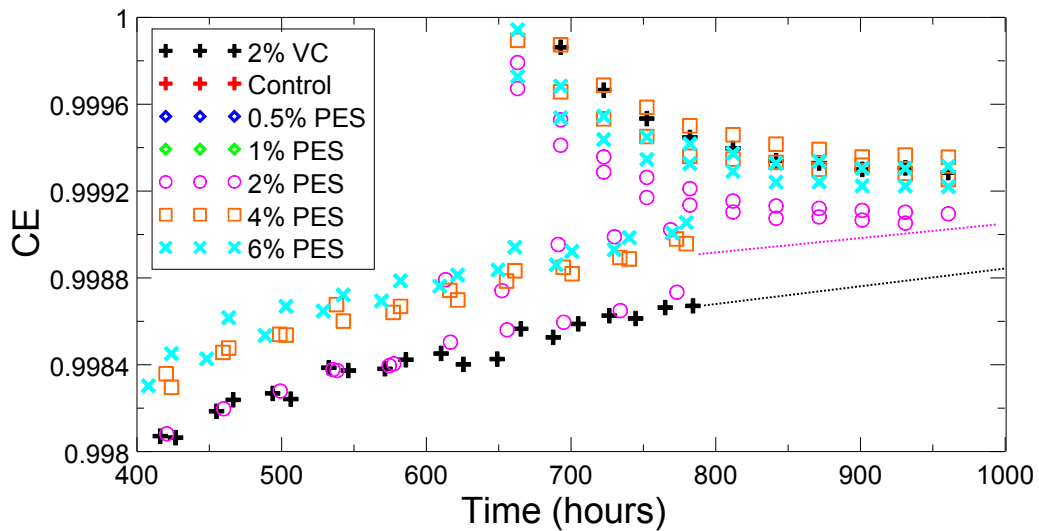


Figure 4.7 The coulombic efficiency of the cycled-only cells (left) and the stored-before-cycled cells (right) as a function of time. The zero of time marks the point after EIS was measured after formation for all the cells. The cells were cycled at C/20 between 2.8 and 4.2 V at 40°C. The black dotted line represents an extrapolation of the CE for 2% VC-containing cells and the magenta dotted line represents an extrapolation of the CE for 2% PES containing cells.

4.1.3 CONCLUSION

Through the use of storage and UHPC cycling experiments, the effectiveness of PES as an additive was investigated. UHPC cycling experiments shows that 4% or 6% PES outperformed 2% VC while 2% PES was comparable to 2% VC. However, the use of 4% or 6% PES comes at the expense of higher impedance in the resulting cells. The voltage drop during storage in PES-containing cells was very similar to that for cells with 2% VC, however, in storage experiments at 40.°C, cells with PES showed less irreversible capacity loss than cells with VC.

4.2 HIGH TEMPERATURE STORAGE STUDY

To further understand the role of PES as an additive and its potential to overcome the temperature sensitivity that plagues VC, a 60°C storage study was performed. The combination of PES with the additive HQ-115 was explored.

4.2.1 EXPERIMENTAL

Machine made 220 mAh Li[Ni_{1/3}Mn_{1/3}Co_{1/3}]O₂ (NMC111)/graphite wound pouch cells balanced for 4.4 V operation were obtained dry (no electrolyte added) from Whenergy (Shandong, China). The pouch cells were heated, filled, and sealed as described in Section 4.1.1. The additives VC, PES, and lithium bis (trifluoromethanesulphonyl) imide (LiN(CF₃SO₂)₂ or 3M Fluorad Lithium HQ-115) were added singly to the control electrolyte at 2% by weight. Several binary combinations of either 1 or 2% by weight of these additives were also studied. Gas measurements and EIS measurements were performed as described in Section 4.1.1. After undergoing the same formation procedure

described in Section 4.1.1, the cells were placed at $60. \pm 0.1^\circ\text{C}$ where their open circuit voltage was monitored and recorded every 6 hours during a 500 hour storage period.

4.2.2 RESULTS AND DISCUSSION

Figure 4.8 summarizes the gas evolution and impedance measurements taken after formation at 40°C and after 500 hours of storage at 60°C . The error bars are the standard deviation of data from pair cells. Figure 4.8a shows that all additive types produced small amounts of gas during formation except for HQ-115 alone. Figure 4.8b shows the EIS spectra after formation at 3.8 V and 10°C . PES-containing cells had larger charge transfer resistances than cells without PES. Figure 4.8c shows the volume of gas evolved during the 500 hour storage period at 60°C . This panel shows that cells with PES alone had only 10% of the gas produced compared to cells with VC alone. All the PES-containing cells exhibited a significant reduction in gas compared with cells that did not contain PES. Figure 4.8c demonstrates the superiority of PES over VC as an additive at high temperature. Figure 4.8d shows the EIS spectra after the 60°C storage period measured at 3.8 V and 10°C . Although all cells show low impedance, the impedance of PES-containing cells have been significantly reduced after the 60°C storage period compared to after formation. The reasons for this are not understood. Figure 4.8c shows that combining HQ-115 with VC caused a reduction in gas evolution compared to 2% VC alone. Although the difference is minor, it appears that adding HQ-115 to 2% PES also caused a reduction in gas evolution compared to 2% PES alone. Clearly, combining PES with other additives may be beneficial to optimize battery performance.

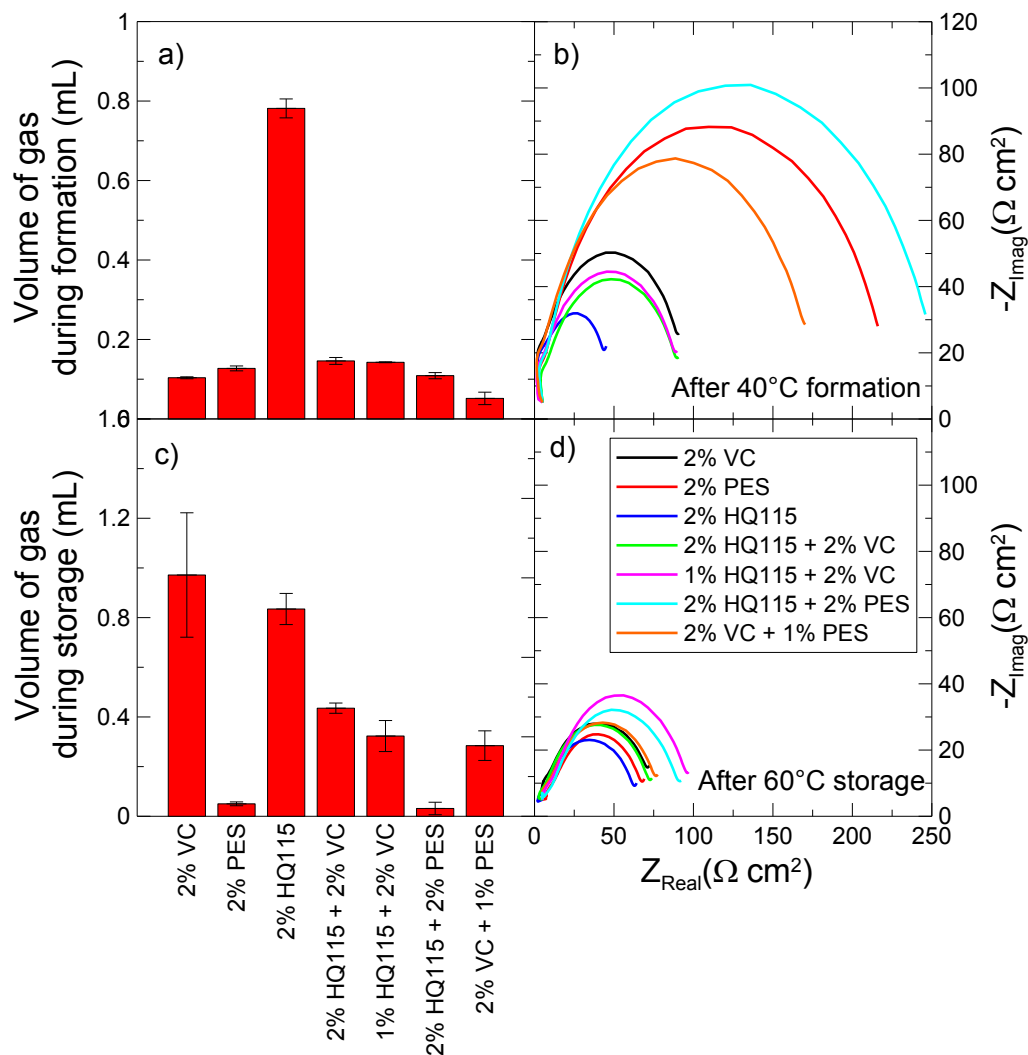


Figure 4.8 Gas evolution during formation at 40°C (a) and during storage at 60°C (c) and the EIS spectra collected at 3.8 V and 10°C after formation (b) and after storage (d).

Figure 4.9 shows the voltage drop from 4.2 V during the 500 hour storage period at 60°C. The error bars are the standard deviation of data from pair cells. The OCV after the storage period is lower than the voltage before the storage period. Figure 4.9 shows that all additives and additive combinations except HQ-115 alone exhibited a relatively small voltage drop during storage. Combining HQ-115 with either 2% VC or 2% PES reduced

the magnitude of the voltage drop compared to 2% VC or 2% PES alone, suggesting useful synergies.

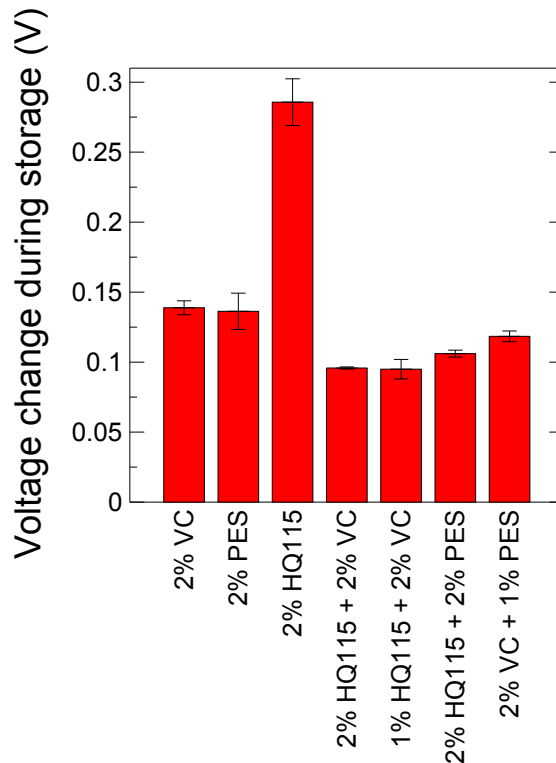


Figure 4.9 The drop in open circuit voltage from 4.2 V during 500 hours of storage at 60°C.

4.2.3 CONCLUSION

Through the use of high temperature storage studies, the effectiveness of PES as an alternative additive to VC was investigated. The gas evolution at high temperatures was dramatically reduced when PES was used. The combination of LiTFSI (HQ-115) with either VC or PES reduced both gassing and voltage drop during 60°C storage. There are no “showstoppers” that prevent PES from reaching the same “famous” status as VC as a general purpose additive, at least in NMC111/graphite cells.

4.3 “211” COMBINATION STUDY

To further understand the role of PES as an additive, cycling and storage experiments were performed on cells containing PES with other high-performing additives. As an extension to the work of Ma et al.³⁷ on ternary and quaternary electrolyte additive mixtures, PES has been studied in combination with a sulfur containing additive (either MMDS or ES) and TTSP or TTSPi. These types of additive combinations were termed “211” combinations.³⁷ Comparisons of the performance of PES in combination with these additives can be made to the performance of VC in combination with these additives.

4.3.1 EXPERIMENTAL

Machine made 220 mAh NMC111/graphite wound pouch cells balanced for 4.4 V operation were obtained dry (no electrolyte added) from Whenergy (Shandong, China). The pouch cells were heated, filled, and sealed as described in Section 4.1.1. The additives prop-1-ene-1,3-sultone (PES, Lianchuang Medicinal Chemistry Co., 98.20%), vinylene carbonate (VC, BASF, 99.97%), methylene methane disulfonate (MMDS, Guangzhou Tinci Co. Ltd, 98.70%), ethylene sulfite (ES, Sigma-Aldrich, > 98%), tris(-trimethyl-silyl)- phosphate (TTSP, TCI America, >98%) and tris(-trimethyl-silyl)- phosphite (TTSPi, TCI America, >95%) were added to the control electrolyte according to the following scheme. The additives selected for combination were PES plus either ES or MMDS plus one of TTSP or TTSPi. PES was added at 2% by weight and the other additives were added at either 1% or 2% by weight. Gas measurements and EIS measurements were performed as described in Section 4.1.1.

After undergoing the same formation procedure described in Section 4.1.1, the cells were placed at $40. \pm 0.1^\circ\text{C}$ where their open circuit voltage was monitored and recorded every 6 hours during a 500 hour storage period. Gas and EIS measurements were performed after the storage period. The cells were then cycled using the Ultra High Precision Charger (UHPC) at Dalhousie University between 2.8 and 4.2 V at $40. \pm 0.1^\circ\text{C}$ and C/22 (10 mA) for 15 cycles.

After the storage and cycling experiments at $40. \pm 0.1^\circ\text{C}$, the same cells underwent a high voltage, high temperature storage experiment. As described in Chapter 3.3, the cells did a precycle of 1.5 cycles between 2.8 and 4.4 V at C/20 and $60. \pm 0.1^\circ\text{C}$. After the precycle, the cells were left to rest at 4.4 V, where their open circuit voltage was monitored and recorded every 6 hours during a 600 hour storage period. Following the storage period, the cells did a postcycle of 1.5 cycles between 2.8 and 4.4 V at C/20.

4.3.2 RESULTS AND DISCUSSION

Figure 4.10 shows the gas evolution during formation at 40°C . Error bars are the standard deviation of data from pair cells. Cells containing ES produced the smallest amount of gas. As the concentrations of MMDS, TTSP, and TTSPi in the electrolyte were increased, the amount of gas produced increased as well.

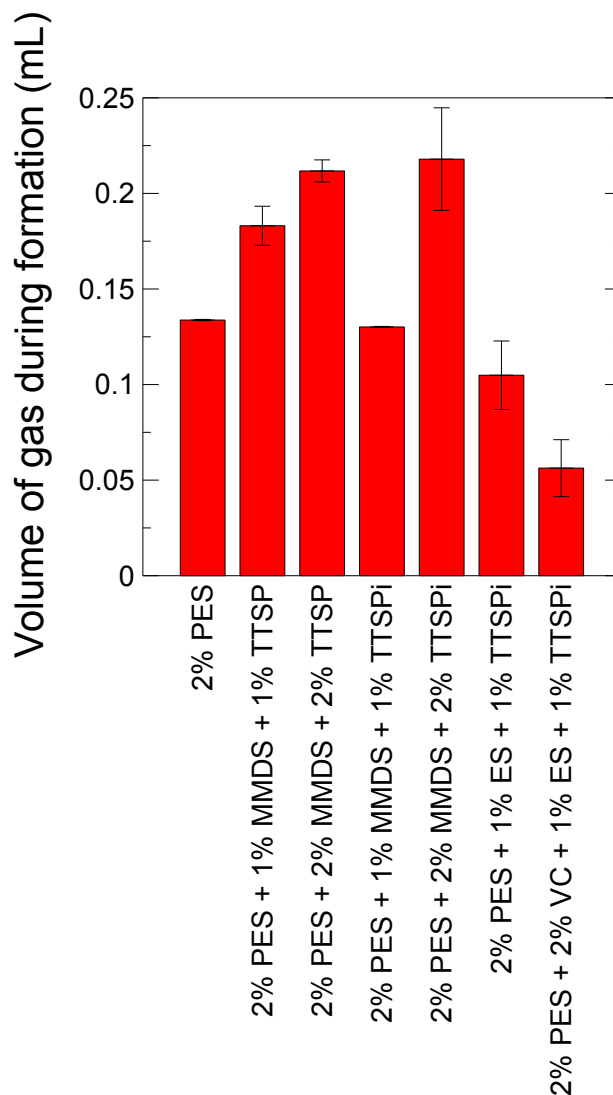


Figure 4.10 Gas evolution during formation at 40°C measured using Archimedes principle.

Figure 4.11 shows the EIS spectra of the cells collected after formation. The EIS data were collected at 3.8 V and 10°C. Figure 4.11 shows that cells containing ES had the lowest impedance and that PES alone resulted in the largest impedance. Increasing the concentration of MMDS with TTSP had no effect on the cell impedance. Increasing the concentration of MMDS with TTSPi resulted in a larger impedance.

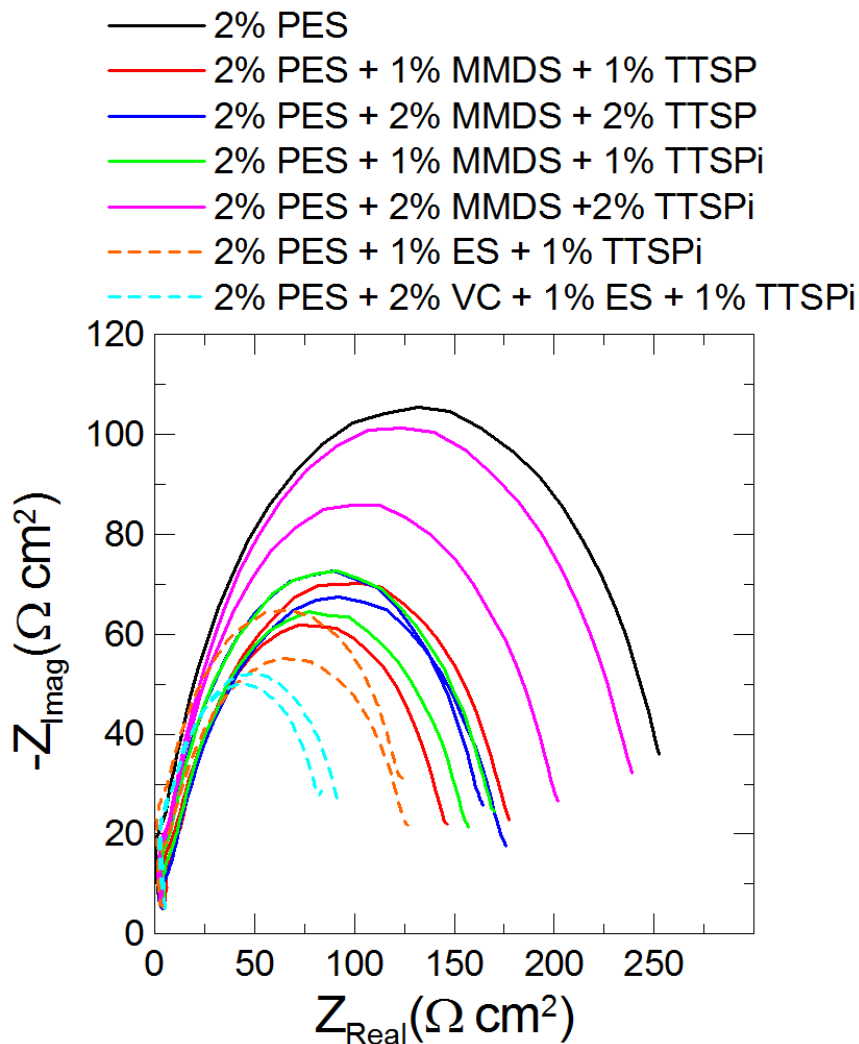


Figure 4.11 EIS spectra of the NMC111/graphite cells collected at 3.8 V and 10°C after formation.

Figure 4.12 summarizes the gas evolution and impedance measurements taken after 500 hours of storage at 40°C and UHPC cycling at 40°C. The error bars are the standard deviation of data from pair cells. Figures 4.12a and 4.12b show that all combinations studied had low gas evolution during storage and cycling. Figures 4.12c and 4.12d show that all combinations studied had reduced impedance after storage and cycling, respectively, compared to after formation. ES-containing cells again had the smallest

impedance after both storage and cycling, similarly to after formation. Cells containing PES alone had a dramatically reduced impedance after storage and cycling compared to after formation. This suggests that PES may help form an SEI layer that effectively reduces parasitic reactions on either the positive or negative electrode, or both, resulting in a decrease in impedance. TTSP-containing cells clearly show reduced impedance compared to TTSPi-containing cells. This suggests that TTSP is a better film-forming additive and perhaps the SEI layers on the positive and negative electrode are more effective at reducing parasitic reactions than those formed in the presence of TTSPi. However, Wang et al. showed that the CE of NMC/graphite cells containing TTSPi was better than cells containing TTSP.⁶⁶

Figure 4.13 shows the total drop in open circuit voltage (OCV) from 4.2 V during the 500 hour storage experiment at 40°C. The error bars are the standard deviation of data from pair cells. The OCV after the storage period is lower than the voltage before the storage period. All combinations studied show similar voltage drops during storage. The addition of TTSP or TTSPi with MMDS leads to a smaller voltage drop than PES alone in the electrolyte.

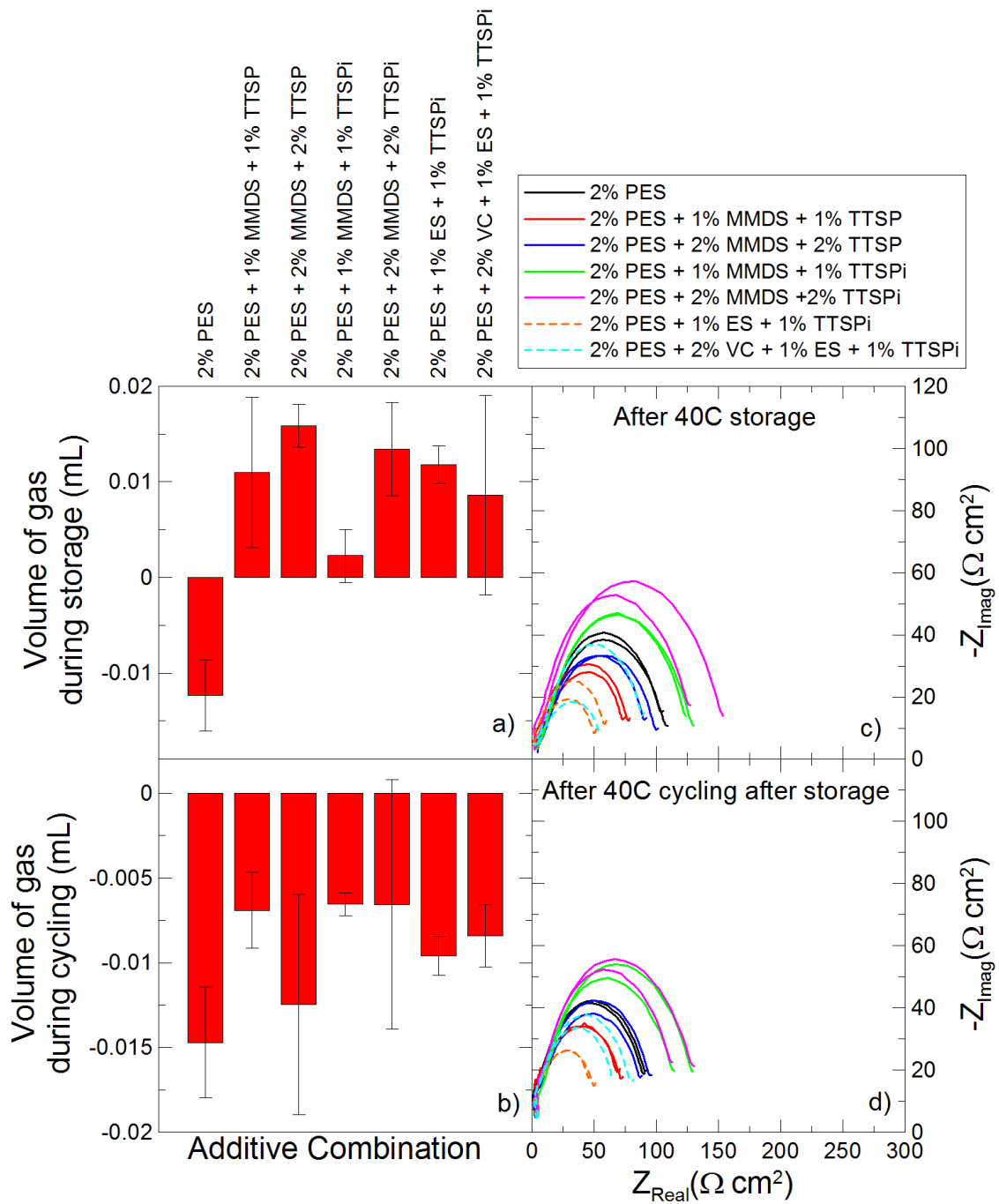


Figure 4.12 Gas evolution during storage at 40°C (a) and during cycling at 40°C (b) and the impedance spectra measured using EIS at 3.8 V and 10°C after storage (c) and after cycling (d).

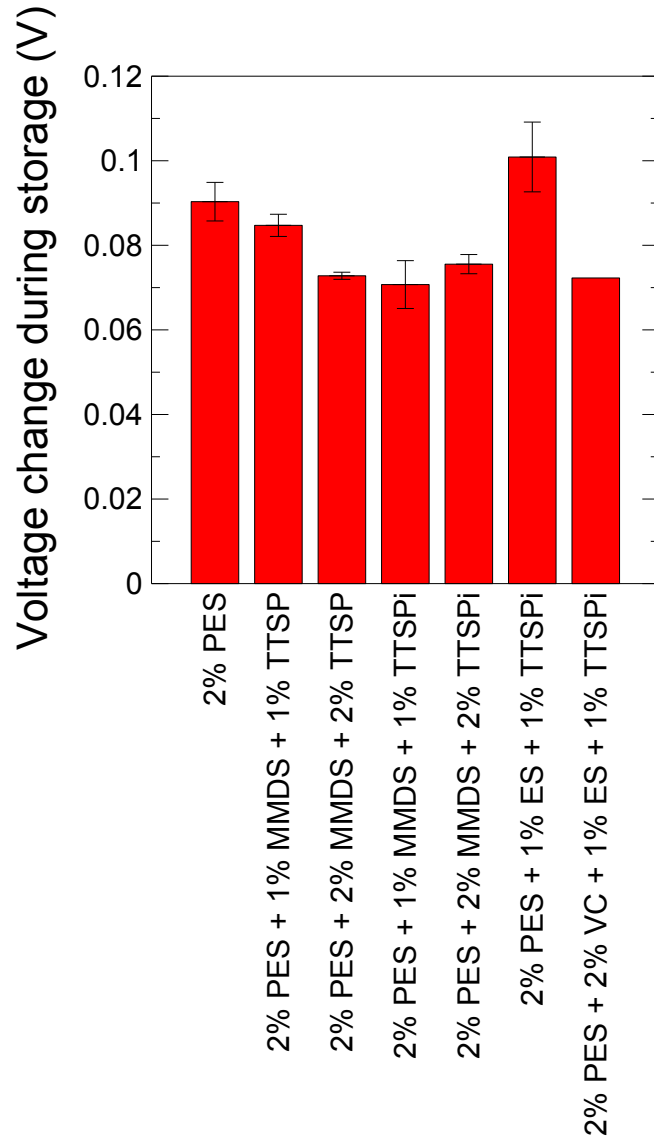


Figure 4.13 The drop in open circuit voltage from 4.2 V during 500 hours of storage at 40°C.

Figure 4.14 shows the results of the UHPC cycling for the cells after the storage period. Figure 4.14a shows the normalized discharge capacity, Figure 4.14b shows the normalized charge end point capacity, and Figure 4.14c shows the CE, all plotted versus cycle number. The true discharge capacity of the cells ranged from 211-220 mAh. As described in Section 4.1.1, the initial increase in capacity and decrease in CE was due to

the lithium in the overhang from the storage period that was slowly made available during cycling. Cells containing PES, VC, ES, and TTSPi showed superior performance compared to all other additive combinations studied. This additive combination had a high discharge capacity with low fade, as well as very low charge slippage, as evidenced by the small slope shown in Figure 4.14b. This additive combination also had the highest coulombic efficiency, reaching a value above 0.9993 after 16 cycles. Conversely, while cells containing PES, ES, and TTSPi (without VC) showed low discharge capacity fade, these cells exhibited severe charge slippage, as evidenced by the large slope shown in Figure 4.14b, indicating detrimental electrolyte oxidation at the positive electrode. These cells also had the lowest CE of the additive combinations studied. The addition of VC with the additives PES, ES, and TTSPi dramatically improved the cycling performance of the NMC111/graphite cells. Cells containing PES, MMDS, and TTSPi performed better during cycling than cells containing PES, MMDS, and TTSP. The TTSPi-containing cells had lower discharge capacity fade, lower charge slippage, and higher CE than TTSP-containing cells. Cells containing PES alone had similar performance to those containing PES, MMDS, and TTSP, if not slightly better.

Figure 4.15 shows the gas evolution measurements taken after the 600 hour storage period at 4.4 V and 60°C. The error bars are the standard deviation of data from pair cells. Despite having undergone a storage period and cycling at 40°C already, when left at open circuit at 4.4 V and 60°C, a significant amount of gas was produced. The gas evolution was most likely due to electrolyte degradation after being exposed to high voltage and high temperature. All experiments presented so far in this thesis involving PES have only involved cells at 4.2 V. The large gas evolution at 4.4 V may be evidence

that PES, alone and in combination with other additives, is only beneficial in the range of potentials below 4.2 V.

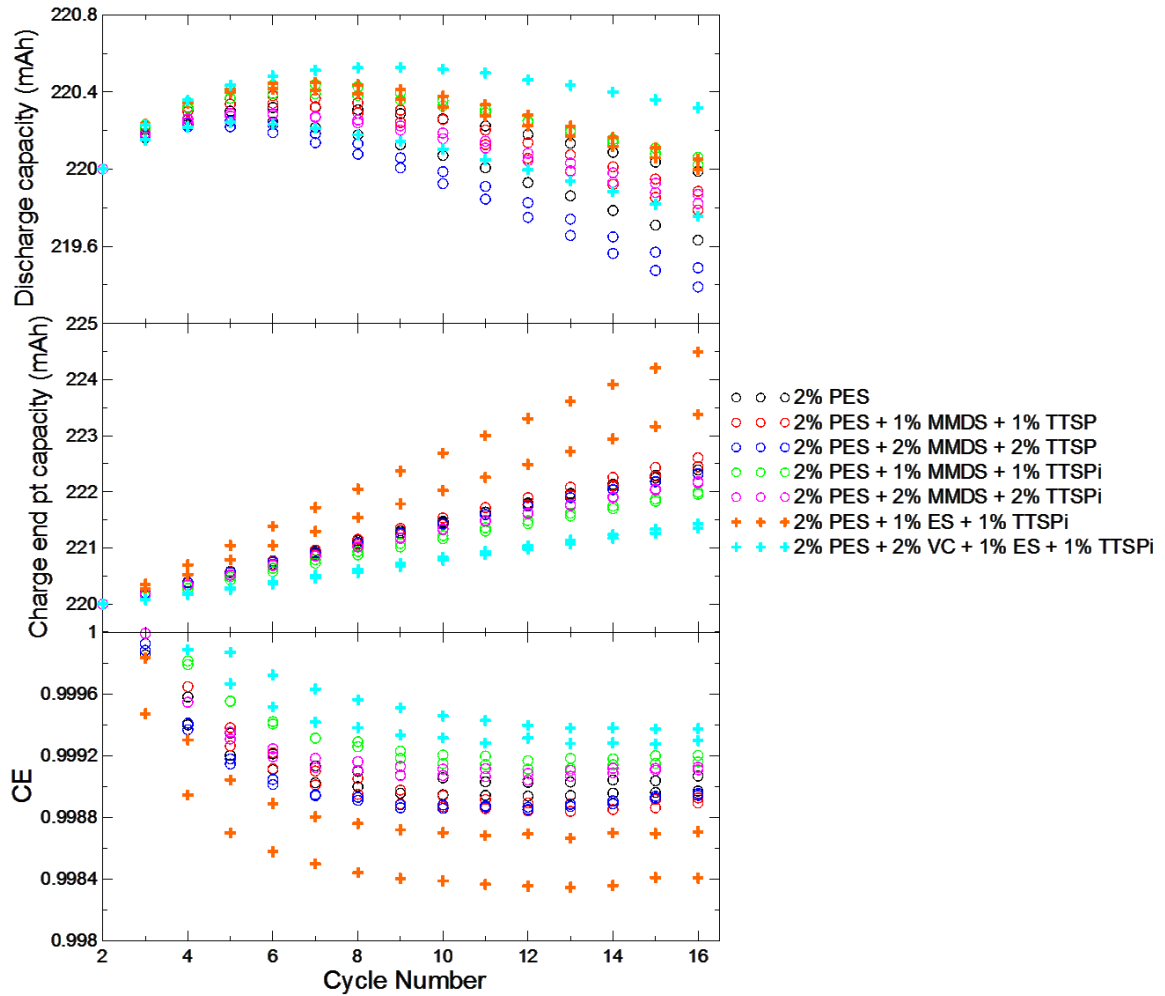


Figure 4.14 The normalized discharge capacity of the cells (a); the normalized charge end point capacity of the cells (b); and the coulombic efficiency of the cells (c), all plotted versus cycle number. The cells were cycled at C/22 between 2.8 and 4.2 V at 40°C

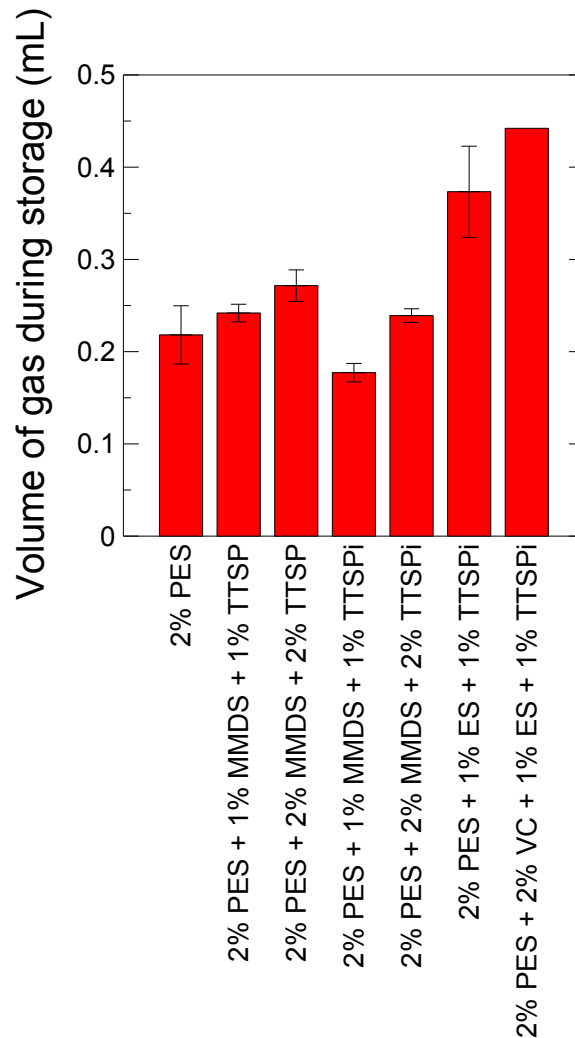


Figure 4.15 Gas evolution during storage at 60°C and 4.4 V measured using Archimedes principle. Cells were not degassed after charging to 4.4 V for the first time.

Connor Aiken at Dalhousie University has used in-situ gas measurements to study the effect of additives and temperature on the volume of gas produced during formation.¹²¹

These experiments allow for the volume of gas to be monitored as a function of time and as a function of voltage. Figure 4.16 shows the volume of gas evolved during formation at 70°C to 4.7 V in NMC442/graphite cells containing 2% PES. There is a gas production peak at approximately 3.5 V, and then the volume of gas begins to decrease in the cell

until approximately 4.3 V, where there is a second gas peak. This figure is an example of the importance of “double-degassing” cells during formation. This means that, during formation, cells should be cut open to release generated gas after charging to 3.5 V, and should be cut open to release generated gas a second time after charging to 4.5 V (or above).

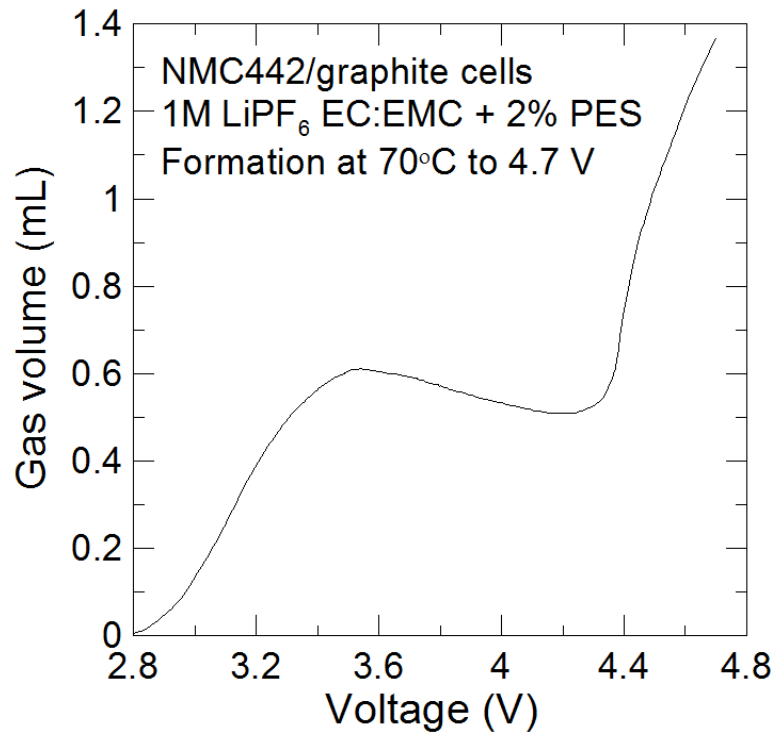


Figure 4.16 Volume of gas evolved during formation at 70°C in NMC442/graphite cells as a function of voltage. Data courtesy of Connor Aiken, Dalhousie University.

The NMC111/graphite cells discussed in this section were not degassed twice. These cells were degassed once after formation to 4.2 V. This is acceptable for the cycling and storage experiments up to 4.2 V, but may account for the large gas evolution during the second storage experiment to 4.4 V, as the cells were not degassed upon the first charge to 4.4 V.

Figure 4.17 shows the voltage versus time during the 600 hour storage period at 4.4 V and 60°C. All additive combinations studied exhibited a severe drop in open-circuit voltage during the storage period. This may be due to the gas evolution that occurred above 4.3 V. The drop in OCV during storage may not have been so severe if these cells were degassed after the first charge to 4.4 V. Furthermore, generation of CO₂ and the subsequent reduction of CO₂ can result in the formation of oxalate, carbonates, and CO.¹²³ A permanent reduction in capacity, and thus drop in OCV during storage, can result when CO₂ is reduced to CO and carbonates. This reduction also increases the thickness of the SEI layer on the negative electrode, as shown by Sloop et al.¹²³ Sloop et al. determined that the evolution of CO₂ lead to the polymerization of EC in both 1M LiPF₆ EC:DMC 1:1 (mole ratio) and 1M LiPF₆ EC:EMC 1:1 (mole ratio) and caused irreversible self-discharge. Therefore, the poor performance of the cells shown in Figure 4.15 and Figure 4.17 may be due to gas production at 4.3 V and the subsequent reduction of gas forming thick SEI layers.

It is important to demonstrate that UHPC measurements have a correlation to long term cycling. Figure 4.18 shows the discharge capacity of NMC111/graphite cells during long term cycling at 55°C and C/2.5 between 2.8 and 4.2 V. Cells containing PES have significantly lower discharge capacity fade than cells containing VC, which is consistent with high precision CE measurements.

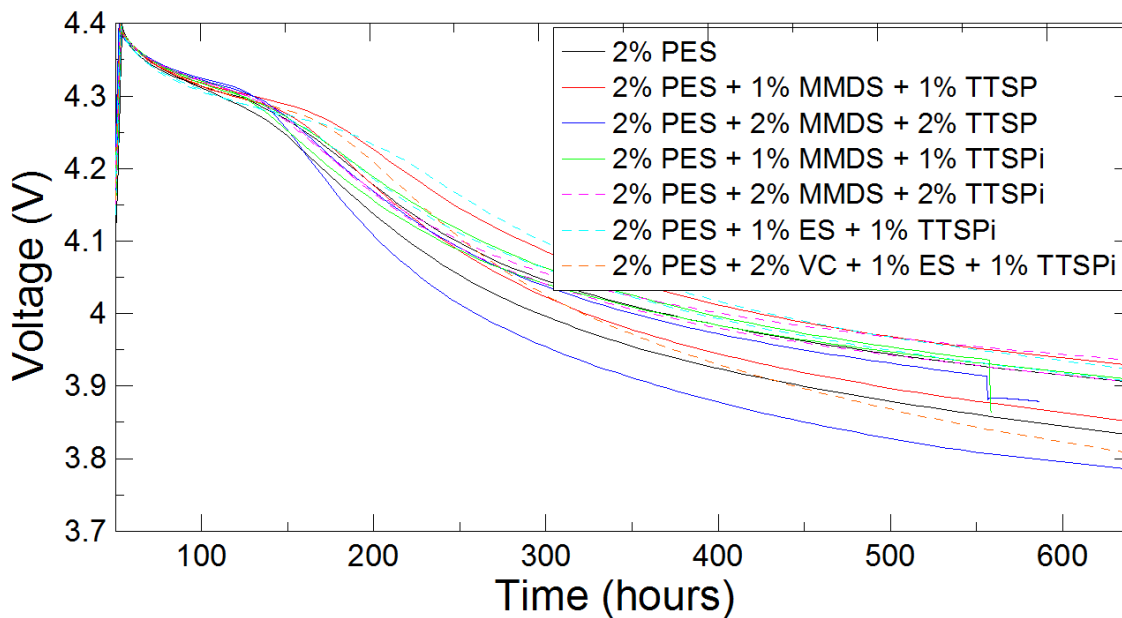


Figure 4.17 The drop in open circuit voltage from 4.4 V during 600 hours of storage at 60°C

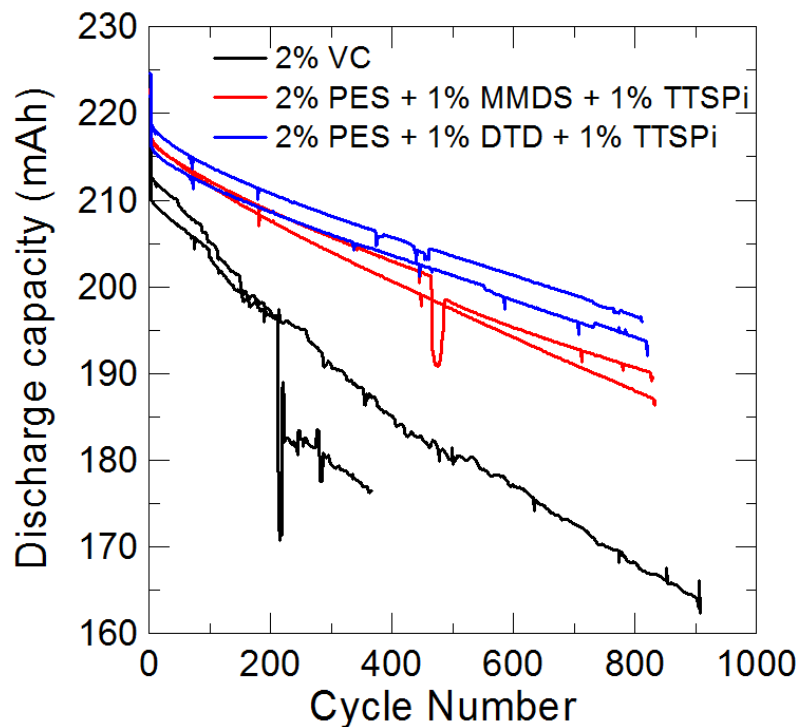


Figure 4.18 The discharge capacity of NMC111/graphite cells as a function of cycle number. The cells were cycled at 55°C and C/2.5 between 2.8 and 4.2 V. Data courtesy of Jian Xia and Lin Ma, Dalhousie University.

4.3.3 CONCLUSION

Through the use of storage and UHPC cycling experiments, the effectiveness of the additive, PES, in combination with other high-performing additives was investigated. While cells containing PES, MMDS and TTSPi have lower discharge capacity fade, lower charge slippage, lower voltage drop during storage and higher CE than cells containing PES, MMDS, and TTSP, this comes at the expense of higher charge transfer impedance. In the range of potentials below 4.2 V, cells containing PES, VC, ES, and TTSPi have the lowest discharge capacity fade, the lowest charge slippage, the highest CE and the lowest charge transfer impedance compared to all additive combinations studied. All additive combinations studied, however, have large gas evolution and severe self-discharge during storage at 4.4 V and 60°C, suggesting that PES with these additive combinations is not useful at high voltage. However, this poor performance may be due to gas produced during the first charge to 4.4 V, which was not removed from the cells. Further experiments exploring the effects of PES on cell performance at high voltage are needed to understand the fate and function of PES at potentials above 4.2 V.

CHAPTER 5. TAP SYSTEM AND FRA MEASUREMENTS

The additive triallyl phosphate (TAP) has been found by Remi Petibon using gas chromatography-mass spectrometry (GC/MS) in two “high voltage electrolytes” produced by Capchem (Shenzhen, China).¹⁰⁵ FEC was also found, using a GC/MS, to be present in one of these electrolytes. Studies of the two Capchem electrolytes as well as studies of the additive TAP have been done to further understand the role of TAP as an additive, and to probe the “high voltage” claim made by Capchem.

5.1 CONCENTRATION STUDY

Studies of a complete range of TAP contents from 0.5% to 6.0% in Li[Ni_{0.4}Mn_{0.4}Co_{0.2}]O₂ (NMC442)/graphite pouch cells were performed. The UHPC at Dalhousie University was used to monitor the coulombic efficiency, charge end point capacity slippage and discharge capacity versus both time and cycle number of the cells. In addition, gas evolution measurements employing Archimedes principle¹²¹ and electrochemical impedance spectroscopy (EIS) measurements were performed.

5.1.1 EXPERIMENTAL

Machine made 240 mAh NMC442/graphite wound pouch cells balanced for 4.7 V operation were obtained dry (no electrolyte added) from Whenergy (Shandong, China). Pouch cells were manufactured and vacuum sealed in a dry room before shipping to

Dalhousie University. After heating to 80°C for 14 hours under vacuum to remove any residual water, the pouch cells were filled with 0.90 g of 1M LiPF₆ in ethylene carbonate (EC): ethyl methyl carbonate (EMC) (Novolyte Technologies, now BASF) in a ratio of 3:7 (by weight) as the control electrolyte. Cells were filled with control electrolyte containing 0.5, 1, 2, 4, and 6% of triallyl phosphate (TAP, Capchem, >94.0%) by weight and compared to cells containing 2% vinylene carbonate (VC, BASF, 99.97%) and cells containing 2% prop-1-ene-1,3-sultone (PES, Lianchuang Medicinal Chemistry Co., 98.20%). Additional cells were filled with 0.90 g of one of two TAP-containing electrolytes made by Capchem. Both Capchem electrolytes contain 2-5% TAP. Capchem 1 was found to have a solvent composition of EC:EMC:DEC 34:27:39 using a GC/MS. Capchem 2 was found to have a solvent composition of EC:EMC:DEC:FEC 33:27:38:2 using a GC/MS by Remi Petibon.

Cells were vacuum sealed using a compact vacuum sealer (MTI Corp.) after electrolyte filling. All cells did a formation cycle at 40 ± 0.1°C, consisting of a 24 hour hold at 1.5 V to ensure adequate electrolyte wetting followed by a C/20 charge to 3.5 V. At this point the cells were transferred into an argon-filled glovebox, cut open just below the heat seal to release generated gas and then vacuum sealed again. Cells then continued formation at 40 ± 0.1°C with a charge to 4.5 V at C/20 and a subsequent C/20 discharge to 3.8 V. After this step, cells were degassed again. Electrochemical impedance spectroscopy was used to measure the combination of charge transfer resistances (both negative and positive electrodes) and resistance due motion of ions through the SEI layers (both negative and positive electrodes), R_{ct} of the cells at 3.8 V and 10. ± 0.1°C. AC impedance

spectra were collected from 100 kHz to 100 mHz with a signal amplitude of 10 mV. These cells were cycled using the Ultra High Precision Charger at Dalhousie University between 2.8 and 4.4 V at $40. \pm 0.1^\circ\text{C}$ and C/22 (10 mA) for 16 cycles. Gas evolution measurements were performed after both degas steps of the formation cycle and after UHPC cycling.

5.1.2 RESULTS AND DISCUSSION

Figure 5.1 shows the gas evolution during formation at 40°C . The red solid bars indicate the gas evolved during formation to 3.5 V. The blue dashed bars indicate the additional gas evolved during formation to 4.5 V. Error bars are the standard deviation of data from pairs of cells. For reference, NMC442/graphite pouch cells filled with control electrolyte (and no additives) produced a total of 1.5 mL of gas during formation up to 4.5 V. Therefore, all electrolytes studied reduce the amount of gas produced during formation compared to electrolyte without any additives. All TAP-containing cells, except for Capchem 2, produce a large volume of gas during formation, most of which is produced below 3.5 V. The presence of FEC in the electrolyte inhibits gas production, most likely because it helps to form an SEI layer on the negative electrode.³ Although the volume of gas evolved in the TAP-containing cells is lower than that of cells containing no additives, TAP is not effective in reducing gas production. The volume of gas produced during formation in the TAP-containing cells was independent of the TAP content in the electrolyte. Capchem 2, VC, and PES –containing cells produce significantly less gas, and PES-containing cells have the lowest gas evolution during formation of all additives studied.

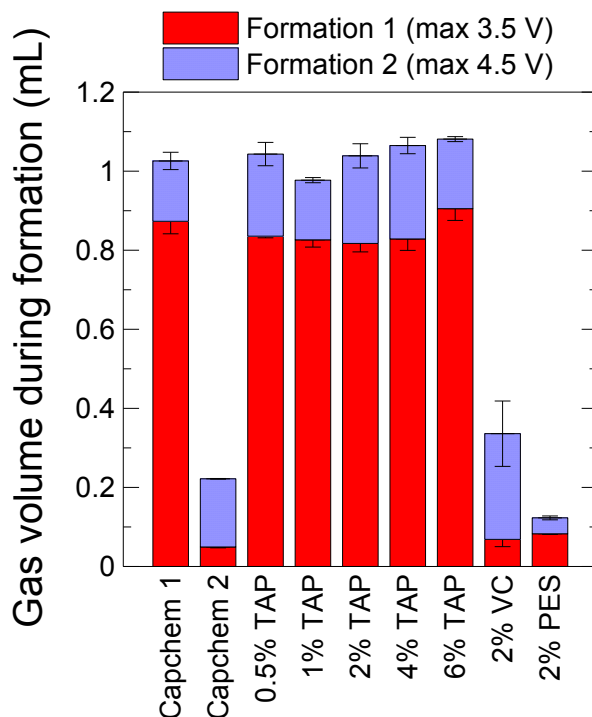


Figure 5.1 Gas evolution during formation at 40°C measured using Archimedes principle.

Figure 5.2 shows the EIS spectra of the cells collected after formation. The EIS data were collected at 3.8 V and 10°C. Figure 5.2 shows that increasing the TAP content in the control electrolyte caused an increase in impedance after formation. This is evidence suggesting that TAP results in the formation of solid resistive species at the negative and/or positive electrodes. As the content of TAP was increased in the electrolyte, TAP may be oxidized or reduced at the corresponding electrodes resulting in a thicker SEI, and thus a higher resistance, \mathcal{R} . While Capchem 1 had low impedance, Capchem 2 had very high impedance. Capchem 2 most likely formed solid resistive species on the negative electrode due to the presence of FEC, whereas Capchem 1 formed mostly gaseous species, not solids, as evidenced by the gas and impedance measurements.

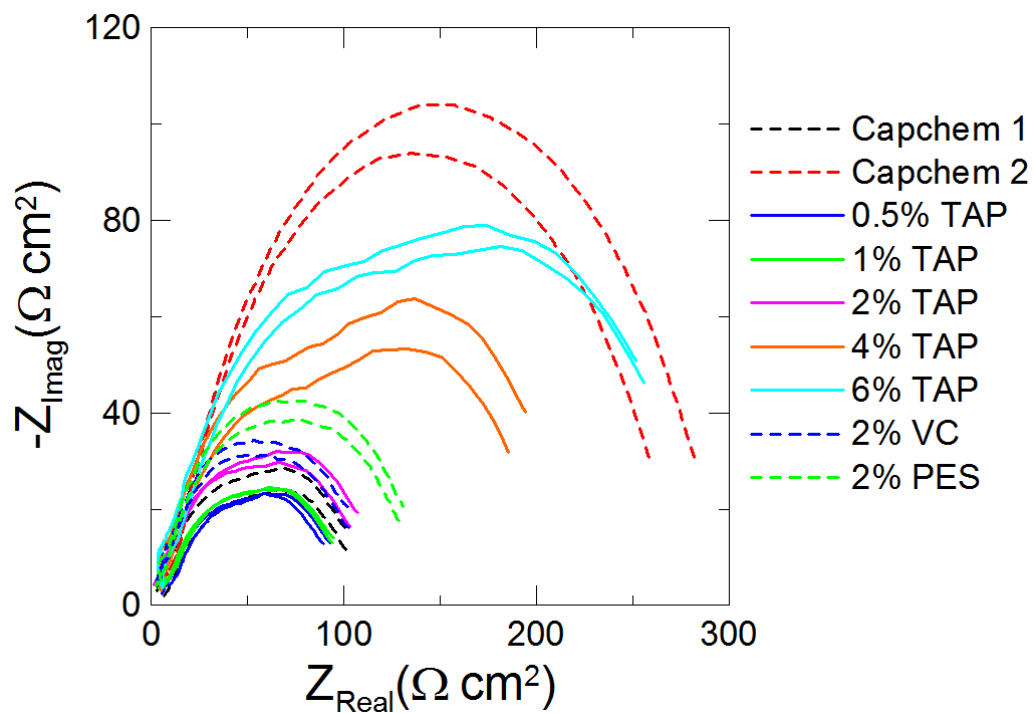


Figure 5.2 EIS spectra of the NMC442/graphite cells collected at 3.8 V and 10°C after formation.

Figure 5.3 summarizes the gas evolution and impedance measurements taken after UHPC cycling at 40°C. The error bars are the standard deviation of data from pairs of cells. Although all cells exhibited low gas evolution during cycling, Figure 5.3a shows that TAP-containing cells produced similar amounts of gas during cycling, all of which were less than that of VC or PES –containing cells. Figure 5.3b shows again that increasing the TAP content in the electrolyte resulted in an increase in charge transfer resistance. All TAP-containing cells increased in impedance during cycling compared to after formation. PES-containing cells had the lowest charge transfer resistance after cycling, and decreased in value after cycling compared to after formation. Although Capchem 2 had large impedance, the impedance was unchanged after cycling compared to after

formation. The impedance spectra shown in Figure 5.3b differs in shape from those shown in Figure 5.2. This was due to different contributions of the positive and negative electrode and the corresponding SEI layers to the cell impedance. This change in shape indicated that the SEI layers were not stable.

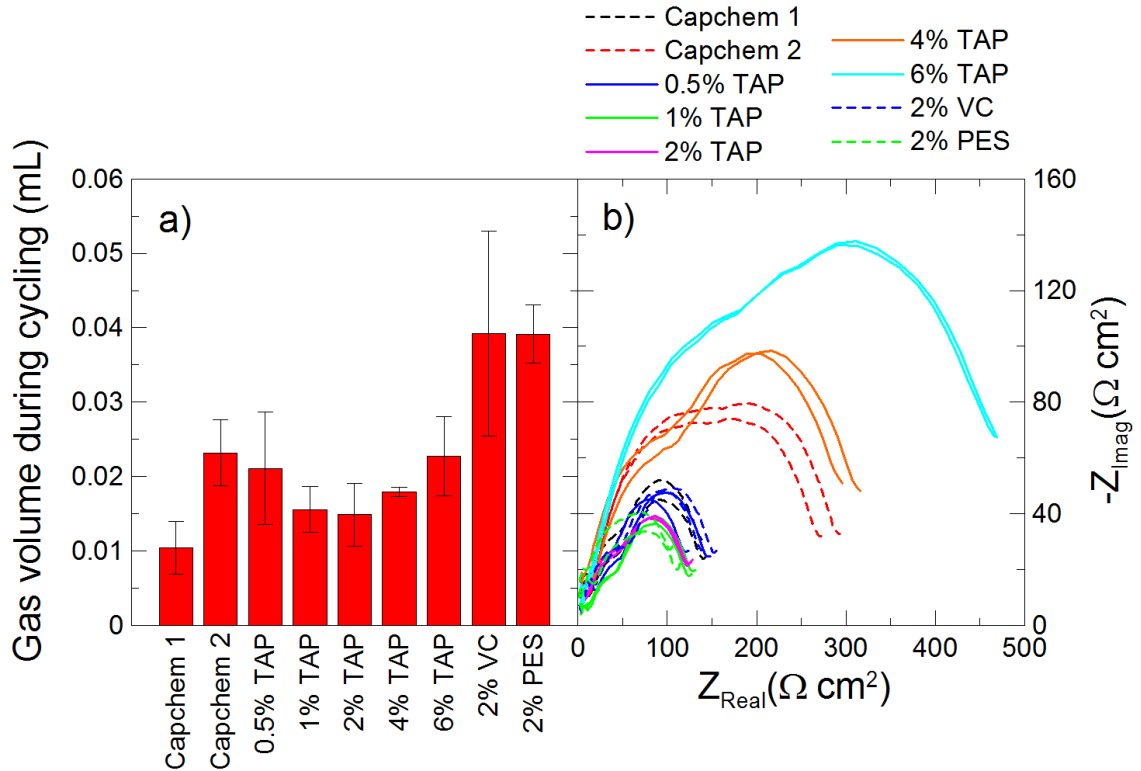


Figure 5.3 Gas evolution during cycling at 40°C (a) and the impedance spectra measured using EIS at 3.8 V and 10°C after cycling (b).

Figure 5.4 shows the results of the UHPC cycling. Figure 5.4a shows the normalized discharge capacity, Figure 5.4b shows the normalized charge end point capacity, and Figure 5.4c shows the CE, all plotted versus cycle number. The true discharge capacity of the cells ranged from 210-227 mAh. Cells containing 4 and 6% TAP have the largest discharge capacity fade, as shown in Figure 5.4a, however they have the smallest charge

end point capacity slippage as evidenced by the small slope in Figure 5.4b. In the absence of impedance growth, the increasing trend, or slippage, of the charge end point capacity is due to electrolyte oxidation at the positive electrode. If there is impedance growth, however, cells will reach the upper cut off voltage earlier than without impedance growth. This can cause discharge capacity fade but reduced charge end point capacity slippage, and therefore result in an apparent untrue improved CE.

Figure 5.5 shows example schematics of a voltage capacity curve during cycling for two cells. Figure 5.5a shows a schematic for a cell without significant impedance growth. The charge and discharge capacity end point slippages are equal, so there is no discharge capacity fade. However, the charge end point capacity slippage is large, and this results in poor CE. This schematic is representative of cells containing 2% PES, which had low impedance and small discharge capacity fade, but large slippage and poor CE. Figure 5.5b shows a schematic for a cell with significant impedance growth. The charge and discharge capacity end points slip at different rates, so there is severe discharge capacity fade. There is low charge end point capacity, however, so the CE is better than that shown in Figure 5.5a. This schematic is representative of cells containing 4 and 6% TAP, which had high impedance and discharge capacity fade, but low slippage and high CE.

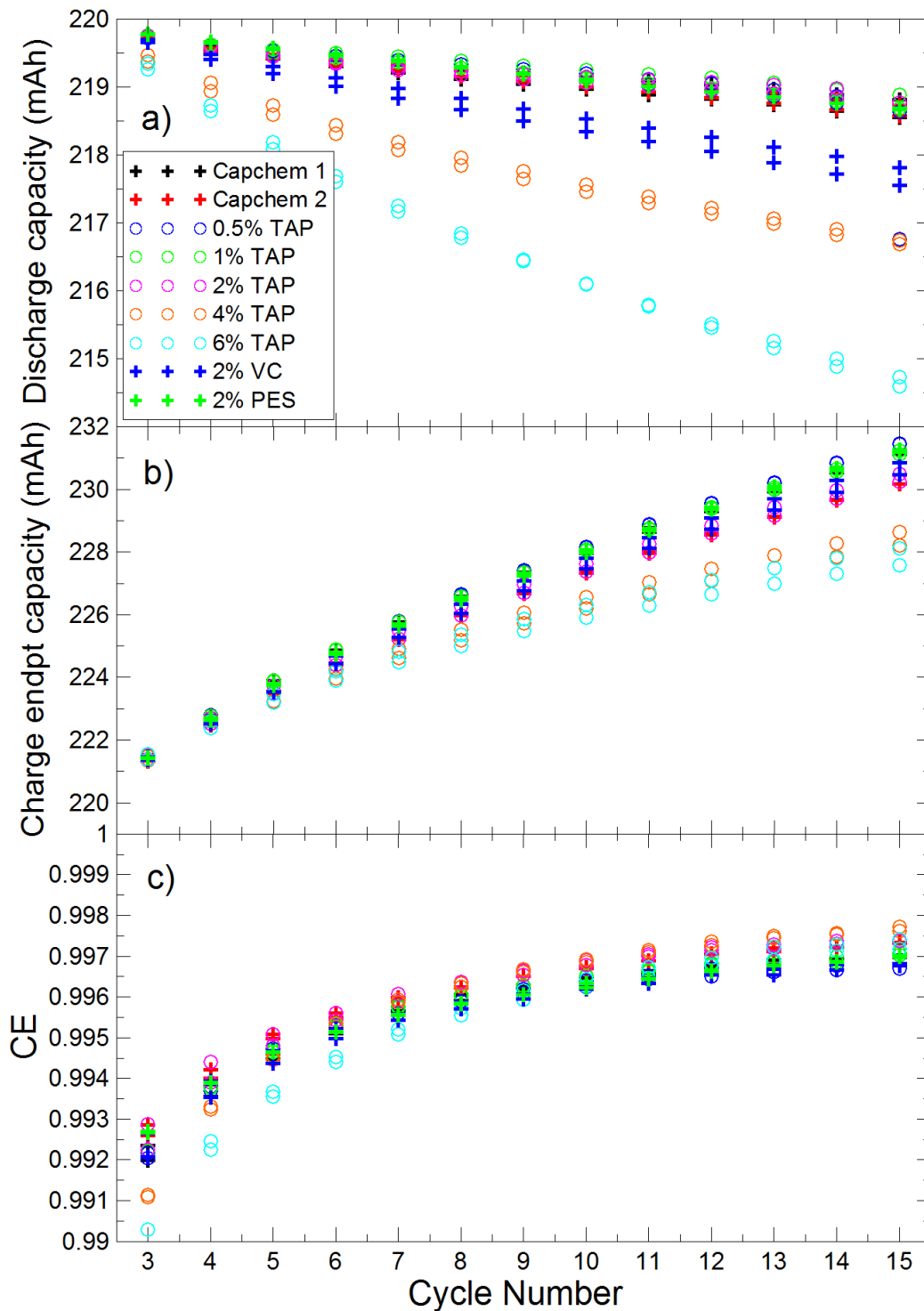


Figure 5.4 The normalized discharge capacity of the cells (a); the normalized charge end point capacity of the cells (b); and the coulombic efficiency of the cells (c), all plotted versus cycle number. The cells were cycled at C/22 between 2.8 and 4.4 V at 40°C.

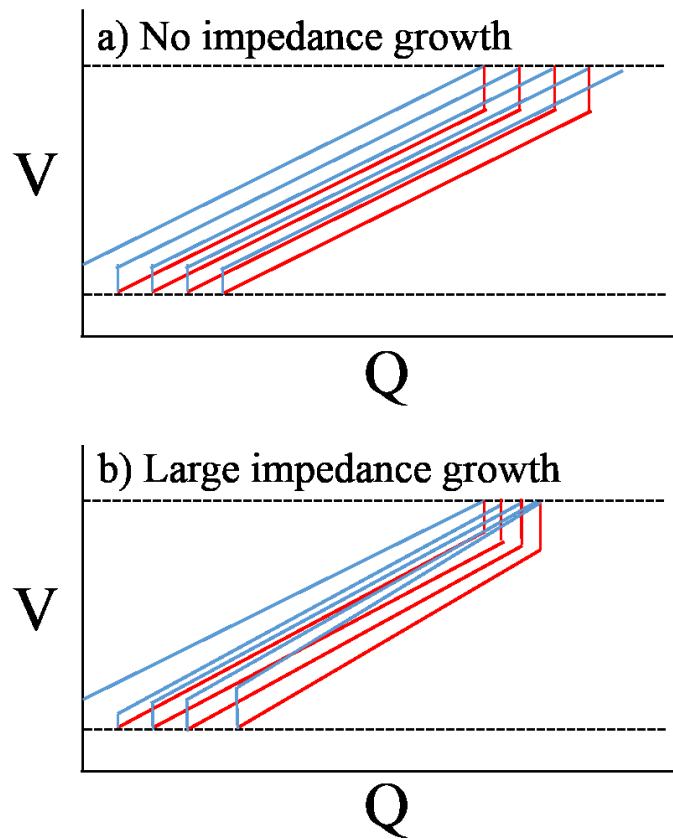


Figure 5.5 Schematic of voltage-capacity curves are a cell with no impedance growth (a) and with large impedance growth (b).

The difference between the average charge and discharge voltages, ΔV , can be plotted versus cycle number to monitor impedance growth. This is useful to determine if the discharge capacity, charge end point capacity, and CE measurements are believable for a given cell. The values of ΔV are plotted versus cycle number for the cells studied in Figure 5.6. All cells show stable values for the difference between the average charge and discharge voltages, except for cells containing 4 and 6% TAP. This explains why these cells had such high CE, and indicate that these measurements are untrue for these cells.

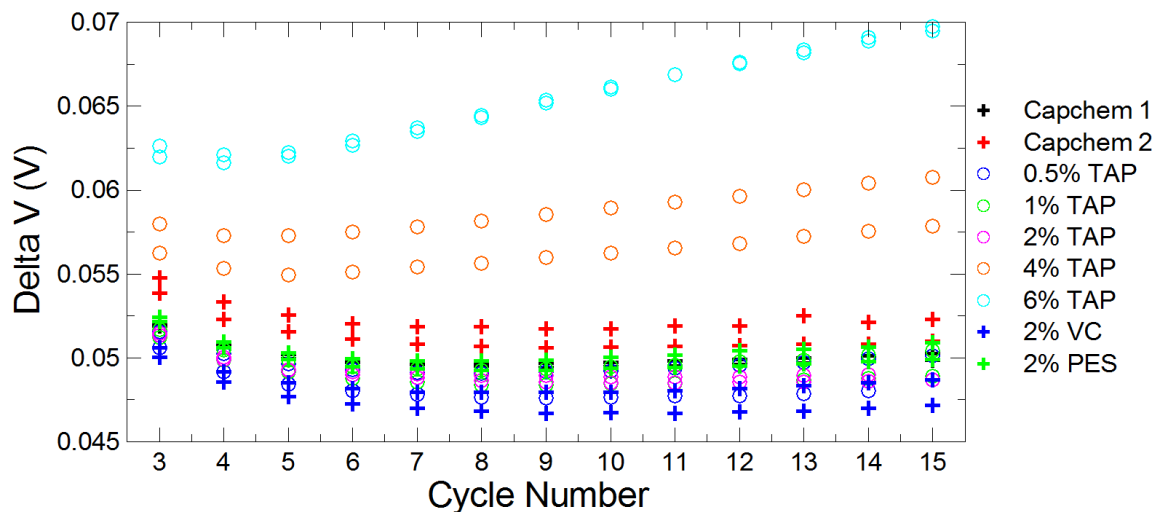


Figure 5.6 The difference between the average charge and discharge voltages of the cells as a function of cycle number.

Figure 5.7 shows a close up of the discharge capacity (top panel) and the CE (bottom panel) for the cells. Cells containing 4 and 6% TAP had the highest coulombic efficiency compared to all other electrolytes studied, but this is a false indication of performance. As the content of TAP in the electrolyte was increased to 4% by weight, the CE also increased. This is due to the large impedance growth as the TAP content increased. VC-containing cells have the lowest CE, indicating that PES and TAP are superior additives in terms of cycling performance. The presence of FEC with TAP results in increased CE and reduced charge end point capacity slippage.

All additive combinations studied have low CE compared to experiments in the range of potentials below 4.2 V, as shown in Chapter 4. This is because at higher voltage, the amount of parasitic reactions increases.

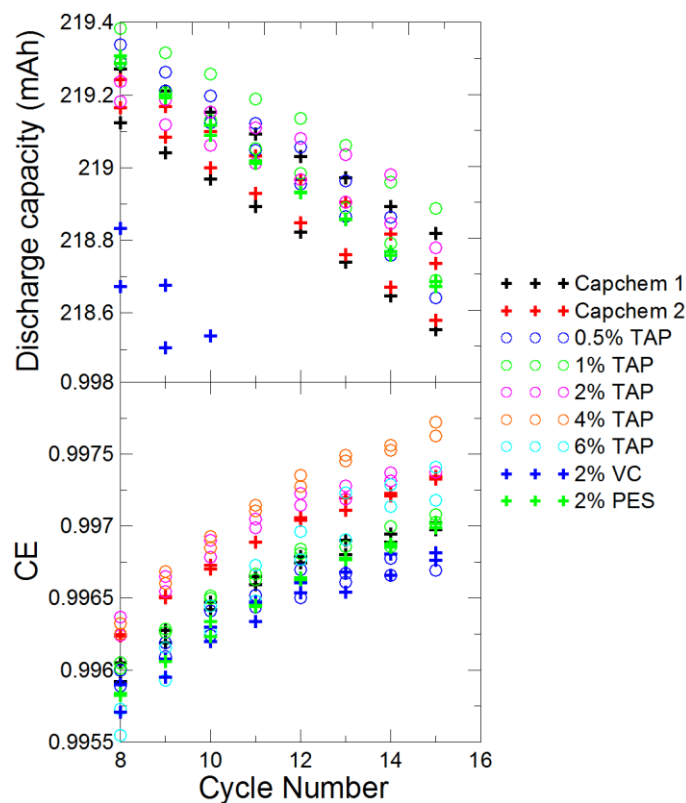


Figure 5.7 A close up of the normalized discharge capacity of the cells (top); and the coulombic efficiency of the cells (bottom), all plotted versus cycle number. The cells were cycled at C/22 between 2.8 and 4.4 V at 40°C.

5.1.3 CONCLUSION

Through the use of UHPC cycling experiments, the effectiveness of TAP as an additive was investigated. Although cells containing VC and PES have low gas evolution during formation and cycling, low charge transfer resistance during formation and cycling, and low discharge capacity fade during cycling, this comes at the expense of low CE. TAP is not effective at reducing gas evolution during formation and formed resistive layers on the electrodes, which became thicker as the content of TAP was increased in the electrolyte. Cells containing 4 and 6% TAP had apparent high values of CE, which were

untrue due to the large impedance growth during cycling and the subsequent severe discharge capacity fade. Further high voltage experiments on the effect of TAP on cell cycling performance and cell impedance are necessary, and are described in Section 5.2.

5.2 FRA STUDY

5.2.1 EXPERIMENTAL

Machine made 240 mAh NMC442/graphite wound pouch cells balanced for 4.7 V operation were obtained dry (no electrolyte added) from Whenergy (Shandong, China). Pouch cells were heated, filled, and sealed with the same method and electrolyte as described in Section 5.1.1. The only electrolyte composition omitted from this FRA study compared to the study described in Section 5.1 was 0.5% TAP, due to lack of available channels and similar performance to cells containing 1% TAP. Therefore, eight NMC442/graphite cells each containing different electrolytes were used for this experiment. Cells underwent the same formation procedure as described in Section 5.1.1.

Cells were cycled using a Maccor series 4000 between 2.8 and 4.4 V at C/5 and 40°C. Every 11 cycles, the cells underwent a charge and discharge at C/20 between 2.8 and 4.4 V while the FRA measured the cell impedance every 0.1 V between 3.6 and 4.4 V. After the FRA sequence, the cells were cycled again between 2.8 and 4.4 V at C/5 for 11 cycles, and the protocol was repeated.

After approximately 40 cycles, some cells were removed due to 1) poor performance or 2) similar performance to other cells being tested. Two additional NMC442/graphite cells

were added to the experiment and filled with 0.90 g of 1M LiPF₆ EC:EMC 3:7 with either 2% PES + 1% MMDS + 1% TTSPi or 2% PES + 2% VC + 1% ES + 1%TTSPi. These cells were added due to the superior cycling and storage performance of cells containing these additive blends as demonstrated in Section 4.3. These cells underwent the same formation procedure as discussed above, and then began cycling with FRA measurements in the same protocol as described above for the original eight cells.

After approximately 65 cycles, the upper cut off voltage during cycling was increased to 4.5 V, and the same 11 cycles-FRA sequence protocol continued. Cells were typically removed from testing once they exhibited a dramatic decrease in discharge capacity that did not stabilize.

5.2.2 RESULTS AND DISCUSSION

Figure 5.8 shows the discharge capacity versus cycle number for the original eight cells. Every 11 cycles there is a gap in the discharge capacity due to the FRA measurement cycle. As the content of TAP was increased in the electrolyte, the discharge capacity decreased. The irreversible capacity loss and the discharge capacity fade were greater as the TAP content increased. Cells containing 2% PES and 1% TAP behaved very similarly and both resulted in the highest discharge capacity and the smallest capacity fade compared to the other electrolytes studied. Capchem 1, Capchem 2 and 2% TAP – containing cells had similar performance with good discharge capacity and small capacity fade. The cell containing 2% VC displayed good performance in terms of discharge capacity for 20 cycles. After 20 cycles, this cell exhibited dramatic discharge capacity

fade, indicating the presence of parasitic reactions and most likely unstable, resistive SEI layers on the electrodes due to electrolyte decomposition.

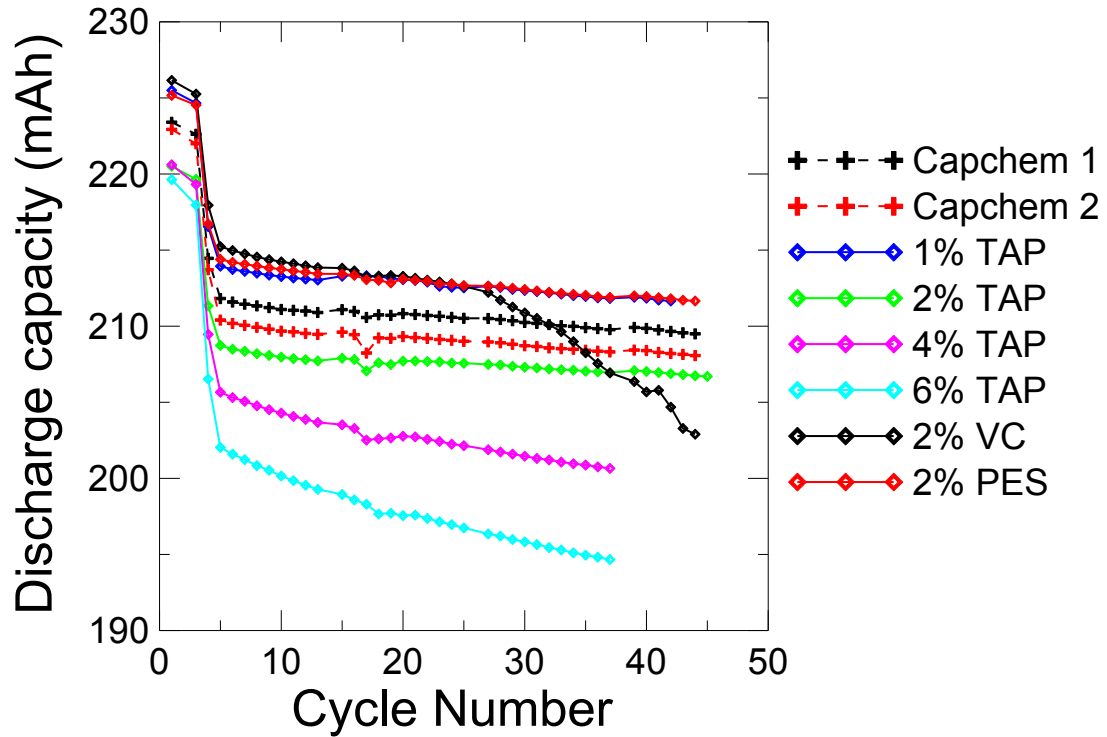


Figure 5.8 Discharge capacity as a function of cycle number for the original eight cells undergoing cycling tests and FRA measurements at 40°C.

Figure 5.9 shows the combined resistance from charge transfer and the motion of ions through the SEI layers as a function of voltage for the original eight cells. Each panel shows the resistance measured during each charge and discharge of the FRA sequence, every 11 cycles, for the cell with the electrolyte additive as labelled. Partial or missing data for an FRA sequence indicates that the cell was removed from testing at that time. All cells exhibited an increase in \mathcal{R} as the voltage increased from 3.8 V. All cells exhibited an increased resistance, \mathcal{R} at all voltages as the cycle number increased.

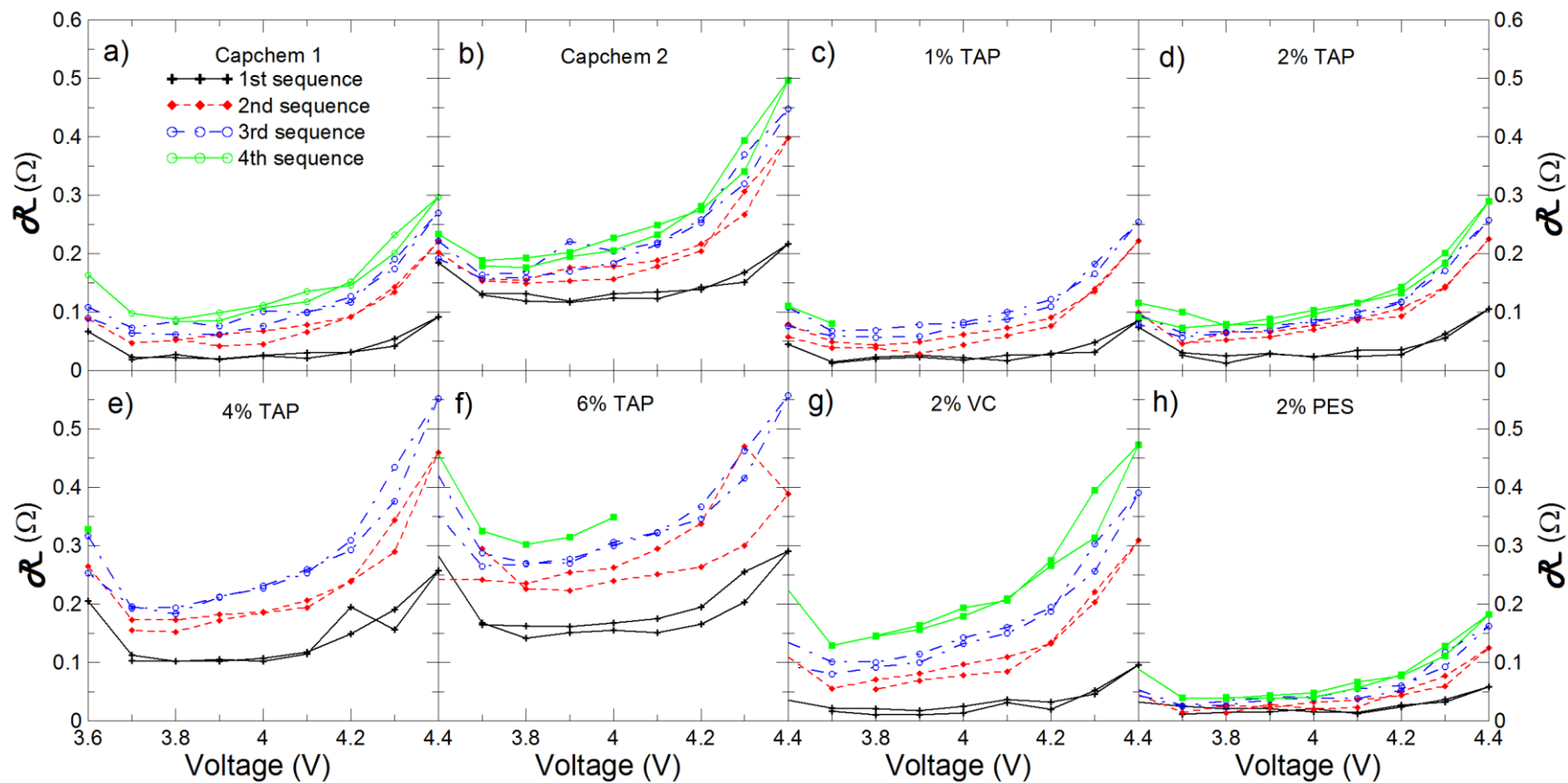


Figure 5.9 The combination of charge transfer resistances (both negative and positive electrodes) and resistance due to motion of ions through the SEI layers (both negative and positive electrodes, \mathcal{R} as a function of voltage for the original eight cells measured every 11 cycles.

Several interesting features are shown in Figure 5.9. All cells exhibited a significant increase in resistance, \mathcal{R} after the first FRA sequence (ie. after 11 cycles), and the impedance measured during the subsequent FRA sequences (every 11 cycles) appear to begin stabilizing for most cells.

As the content of TAP was increased in the electrolyte, the resistance, \mathcal{R} also increased. This suggests that the increased content of TAP resulted in thicker, and thus more resistive, SEI layers. This is consistent with the findings in Section 5.1. The resistance as a function of voltage for the Capchem 1 –containing cell was similar to that of the 2% TAP –containing cell. Capchem 2 and VC –containing cells had large impedance, which did not appear to stabilize during subsequent cycles. The 2% PES –containing cell had incredibly low impedance at all voltages measured.

Although the resistances of all cells increased with voltage, particularly at 4.4 V, the resistance measured after charging to 4.4 V returned to the value (or very similar) of the resistance measured before charging to 4.4 V. Despite having high impedance at 4.4 V, this large impedance was not permanent upon discharge, and the resistance, \mathcal{R} was mostly reversible during one FRA charge and discharge sequence. This suggests that there was temporary electrolyte oxidation at 4.4 V in which electrolyte formed resistive species on the positive electrode SEI. Another possibility for the cause of the reversible impedance is a physical restructuring of the positive electrode upon delithiation, and a restoration to the previous physical structure upon lithiation. However, this does not account for the significant differences observed for different electrolytes.

Figure 5.10 shows the discharge capacity as a function of cycle number for the cells that were chosen to continue testing. The vertical dashed line indicates when the upper cut off voltage was increased to 4.5 V. This figure also includes the additional cell containing 2% PES + 1% MMDS + 1% TTSPi, which will now be referred to as PES211. The other additional cell containing 2% PES + 2% VC + 1% ES + 1% TTSPi is not included in any figures, as it exhibited severe capacity fade in very few cycles. Despite the superior performance of this additive blend in experiments to 4.2 V, as shown in Section 4.3, this additive blend was not useful in experiments up to 4.4 V and has thus not been included in any figures or further discussions.

As expected, the discharge capacity of all cells increased when the voltage range was increased, due to the increased energy density when the average cell voltage is increased. However, an increased average cell voltage also increases the amount of parasitic reactions that occur. The Capchem 2 –containing cell had severe discharge capacity fade immediately following the increase in voltage, after 65 total cycles. The Capchem 1 – containing cell had higher discharge capacity, but also had severe capacity fade after 90 cycles. Although the 2% PES –containing cell had the highest discharge capacity, this cell also exhibited severe capacity fade after 115 cycles. The 2% TAP – containing cell exhibited a more gradual decrease in discharge capacity, until approximately 150 cycles. The slight increase in capacity of this cell at 210 cycles resulted from clamping the cell, in an effort to increase the stack pressure and improve cell performance. The clamp was not effective, since the capacity increased minimally and then decreased rapidly. The PES211 –containing cell had the best discharge capacity and 90% capacity retention (at

cycle 175) during cycling to 4.5 V. This cell has the most cycles before severe capacity fade, which has not occurred yet, and is still under test.

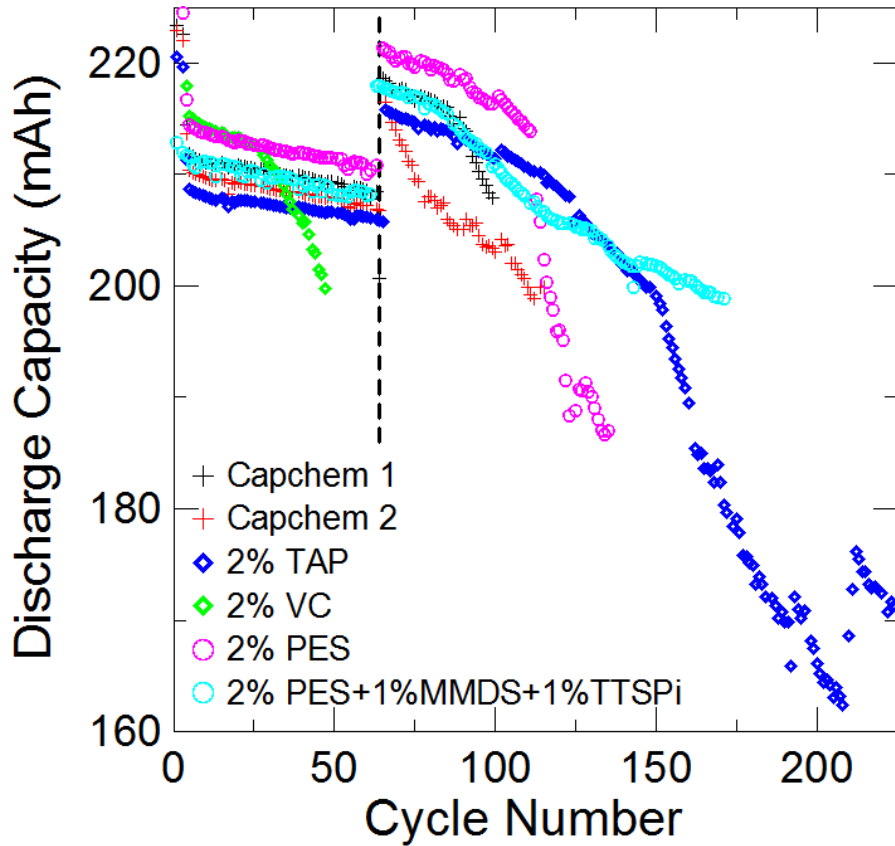


Figure 5.10 Discharge capacity as a function of cycle number for the cell chosen for continued cycling tests and FRA measurements at 40°C.

Figure 5.11 is a Bode representation of an example impedance spectra of the cell containing 2% TAP. The top panel shows the real component of impedance and the bottom panel shows the imaginary component of impedance, both as a function of frequency. The black dotted line indicates the raw data, and the blue solid line indicates the contribution of the experimental setup to the impedance measured using a 1 ohm resistor. A 1 ohm resistor was used for simplicity. The experimental setup mostly

contributes to the imaginary component of impedance at high frequencies. After subtracting 1 ohm from the real component of impedance from the resistor, the resulting calibration data was subtracted from all raw data presented in this thesis. The red dotted line indicates the final data.

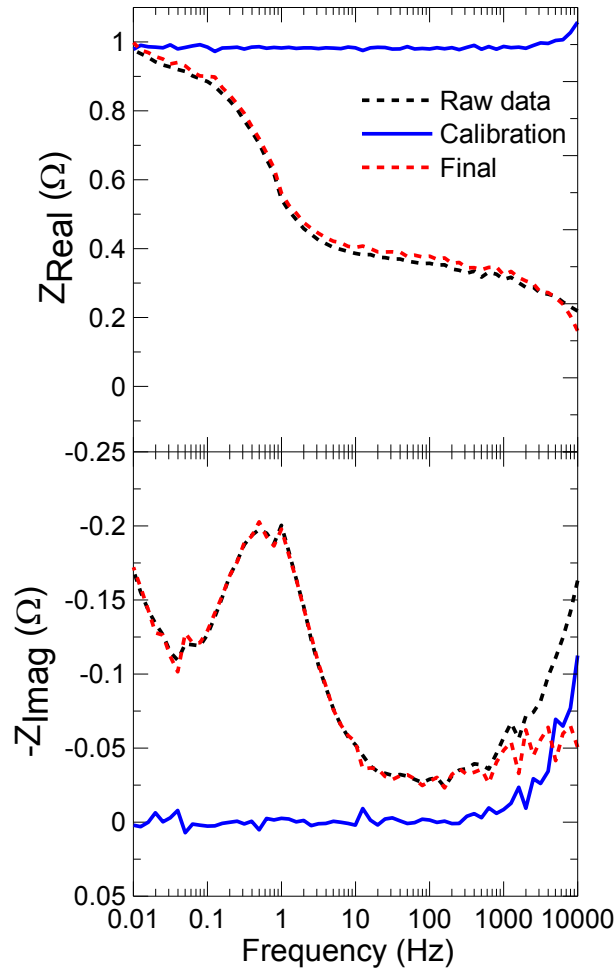


Figure 5.11 A Bode representation of the raw data, calibration data, and final data of an example cell containing 2% TAP.

Figure 5.12 is a Nyquist representation of the impedance spectra of the cell containing 2% TAP at each FRA sequence, every 11 cycles, measured at 4.4 V. The spectra grows

with increasing cycle number, as indicated in Figure 5.12. The shift of the first minimum of the spectra to larger values in the x-axis indicates an increase in the electrolyte resistance with increasing cycle number. The high frequency tail that occurs at low values of the real axis is most likely an artifact due to the subtracted calibration data not accounting for all impedance contributions from the experimental setup.

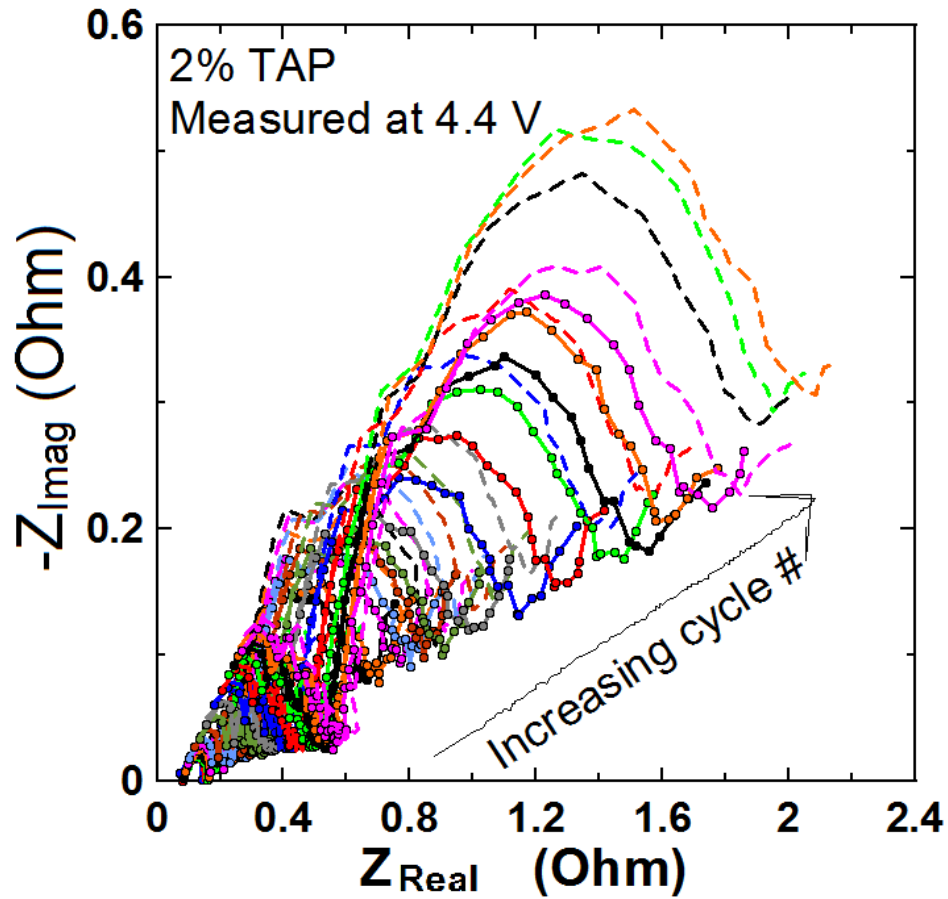


Figure 5.12 Impedance spectra of the 2% TAP-containing cell for every FRA cycle, measured at 4.4 V.

Figure 5.13 is a Nyquist representation of the impedance spectra of the cell containing 2% TAP for every measured voltage of the FRA sequence during cycle 149. The dotted

line indicates measurements taken during discharge. The spectra grows with increasing voltage. The electrolyte resistance is constant during one cycle.

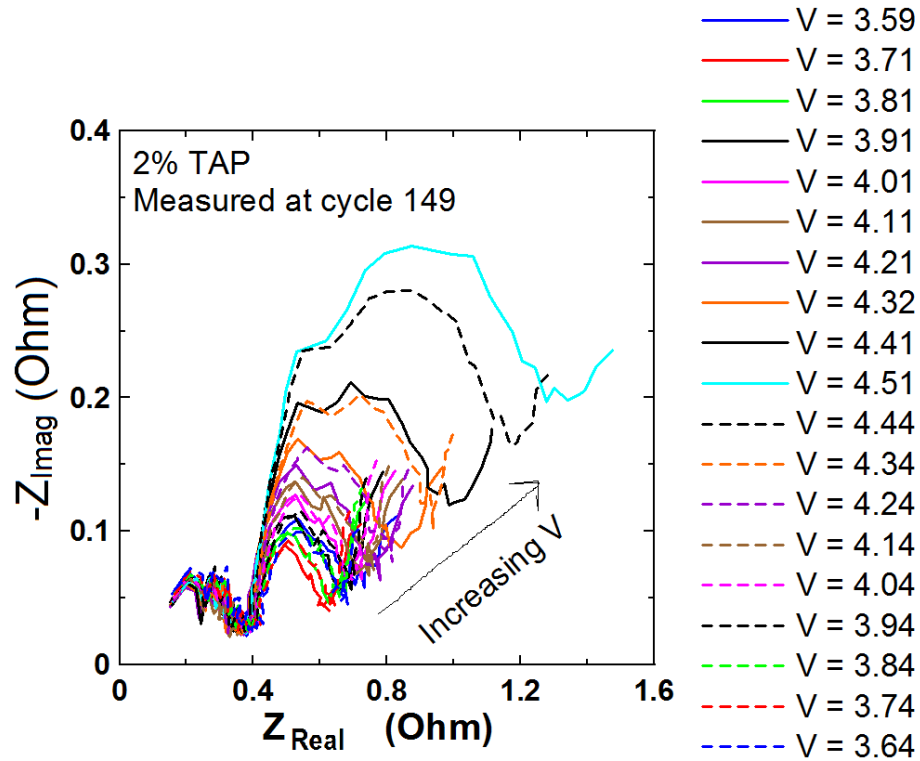


Figure 5.13 Impedance spectra of the 2% TAP-containing cell at every voltage measured during cycle 149.

Figure 5.14 shows the resistance, \mathcal{R} as a function of voltage for the six cells chosen for continued testing. Each panel shows the resistance measured during each charge and discharge of the FRA sequence, every 11 cycles, for the cell with the electrolyte additive as labelled. Partial or missing data for an FRA sequence indicates that the cell was removed from testing at that time.

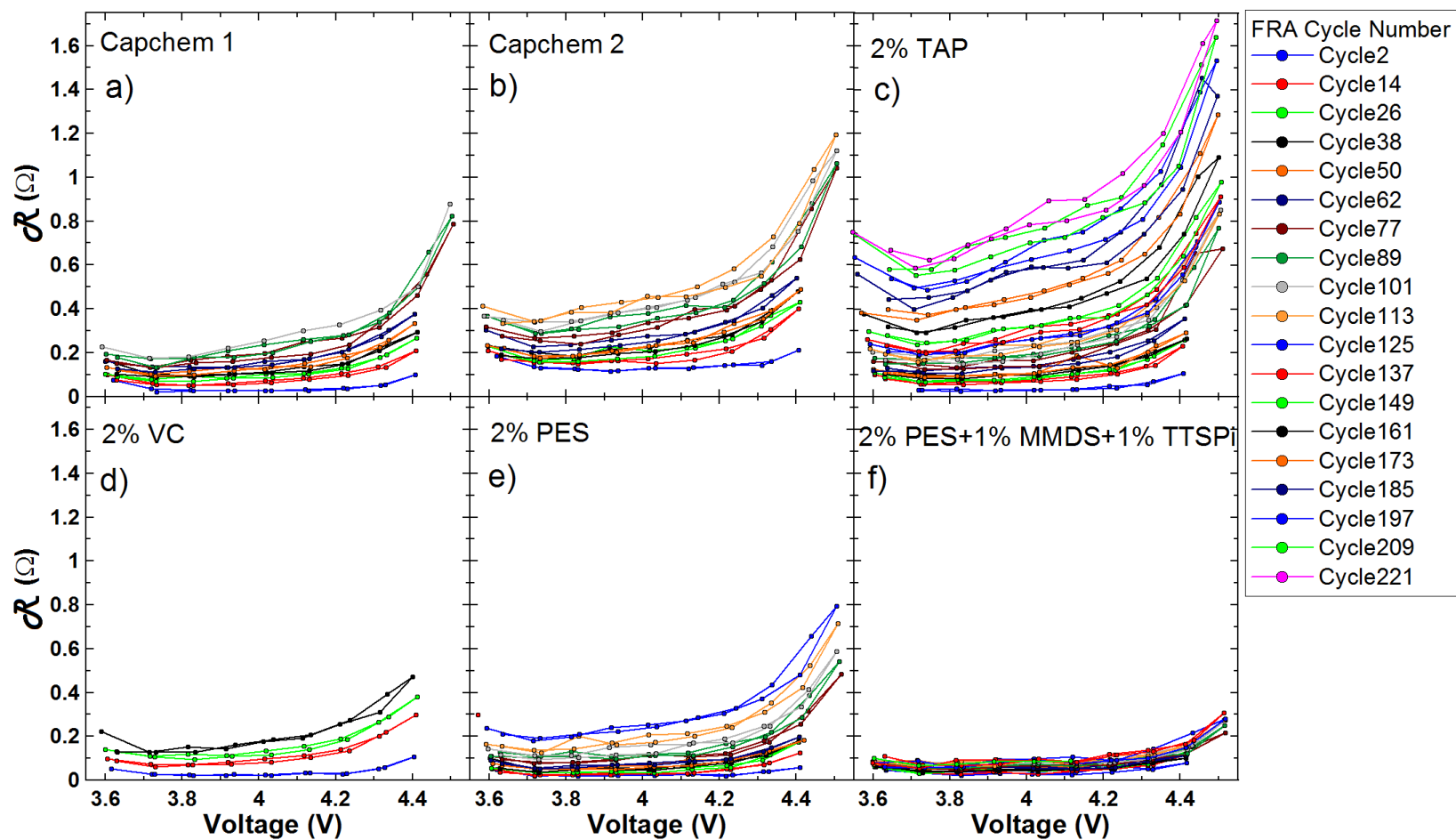


Figure 5.14 The combination of charge transfer resistances (both negative and positive electrodes) and resistance due to motion of ions through the SEI layers (both negative and positive electrodes), \mathcal{R} as a function of voltage for the cells chosen for continued testing measured every 11 cycles.

Figure 5.14 has many interesting features. As shown in Figure 5.9, all cells exhibited an increase in resistance as the voltage increased from 3.8 V and all cells exhibited an increased resistance at all voltages as the cycle number increased. The cell containing PES211 had very low impedance measured at all voltages during every FRA cycle. When the upper cutoff voltage was increased to 4.5 V, the impedance of all cells increased dramatically, except for PES211. Despite this increased impedance at 4.5 V, the impedance measured at 4.4 V upon discharge decreased such that the value is nearly the same as the value measured upon charge.

The reversibility in resistance, particularly from 4.5 V to 4.4 V, is thought-provoking. Possible explanations for this are 1) resistive species are temporarily formed at 4.5 V, and return to solution upon discharge to 4.4 V; or 2) physical restructuring of the electrodes or SEI layers caused by high potential increases the impedance temporarily; 3) others.

Graphite has a volume expansion of approximately 10% during intercalation.¹²⁴ Although this change in volume is small, particularly compared to the 280% expansion exhibited by silicon negative electrodes, it may still lead to stress and electrode degradation.¹²⁴ Qi and Harris investigated the strain during lithiation in graphite electrodes, and they determined that stress related to the volume expansion can cause fracture of active material, particularly with prolonged cycling.¹²⁴ Similar fracture of active material may occur at the positive electrodes during delithiation. If the volume expansion and stress during intercalation is not severe enough to cause particle fracture, it may still cause a temporary increase in impedance during full lithiation and delithiation. This should be

independent of the additives in the electrolyte, so it cannot account for the dramatic differences observed in the impedance for different additives.

Zhang et al. observed that the charge transfer resistance of graphite electrodes in 1M LiPF₆ EC:PC:EMC 1:1:3 and 1M LiPF₆ in EC:EMC 3:7 is a function of potential.¹²⁵ They also observed reversible behaviour in the impedance when the cells were cycled between 1 and 0.02 V. They suggested that the reversible nature of the impedance with voltage was due to physical restructuring of the SEI on the negative electrode from volume expansion during cycling.¹²⁵ They also suggested that there is dissolution of SEI species into the electrolyte during cycling. The reversible nature of the impedance of positive electrodes was explained by Aurbach et al.¹²⁶ and Levi et al.¹²⁷

Aurbach et al. measured the R_{ct} of LiNiO₂ electrodes between 3.6 and 4.2 V.¹²⁶ They found that the R_{ct} was at a minimum at 3.7 V, and that the R_{ct} increased dramatically below 3.65 V and above 4.05 V. Aurbach et al. also measured the R_{ct} of LiMn₂O₄ electrodes between 3.0 and 4.4 V, a range chosen such that the electrode had good stability.¹²⁶ They found that the high frequency feature (up to 200 kHz) of the impedance spectra increased during the first 6 cycles, unlike the LiNiO₂ electrode. This feature then stabilized during subsequent cycles, and the impedance was reversible. They observed that the resistance and interfacial capacitance increased dramatically, from 46 to 227 Ω and 1.7 to 9 mF, respectively, during 45 cycles at C/7. This increase was claimed to be caused by destructive processes, such as Mn dissolution and electrode degradation due to acidic electrolyte components. Levi et al. measured the R_{ct} of LiCoO₂ electrodes between

3.8 and 4.1 V.¹²⁷ They found that the R_{ct} was at a maximum at 3.8 V, and then decreased with increasing voltage, which is not consistent with the findings in this thesis. However, since NMC442/graphite cells were used in this thesis, it is possible that the increasing impedance with increasing voltage observed with LiNiO_2 and LiMn_2O_4 electrodes dominates, and not the decreasing impedance with increasing voltage observed with LiCoO_2 electrodes. Therefore, the findings by Zhang et al.¹²⁵ and Aurbach et al.¹²⁶ are consistent with the findings presented in this thesis of the reversible impedance of NMC442/graphite cells that increased with voltage.

Love and Swider-Lyons recognized the reversible nature of impedance with LiCoO_2 positive electrodes.¹²⁸ They studied the use of impedance measurements to diagnose overcharged Li-ion cells. They observed that the charge transfer resistance was reversible between 2.8 and 4.2 V, and only increased slightly during 200 cycles.¹²⁸ The charge transfer resistance was not reversible when the cells were overcharged, as this caused degradation and the formation of an insulating layer on the positive electrode. Therefore, by monitoring the impedance, overcharged cells could be differentiated from healthy cells.

Figure 5.15 shows the resistance, \mathcal{R} , versus cycle number measured at 4.4 V for three types of cells. A change in slope occurs around 65 cycles, when the upper cut off voltage was increased to 4.5 V, for the 2% PES-containing cell. The increase in slope of the 4.5 V data compared to the 4.4 V data indicates the increase in parasitic reactions and resistive species formed on the electrodes when in the presence of 2% PES. The PES211-

containing cell does not exhibit any change in slope, as shown in Figure 5.15b. This is consistent with the gradual capacity fade shown in Figure 5.10, and demonstrates the superiority of the PES211 additive combination. The slope for the 2% TAP-containing cell is constant until 150 cycles and then there is an increase in slope. This is consistent with the severe discharge capacity fade exhibited by this cell at 150 cycles, as shown in Figure 5.10. This also indicates that, although the impedance of the 2% TAP-containing cell continued to increase with cycle number, it was not immediately affected by the increase in upper cut off voltage.

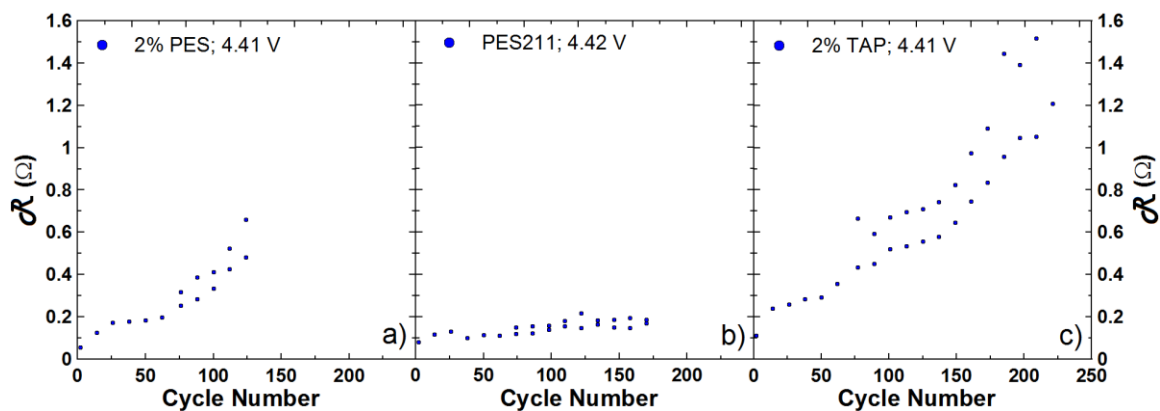


Figure 5.15 The combination of charge transfer resistances (both negative and positive electrodes) and resistance due to motion of ions through the SEI layers (both negative and positive electrodes), \mathcal{R} , measured at 4.4 V as a function of cycle number for the cell containing 2% PES (a), PES211 (b), and 2% TAP (c).

Further experiments must be done to probe the reversible nature of the impedance. Upon charging to an upper cut off voltage of 4.6 V, perhaps the impedance will be less reversible. Impedance measurements at low voltage (ie. down to 2.8 V) are also necessary.

5.2.3 CONCLUSION

Through the use of cycling and impedance measurements, the effectiveness of TAP and PES as electrolyte additives for high voltage applications was investigated. All cells, except that containing PES211, exhibited an increase in impedance with increasing voltage and increasing cycle number, with a dramatic increase in impedance during 4.5 V cycling. PES and PES211 result in extremely low impedance at all voltages during cycling. The cell containing PES211 was the only cell studied that did not exhibit severe capacity fade, and is a promising additive blend for high voltage applications. Further experiments investigating the nature of the reversible impedance are needed.

CHAPTER 6. CONCLUSION

6.1 CONCLUSIONS

Lithium-ion batteries are used in portable electronics, electric vehicles, and grid energy storage. Electric vehicles and grid energy storage require battery lifetimes of 10-30 years, so improved Li-ion batteries are necessary for the success of these applications. Electrolyte additives are one of the most effective and economical ways to improve Li-ion batteries. Investigating the effects of electrolyte additives in Li-ion cells and understanding their fate and function are therefore essential.

The SEI layers on the positive and negative electrodes play a critical role in the stability, performance, and safety of Li-ion cells. Additives are known to affect the formation and growth of the SEI layers, however the composition and growth mechanisms of the SEI layers are still poorly understood. The importance of using high precision coulometry experiments to evaluate electrolyte additives coupled with gas evolution and impedance measurements to understand the function of electrolyte additives was discussed in Chapter 2 and Chapter 3.

Cells containing the additive PES alone were found to have comparable cycling performance to those containing VC alone in experiments up to 4.2 V, and had superior performance in experiments up to 4.5 V. The main advantage of PES is the elimination of nearly all gas production during storage at 60°C and 4.2 V. Combinations of PES and other additives also result in gas reduction and improved performance during storage and cycling. Cells containing PES alone and PES in combination with other additives have

remarkably low impedance, even during cycling to 4.5 V. The low gas evolution and low impedance of PES-containing cells indicates that PES is involved in forming desired SEI layers.

Cells containing the additive TAP were found to have very high impedance which increased as a function of TAP concentration. However, in cycling experiments up to 4.4 V, TAP-containing cells showed low charge end point capacity slippage and high CE. The CE measured for all NMC442/graphite cells in experiments up to 4.4 V were dramatically lower than that measured for NMC111/graphite cells in experiments up to 4.2 V. Therefore, there is still a great amount of work to be done to understand SEI formation and electrolyte degradation during high voltage experiments in order to produce Li-ion cells with higher energy density and longer lifetimes.

Experiments combining cycling with impedance measurements concluded that the resistance of all cells increased with cycle number and with increasing voltage. However, during one charge-discharge FRA measurement, the impedance was reversible. The reversible nature of the impedance provides insight to the SEI formation and growth processes. Further experiments designed to understand the reason for the reversible impedance changes are necessary, and suggestions are described in Section 6.2.

6.2 FUTURE WORK

The work presented in this thesis demonstrated the advantage of particular electrolyte additives, such as PES, and additive blends through several experimental techniques.

High precision cycling and storage experiments are very valuable and can distinguish beneficial additives from non-beneficial additives. Electrolyte additives and the way in which they improve Li-ion cells are still poorly understood. Further experiments designed to understand the fate and function of well-performing additives in Li-ion cells are necessary. By understanding how additives work, why they work, and where in a Li-ion cell they are beneficial, new additives can be engineered and the selection of additives for specific applications may be possible.

Analyzing the electrolyte in Li-ion cells as a function of time or cycle number using GC/MS can provide insight to when the additives are consumed and what byproducts are formed. Using liquid-liquid extraction, the organic components of the electrolyte can be analyzed using GC/MS, without damage to the equipment.¹²⁹ For example, the electrolyte was extracted from two NMC111/graphite cells after formation. One cell contained 1M LiPF₆ EC:EMC 3:7 with 2% DTD, and the other with 2% DTD + 2% VC. Figure 6.1 shows the chromatogram (total ion count) for both cells, as labelled. Compounds labelled in red are only observed in the presence of VC and compounds labelled in black are only observed in the absence of VC. Compounds labelled in blue are observed in both cells. In the absence of VC, DTD is fully consumed during formation. Several additional peaks are observed in the absence of VC, including DMC and DEC, indicating transesterification. In the presence of VC, DTD is not fully consumed, and there is no evidence of transesterification.

Analyzing the gas produced in cells during formation, cycling, and storage experiments using GC/MS can also provide useful information about electrolyte degradation and SEI formation.

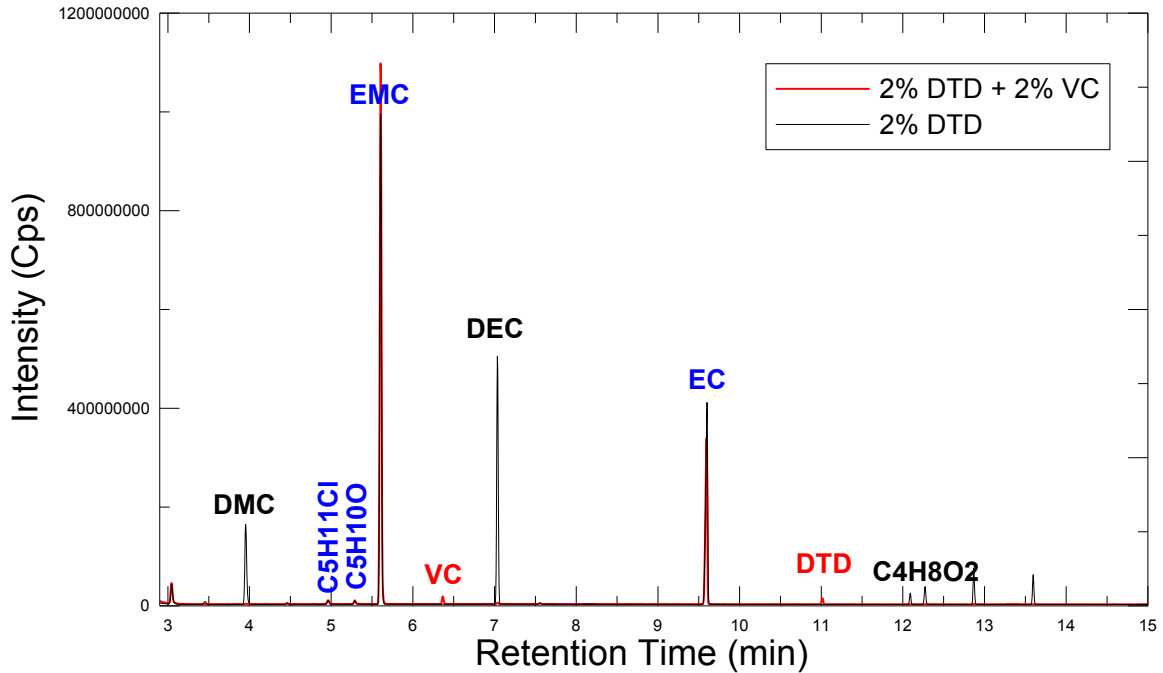


Figure 6.1 Chromatogram (total ion counts) of extracted electrolyte from NMC111/graphite cells initially containing 2% DTD or 2% DTD + 2% VC.

Testing Li-ion cells under practical conditions for specific applications is of course necessary. Success of electrolyte additives under typical laboratory tests is not always indicative of real-world performance. The effect of a hold or rest period at high voltage on the performance of Li-ion cells, for example, is an important experiment. Phones, computers, and electric vehicles relying on Li-ion batteries will often sit at high voltage for extended periods of time due to convenience for the user. However, this rest or hold at

high voltage may have detrimental effects on the performance of Li-ion cells. The amount of parasitic reactions may be significantly increased during aging at high voltage.

As a preliminary test of the effect of prolonged high voltage exposure of Li-ion cells, three electrolytes in NMC442/graphite cells were tested. Cells filled with 2% TAP, PES211, and 4% PES + 1% MMDS + 1% TTSPi (referred to as PES411) were cycled using a Maccor series 4000 combined with impedance measurements using a Maccor FRA model 0356. After a formation cycle as described in Chapter 5, these cells underwent three cycles between 2.8 and 4.4 V at C/5 with a 24 hour hold at 4.4 V every cycle. After three cycles at C/5, the cells underwent one cycle at C/20 between 2.8 and 4.4 V with FRA measurements every 0.1 V between 3.6 and 4.4 V. This protocol was then repeated.

Figure 6.2 shows the discharge capacity for the cells as a function of cycle number. All cells exhibit large capacity fade when subjected to a 24 hour hold at 4.4 V compared to without a hold (shown in Section 5.2). Similar cells cycling without a hold exhibited less than a 10% fade in discharge capacity after 65 cycles, as shown in Figure 5.8. The cell containing PES411 has severe capacity fade after only 15 cycles.

Figure 6.3 shows the resistance, \mathcal{R} , as a function of voltage for the three cells measured at each FRA sequence, every 3 cycles. All cells exhibit larger impedance when subjected to a hold at high voltage compared to without a hold (as shown in Section 5.2). Furthermore, the resistance does not stabilize with increasing cycle number, indicating the presence of parasitic reactions and the formation of unstable SEI layers.

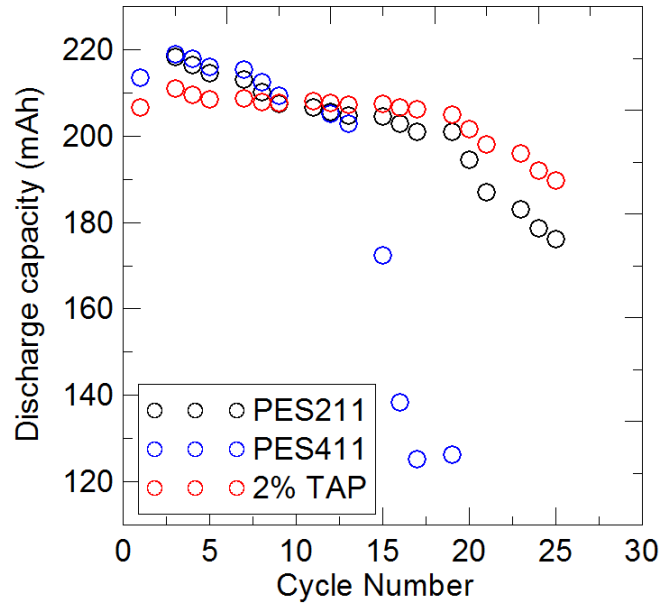


Figure 6.2 Discharge capacity for NMC442/graphite cells undergoing cycling tests with a 24 hour hold at 4.4 V and 40°C.

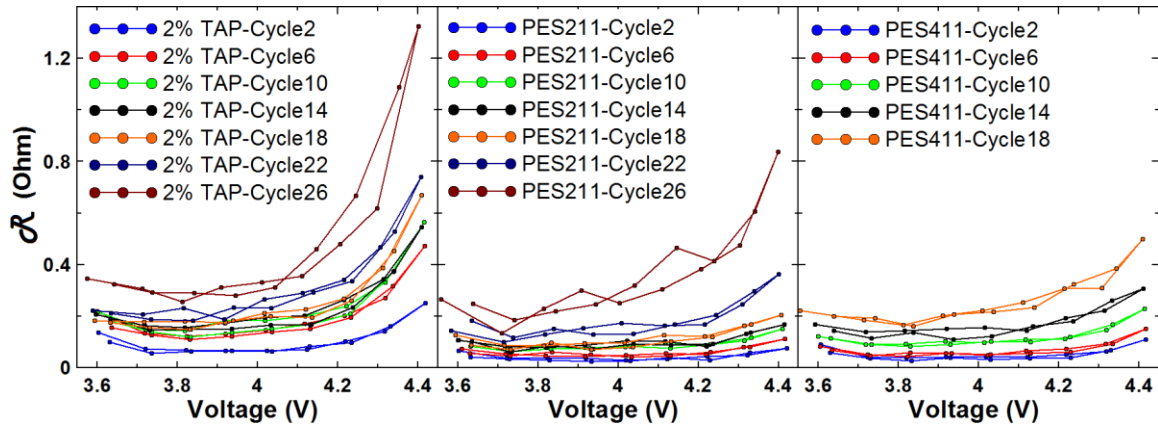


Figure 6.3 The combination of charge transfer resistances (both negative and positive electrodes) and resistance due to motion of ions through the SEI layers (both negative and positive electrodes), \mathcal{R} as a function of voltage for three cells for each measured FRA sequence.

Impedance measurements during cycling are indicative of the amount of parasitic reactions, electrolyte degradation, and provide information about the SEI layers on the positive and negative electrodes. Analysis of the electrolyte and produced gas inside cells at regular intervals during cycling with FRA measurements will be very useful in determining the effect of electrolyte additives on Li-ion cell performance. These measurements will also enable further understanding of the mechanisms occurring in Li-ion cells and the formation and growth of the SEI layers.

To further probe the effect of high voltage cycling on cell impedance and understand the reversible changes in impedance, symmetric cells can be used. A symmetric cell is a cell that contains two of the same electrodes. For example, a negative symmetric cell would consist of two graphite electrodes. The effect of electrolyte additives on each electrode can be investigated by measuring the impedance of symmetric cells. Petibon et al. proved that EIS measurements on symmetric cells provide information about where in a full cell an additive is most beneficial.^{5,59}

Surface analysis techniques, such as XPS, are also highly useful in understanding the effects of additives on the SEI layers. XPS can be used to determine the chemical nature of the SEI. The results can be compared for various additives and additive combinations to observe how additives influence the SEI composition. XPS can provide insight to why particular additives are beneficial.

REFERENCES

1. K. Xu, *Chem. Rev.*, **104**, 4303–4417 (2004).
2. *Linden's Handbook of Batteries, 4th Edition*, McGraw-Hill Professional; 4 edition, (2010), p. 1200.
3. S. S. Zhang, *J. Power Sources*, **162**, 1379–1394 (2006).
4. L. E. Downie, K. J. Nelson, R. Petibon, V. L. Chevrier, and J. R. Dahn, *ECS Electrochem. Lett.*, **2**, A106–A109 (2013).
5. R. Petibon, C. P. Aiken, N. N. Sinha, J. C. Burns, H. Ye, C. M. VanElzen, G. Jain, S. Trussler, and J. R. Dahn, *J. Electrochem. Soc.*, **160**, A117–A124 (2012).
6. J. C. Burns, G. Jain, A. J. Smith, K. W. Eberman, E. Scott, J. P. Gardner, and J. R. Dahn, *J. Electrochem. Soc.*, **158**, A255 (2011).
7. <http://nissannews.com/en-US/nissan/usa/channels/U-S-Sales-Reports/releases/nissan-group-reports-may-2014-u-s-sales>.
8. <http://media.gm.ca/media/us/en/gm/news.detail.html/content/Pages/news/us/en/2014/Jun/gmsales.html>.
9. J. R. Dahn, T. Zheng, Y. Liu, and J. S. Xue, *Science*, **270**, 590–593 (1995).
10. M. N. Obrovac and L. Christensen, *Electrochem. Solid-State Lett.*, **7**, A93 (2004).
11. M. N. Obrovac and L. J. Krause, *J. Electrochem. Soc.*, **154**, A103 (2007).
12. Z. Lu, D. D. MacNeil, and J. R. Dahn, *Electrochem. Solid-State Lett.*, **4**, A200 (2001).
13. 3M, *3M™ Battery Materials: Enabling Lighter, Smaller, Safer and Higher Performance Lithium-ion Batteries*, (2011).
14. R. Fong, U. von Sacken, and J. R. Dahn, *J. Electrochem. Soc.*, **137**, 2009 (1990).
15. E. Peled, *J. Electrochem. Soc.*, **126**, 2047–2051 (1979).
16. P. Verma, P. Maire, and P. Novák, *Electrochim. Acta*, **55**, 6332–6341 (2010).

17. D. Aurbach, *J. Power Sources*, **89**, 206–218 (2000).
18. E. Peled and G. Ardel, *J. Electrochem. Soc.*, **144**, 208–210 (1997).
19. K. Edström, M. Herstedt, and D. P. Abraham, *J. Power Sources*, **153**, 380–384 (2006).
20. A. J. Smith, J. C. Burns, X. Zhao, D. Xiong, and J. R. Dahn, *J. Electrochem. Soc.*, **158**, A447 (2011).
21. Q. Zhang and R. E. White, *J. Power Sources*, **179**, 793–798 (2008).
22. D. Aurbach, B. Markovsky, A. Shechter, and R. Gan, *J. Electrochem. Soc.*, **143** (1996).
23. P. Ganesh, P. R. C. Kent, and D. Jiang, *J. Phys. Chem. C*, **116**, 24476–24481 (2012).
24. D. Aurbach, B. Markovsky, A. Rodkin, M. Cojocaru, E. Levi, and H.-J. Kim, *Electrochim. Acta*, **47**, 1899–1911 (2002).
25. S. Shi, P. Lu, Z. Liu, Y. Qi, L. G. Hector, H. Li, and S. J. Harris, *J. Am. Chem. Soc.*, **134**, 15476–87 (2012).
26. G. V. Zhuang and P. N. Ross, *Electrochem. Solid-State Lett.*, **6**, A136 (2003).
27. S. S. Harilal, J. P. Allain, a. Hassanein, M. R. Hendricks, and M. Nieto-Perez, *Appl. Surf. Sci.*, **255**, 8539–8543 (2009).
28. L. Zhao, I. Watanabe, T. Doi, S. Okada, and J. Yamaki, *J. Power Sources*, **161**, 1275–1280 (2006).
29. R. Dedryvère, S. Leroy, H. Martinez, F. Blanchard, D. Lemordant, and D. Gonbeau, *J. Phys. Chem. B*, **110**, 12986–92 (2006).
30. M. Nie, D. Chalasani, D. P. Abraham, Y. Chen, A. Bose, and B. L. Lucht, *J. Phys. Chem. C*, **117**, 1257–1267 (2013).
31. M. Nie and B. L. Lucht, *J. Electrochem. Soc.*, **161**, A1001–A1006 (2014).
32. M. Nie, *Priv. Commun.* (2014).
33. R. Dedryvère, L. Gireaud, S. Grugeon, S. Laruelle, J.-M. Tarascon, and D. Gonbeau, *J. Phys. Chem. B*, **109**, 15868–75 (2005).

34. R. Dedryvère, S. Laruelle, S. Grugeon, L. Gireaud, J.-M. Tarascon, and D. Gonbeau, *J. Electrochem. Soc.*, **152**, A689 (2005).
35. R. Dedryvère, D. Foix, S. Franger, S. Patoux, L. Daniel, and D. Gonbeau, *J. Phys. Chem. C*, **114**, 10999–11008 (2010).
36. M. Moshkovich, M. Cojocaru, H. . Gottlieb, and D. Aurbach, *J. Electroanal. Chem.*, **497**, 84–96 (2001).
37. L. Ma, D. Y. Wang, L. E. Downie, J. Xia, K. J. Nelson, N. N. Sinha, and J. R. Dahn, *J. Electrochem. Soc.*, **161**, A1261–A1265 (2014).
38. D. Y. Wang, N. N. Sinha, R. Petibon, J. C. Burns, and J. R. Dahn, *J. Power Sources*, **251**, 311–318 (2014).
39. M. Hu, X. Pang, and Z. Zhou, *J. Power Sources*, **237**, 229–242 (2013).
40. M. G. S. R. Thomas, P. G. Bruce, and J. B. Goodenough, *J. Electrochem. Soc.*, **132**, 1521 (1985).
41. D. Guyomard and J. M. Tarascon, *J. Electrochem. Soc.*, **139**, 937 (1992).
42. D. Aurbach, K. Gamolsky, B. Markovsky, G. Salitra, Y. Gofer, U. Heider, R. Oesten, and M. Schmidt, *J. Electrochem. Soc.*, **147**, 1322 (2000).
43. P. B. Balbuena and Y. Wang, Eds., *Lithium-ion Batteries: Solid-electrolyte Interphase*, Imperial College Press, (2004), p. 407.
44. M. Broussely, P. Biensan, F. Bonhomme, P. Blanchard, S. Herreyre, K. Nechev, and R. J. Staniewicz, *J. Power Sources*, **146**, 90–96 (2005).
45. L. Yang and B. L. Lucht, *Electrochem. Solid-State Lett.*, **12**, A229 (2009).
46. W. Choi and A. Manthiram, *J. Electrochem. Soc.*, **153**, A1760 (2006).
47. K. Yamamoto, T. Minato, S. Mori, D. Takamatsu, Y. Orikasa, H. Tanida, K. Nakanishi, H. Murayama, T. Masese, T. Mori, H. Arai, Y. Koyama, Z. Ogumi, and Y. Uchimoto, *J. Phys. Chem. C*, **118**, 9538–9543 (2014).
48. Y. Zhang, C. Y. Chung, L. X. Sun, and M. Zhu, *Mater. Chem. Phys.*, **107**, 254–260 (2008).
49. C. Yogi, D. Takamatsu, K. Yamanaka, H. Arai, Y. Uchimoto, K. Kojima, I. Watanabe, T. Ohta, and Z. Ogumi, *J. Power Sources*, **248**, 994–999 (2014).

50. S. Dalavi, M. Xu, B. Knight, and B. L. Lucht, *Electrochem. Solid-State Lett.*, **15**, A28–A31 (2011).
51. Z. Chen, Y. Qin, K. Amine, and Y.-K. Sun, *J. Mater. Chem.*, **20**, 7606 (2010).
52. Y.-K. Sun, S.-W. Cho, S.-W. Lee, C. S. Yoon, and K. Amine, *J. Electrochem. Soc.*, **154**, A168 (2007).
53. D. Aurbach and Y. Gofer, *J. Electrochem. Soc.*, **136**, 3198–3205 (1989).
54. D. Aurbach, Y. Ein-Eli, O. Chusid, Y. Carmeli, M. Babai, and H. Yamin, *J. Electrochem. Soc.*, **141**, 603 (1994).
55. D. Aurbach, E. Zinigrad, Y. Cohen, and H. Teller, *Solid State Ionics*, **148**, 405–416 (2002).
56. J. C. Burns, A. Kassam, N. N. Sinha, L. E. Downie, L. Solnickova, B. M. Way, and J. R. Dahn, *J. Electrochem. Soc.*, **160**, A1451–A1456 (2013).
57. J. C. Burns, N. N. Sinha, G. Jain, H. Ye, C. M. VanElzen, E. Scott, A. Xiao, W. M. Lamanna, and J. R. Dahn, *J. Electrochem. Soc.*, **160**, A2281–A2287 (2013).
58. J. C. Burns, N. N. Sinha, G. Jain, H. Ye, C. M. VanElzen, W. M. Lamanna, A. Xiao, E. Scott, J. Choi, and J. R. Dahn, *J. Electrochem. Soc.*, **159**, A1095–A1104 (2012).
59. R. Petibon, N. N. Sinha, J. C. Burns, C. P. Aiken, H. Ye, C. M. VanElzen, G. Jain, S. Trussler, and J. R. Dahn, *J. Power Sources*, **251**, 187–194 (2014).
60. N. N. Sinha, A. J. Smith, J. C. Burns, G. Jain, K. W. Eberman, E. Scott, J. P. Gardner, and J. R. Dahn, *J. Electrochem. Soc.*, **158**, A1194 (2011).
61. H. M. Jung, S.-H. Park, J. Jeon, Y. Choi, S. Yoon, J.-J. Cho, S. Oh, S. Kang, Y.-K. Han, and H. Lee, *J. Mater. Chem. A*, **1**, 11975 (2013).
62. J. Jeon, S. Yoon, T. Park, J.-J. Cho, S. Kang, Y.-K. Han, and H. Lee, *J. Mater. Chem.*, **22**, 21003 (2012).
63. J. Xia, N. N. Sinha, L. P. Chen, G. Y. Kim, D. J. Xiong, and J. R. Dahn, *J. Electrochem. Soc.*, **161**, A84–A88 (2013).
64. B. Li, M. Xu, B. Li, Y. Liu, L. Yang, W. Li, and S. Hu, *Electrochim. Acta*, **105**, 1–6 (2013).

65. B. Li, Y. Wang, H. Rong, Y. Wang, J. Liu, L. Xing, M. Xu, and W. Li, *J. Mater. Chem. A*, **1**, 12954 (2013).
66. D. Y. Wang, J. Xia, L. Ma, K. J. Nelson, J. E. Harlow, D. Xiong, L. E. Downie, R. Petibon, J. C. Burns, A. Xiao, W. M. Lamanna, and J. R. Dahn, *J. Electrochem. Soc.* (2014).
67. L. Xia, D. Wang, H. Yang, Y. Cao, and X. Ai, *Electrochem. commun.*, **25**, 98–100 (2012).
68. H. Lee, S. Choi, S. Choi, H.-J. Kim, Y. Choi, S. Yoon, and J.-J. Cho, *Electrochem. commun.*, **9**, 801–806 (2007).
69. X. Zuo, M. Xu, W. Li, D. Su, and J. Liu, *Electrochem. Solid-State Lett.*, **9**, A196 (2006).
70. M. Q. Xu, W. S. Li, X. X. Zuo, J. S. Liu, and X. Xu, *J. Power Sources*, **174**, 705–710 (2007).
71. J. R. Dahn, J. Jiang, L. M. Moshurchak, M. D. Fleischauer, C. Buhrmester, and L. J. Krause, *J. Electrochem. Soc.*, **152**, A1283 (2005).
72. J. Chen, C. Buhrmester, and J. R. Dahn, *Electrochem. Solid-State Lett.*, **8**, A59 (2005).
73. S. Komaba, T. Itabashi, T. Ohtsuka, H. Groult, N. Kumagai, B. Kaplan, and H. Yashiro, *J. Electrochem. Soc.*, **152**, A937 (2005).
74. Z. Zhang, L. Zhang, and K. Amine, *Advanced Electrolyte Additives for PHEV/EV Lithium-ion Battery*, (2011).
75. H. J. Santner, K.-C. Möller, J. Ivančo, M. G. Ramsey, F. P. Netzer, S. Yamaguchi, J. O. Besenhard, and M. Winter, *J. Power Sources*, **119-121**, 368–372 (2003).
76. R. Shimizu, T. Yamaguchi, C. Jung, H. Chung, and Y. Chang, **2**, US7776475 B2 (2010).
77. T. R. Jow, *Electrolytes for Lithium and Lithium-Ion Batteries* T. R. Jow, K. Xu, O. Borodin, and M. Ue, Editors, Springer New York, New York, NY, (2014).
78. J.-T. Lee, Y.-W. Lin, and Y.-S. Jan, *J. Power Sources*, **132**, 244–248 (2004).
79. K. Abe, K. Miyoshi, T. Hattori, Y. Ushigoe, and H. Yoshitake, *J. Power Sources*, **184**, 449–455 (2008).

80. K. Abe, T. Hattori, K. Kawabe, Y. Ushigoe, and H. Yoshitake, *J. Electrochem. Soc.*, **154**, A810 (2007).
81. M. . Smart, B. . Ratnakumar, V. . Ryan-Mowrey, S. Surampudi, G. K. . Prakash, J. Hu, and I. Cheung, *J. Power Sources*, **119-121**, 359–367 (2003).
82. M. C. Smart, B. V. Ratnakumar, V. S. Ryan, S. Surampudi, G. K. S. Prakashb, J. Hub, and I. Cheung, *J. Power Sources* (2002).
83. Y. Lee, K. Nam, E. Hwang, Y. Kwon, D. Kang, S. Kim, S.-W. Song, L. Co, and M. O. Battery, *J. Phys. Chem. C*, **118**, 10631–10639 (2014).
84. Y. Matsuda, T. Nakajima, Y. Ohzawa, M. Koh, A. Yamauchi, M. Kagawa, and H. Aoyama, *J. Fluor. Chem.*, **132**, 1174–1181 (2011).
85. H. F. Xiang, H. Y. Xu, Z. Z. Wang, and C. H. Chen, *J. Power Sources*, **173**, 562–564 (2007).
86. Y. Ein-Eli, *J. Electroanal. Chem.*, **531**, 95–99 (2002).
87. K. Abe, H. Yoshitake, T. Kitakura, T. Hattori, H. Wang, and M. Yoshio, *Electrochim. Acta*, **49**, 4613–4622 (2004).
88. X. X. Li, Z. Yin, and C. Wang, *Ionics*, **20**, 795–801 (2013).
89. J. Xia, N. N. Sinha, L. P. Chen, and J. R. Dahn, *J. Electrochem. Soc.*, **161**, A264–A274 (2013).
90. G. H. Wrodnigg, *J. Electrochem. Soc.*, **146**, 470 (1999).
91. B. T. Yu, W. H. Qiu, F. S. Li, and L. Cheng, *J. Power Sources*, **158**, 1373–1378 (2006).
92. M.-H. Ryou, G.-B. Han, Y. M. Lee, J.-N. Lee, D. J. Lee, Y. O. Yoon, and J.-K. Park, *Electrochim. Acta*, **55**, 2073–2077 (2010).
93. S. S. Zhang, K. Xu, and T. R. Jow, *J. Power Sources*, **156**, 629–633 (2006).
94. S. K. Martha, E. Markevich, V. Burgel, G. Salitra, E. Zinigrad, B. Markovsky, H. Sclar, Z. Pramovich, O. Heik, D. Aurbach, I. Exnar, H. Buqa, T. Drezen, G. Semrau, M. Schmidt, D. Kovacheva, and N. Saliyski, *J. Power Sources*, **189**, 288–296 (2009).
95. M. Hu, J. Wei, L. Xing, and Z. Zhou, *J. Appl. Electrochem.*, **42**, 291–296 (2012).

96. S. Li, W. Zhao, X. Cui, Y. Zhao, B. Li, H. Zhang, Y. Li, G. Li, X. Ye, and Y. Luo, *Electrochim. Acta*, **91**, 282–292 (2013).
97. J. Ufheil, M. C. Baertsch, A. Würsig, and P. Novák, *Electrochim. Acta*, **50**, 1733–1738 (2005).
98. X. Zuo, C. Fan, X. Xiao, J. Liu, and J. Nan, *J. Power Sources*, **219**, 94–99 (2012).
99. Y. Yang and J. Li, in *Gordon Research Conference: Batteries*, Ventura, CA (2014).
100. S. Chen, G. Zhong, X. Cao, Y. Gao, Y. Jin, A. Wu, Z. Gong, R. Fu, Y. Zhao, and Y. Yang, *ECS Electrochem. Lett.*, **2**, A115–A117 (2013).
101. J. Xia, L. Ma, C. P. Aiken, K. J. Nelson, L. P. Chen, and J. R. Dahn, *J. Electrochem. Soc.* (2014).
102. S. Malmgren, M. Hahlin, H. Rensmo, and P. Johansson, *J. Phys. Chem. C*, **117**, 23476–23486 (2013).
103. Y.-S. Kim, T.-H. Kim, H. Lee, and H.-K. Song, *Energy Environ. Sci.*, **4**, 4038 (2011).
104. Y. Ein-Eli, S. R. Thomas, and V. R. Kocht, *J. Electrochem. Soc.*, **144**, 1159–1165 (1997).
105. 石桥 and 谿谷春, *CN103594729 A* (2014).
106. N. N. Sinha, J. C. Burns, and J. R. Dahn, in *224th ECS Meeting*, (2013).
107. T. M. Bond, J. C. Burns, D. A. Stevens, H. M. Dahn, and J. R. Dahn, *J. Electrochem. Soc.*, **160**, A521–A527 (2013).
108. N. N. Sinha, J. C. Burns, and J. R. Dahn, *J. Electrochem. Soc.*, **161**, A1084–A1089 (2014).
109. X. L. Yao, S. Xie, C. H. Chen, Q. S. Wang, J. H. Sun, Y. L. Li, and S. X. Lu, *J. Power Sources*, **144**, 170–175 (2005).
110. P. Ping, Q. S. Wang, J. H. Sun, X. Xia, and J. R. Dahn, *J. Electrochem. Soc.*, **159**, A1467–A1473 (2012).
111. X. Xia, P. Ping, and J. R. Dahn, *J. Electrochem. Soc.*, **159**, A1460–A1466 (2012).
112. S. S. Zhang, K. Xu, and T. R. Jow, *Electrochem. Solid-State Lett.*, **5**, A206 (2002).

113. S. S. Zhang, K. Xu, and T. R. Jow, *J. Power Sources*, **113**, 166–172 (2003).
114. A. von Cresce and K. Xu, *J. Electrochem. Soc.*, **158**, A337 (2011).
115. S. Tan, Z. Zhang, Y. Li, J. Zheng, Z. Zhou, and Y. Yang, *J. Electrochem. Soc.*, **160**, A285–A292 (2012).
116. Z. Cai, Y. Liu, J. Zhao, L. Li, Y. Zhang, and J. Zhang, *J. Power Sources*, **202**, 341–346 (2012).
117. G. Yan, X. Li, Z. Wang, H. Guo, and C. Wang, *J. Power Sources*, **248**, 1306–1311 (2014).
118. J. Li, W. Yao, Y. S. Meng, and Y. Yang, *J. Phys. Chem. C*, **112**, 12550–12556 (2008).
119. R. Fathi, J. C. Burns, D. A. Stevens, H. Ye, C. Hu, G. Jain, E. Scott, C. Schmidt, and J. R. Dahn, *J. Electrochem. Soc.*, **161**, A1572–A1579 (2014).
120. A. J. Smith, J. C. Burns, D. Xiong, and J. R. Dahn, *J. Electrochem. Soc.*, **158**, A1136 (2011).
121. C. P. Aiken, J. Xia, D. Y. Wang, D. A. Stevens, S. Trussler, and J. R. Dahn, *J. Electrochem. Soc.*, **161**, A1548–A1554 (2014).
122. A. J. Smith, J. C. Burns, S. Trussler, and J. R. Dahn, *J. Electrochem. Soc.*, **157**, A196 (2010).
123. S. E. Sloop, J. B. Kerr, and K. Kinoshita, *J. Power Sources*, **119-121**, 330–337 (2003).
124. Y. Qi and S. J. Harris, *J. Electrochem. Soc.*, **157**, A741 (2010).
125. S. Zhang, M. S. Ding, K. Xu, J. Allen, and T. R. Jow, *Electrochem. Solid-State Lett.*, **4**, A206 (2001).
126. D. Aurbach, M. D. Levi, E. Levi, H. Telier, B. Markovsky, and G. Salitra, *J. Electrochem. Soc.*, **145**, 3024–3034 (1998).
127. M. D. Levi, G. Salitra, B. Markovsky, H. Teller, D. Aurbach, U. Heider, and L. Heider, *J. Electrochem. Soc.*, **146**, 1279–1289 (1999).
128. C. T. Love and K. Swider-Lyons, *Electrochem. Solid-State Lett.*, **15**, A53 (2012).

129. R. Petibon, L. Rotermund, K. J. Nelson, A. S. Gozdz, J. Xia, and J. R. Dahn, *J. Electrochem. Soc.*, **161**, A1167–A1172 (2014).